European Journal of Medicinal Chemistry 236 (2022) 114354

Contents lists available at ScienceDirect

European Journal of Medicinal Chemistry

journal homepage: http://www.elsevier.com/locate/ejmech

Design, synthesis, and *in vitro* and *in vivo* characterization of new memantine analogs for Alzheimer's disease

Andreea L. Turcu [a, b], Júlia Companys-Alemany [c], Matthew B. Phillips [d], Dhilon S. Patel [e], Christian Griñán-Ferré [c], M. Isabel Loza [f], José M. Brea [f], Belén Pérez [g], David Soto [b, h], Francesc X. Sureda [i], Maria G. Kurnikova [e], Jon W. Johnson [d], Mercè Pallàs [c], Santiago Vázquez [a, *]

[a] *Laboratori de Química Farmacèutica (Unitat Associada al CSIC), Facultat de Farmàcia i Ciències de l'Alimentació i Institut de Biomedicina (IBUB), Universitat de Barcelona, Av. Joan XXIII, 27-31, 08028, Barcelona, Spain*
[b] *Neurophysiology Laboratory, Department of Biomedicine, Faculty of Medicine and Health Sciences, Institute of Neurosciences, University of Barcelona, 08036, Barcelona, Spain*
[c] *Pharmacology Section, Department of Pharmacology, Toxicology and Therapeutic Chemistry, Faculty of Pharmacy and Food Sciences, Institute of Neurosciences (NeuroUB), Universitat de Barcelona, Av. Joan XXIII 27-31, 08028, Barcelona, Spain*
[d] *Department of Neuroscience and Center for Neuroscience, University of Pittsburgh, Pittsburgh, PA, 15260, USA*
[e] *Chemistry Department, Carnegie Mellon University, 4400 Fifth Ave, Pittsburgh, PA, 15213, USA*
[f] *Innopharma Screening Platform, Biofarma Research Group, Centro de Investigación en Medicina Molecular y Enfermedades Crónicas, Universidad de Santiago de Compostela, Edificio CIMUS, Av. Barcelona, S/N, E, 15706, Santiago de Compostela, Spain*
[g] *Department of Pharmacology, Therapeutics and Toxicology, Autonomous University of Barcelona, E-08193, Bellaterra, Spain*
[h] *August Pi i Sunyer Biomedical Research Institute (IDIBAPS), Barcelona, Spain*
[i] *Pharmacology Unit, Faculty of Medicine and Health Sciences, Universitat Rovira i Virgili, C./ St. Llorenç 21, 43201, Reus, Tarragona, Spain*

ARTICLE INFO

Article history:
Received 27 February 2022
Received in revised form
31 March 2022
Accepted 1 April 2022
Available online 8 April 2022

Keywords:
Alzheimer's disease
Benzohomoadamantane
Caenorhabditis elegans
Electrophysiology
5XFAD
Memantine analogs

ABSTRACT

Currently, of the few accessible symptomatic therapies for Alzheimer's disease (AD), memantine is the only *N*-methyl-D-aspartate receptor (NMDAR) blocker approved by the FDA. This work further explores a series of memantine analogs featuring a benzohomoadamantane scaffold. Most of the newly synthesized compounds block NMDARs in the micromolar range, but with lower potency than previously reported hit **IIc**, results that were supported by molecular dynamics simulations. Subsequently, electrophysiological studies with the more potent compounds allowed classification of **IIc**, a low micromolar, uncompetitive, voltage-dependent, NMDAR blocker, as a memantine-like compound. The excellent *in vitro* DMPK properties of **IIc** made it a promising candidate for *in vivo* studies in *Caenorhabditis elegans* (*C. elegans*) and in the 5XFAD mouse model of AD. Administration of **IIc** or memantine improved locomotion and rescues chemotaxis behavior in *C. elegans*. Furthermore, both compounds enhanced working memory in 5XFAD mice and modified NMDAR and CREB signaling, which may prevent synaptic dysfunction and modulate neurodegenerative progression.

1. Introduction

Alzheimer's disease (AD) is a major and rising public health concern due to not only its increasing global prevalence, but also the lack of effective treatment options [1–3]. To date, only four drugs have approval for treating AD. Unfortunately, these drugs only improve cognitive and behavioral symptoms without modifying the course of the disease. Despite intensive efforts to develop new AD pharmacotherapeutics [4], progress has been slow and difficult. For example, a new drug, aducanumab [5], has recently been approved by the Food and Drug Administration (FDA). However, its approval is mired in controversy due to risk of severe side effects and conflicting reports of efficacy [6–9].

The first drugs developed for AD, the acetylcholinesterase inhibitors (AChEIs), aim to revert the cholinergic deficit responsible for the cognitive impairment of patients [10]. In addition to currently available AChEIs (donepezil, rivastigmine and

* Corresponding author.
E-mail address: svazquez@ub.edu (S. Vázquez).

https://doi.org/10.1016/j.ejmech.2022.114354

galantamine), multiple AChEIs have been developed over the last few years. However, few novel AChEIs have reached clinical trials and none have arrived at the market [11–16].

Another drug approved by the FDA is memantine, a *N*-methyl-D-aspartate receptors (NMDAR) uncompetitive antagonist [17,18]. Memantine acts as an open channel blocker that is thought to prevent NMDAR overactivation and glutamate-mediated neurotoxicity in the pathogenesis of AD [19,20]. It has better therapeutic tolerability and favorable safety relative to other NMDAR channel blockers because of its ability to preferentially block extrasynaptic NMDARs, which have been associated with activation of cell death pathways [21]. Memantine is characterized by faster blocking/unblocking kinetics, strong voltage dependency, and moderate affinity for NMDAR [22]. Due to its excellent drug profile, numerous companies and academic groups have developed new analogs of memantine. Although only neramexane has reached clinical trials [23], much effort is still ongoing for developing new NMDAR open channel blockers with pharmacological profiles similar to memantine for use as potential therapies for AD and other neurodegenerative diseases [24–34]. In addition, other NMDAR open channel blockers are also currently being developed for the treatment of tinnitus and as a new class of drugs with fast-onset antidepressant effects [35–41].

Recently, our research group has synthesized new memantine analogs based on a novel benzopolycyclic ring (Fig. 1). First, compounds with the general structure **I** were synthesized, but they were found to be less potent than memantine (e.g., **Ia** and **Ib**) [42,43]. Interestingly, the replacement of the oxygen atom at the C8 position of **Ia** (IC_{50} = 98 ± 26 μM) by a methylene unit led to the seven-fold more potent amine **IIa** (IC_{50} = 13.6 ± 3.4 μM). Thereafter, further variations at the C9 position in the general structure **II** generated compounds with promising potency, in the low-moderate micromolar range. Indeed, three of these derivatives displayed potencies very similar to (**IIc** and **IIg**) or even stronger than (**IIb**) memantine (Fig. 1) [44].

In our endeavor to find novel analogs of memantine, herein we report further structure-activity relationships (SAR) on the benzohomoadamantane scaffold, i.e., derivatives of general structure **III**, in order to select a proper candidate for additional *in vitro* pharmacokinetic studies, and subsequently perform an *in vivo* study in a 5XFAD murine model of AD.

2. Results and discussion

2.1. Design and synthesis of new NMDAR channel blockers

First, to explore alternative substituents at the C9 position, we synthesized **2** (Scheme 1). It is known that H/D bioisosteric replacement may lead to compounds with the same activity and selectivity [45–47]. Furthermore, considering that the C9 position is susceptible to being metabolized, the presence of deuterium may be a good strategy to avoid rapid metabolization and prolong the pharmacokinetic stability of the compound [48]. The approach followed for the synthesis of **2** was similar to that previously applied to the preparation of **IIb** [44]. Thus, the reaction of known alcohol **1** [44] with thionyl bromide followed by radical dehalogenation of the unstable bromo intermediate, generated the amine **2** in moderate overall yield (Scheme 1).

We have previously reported that the NMDAR antagonist activities of amantadine and its ring-contracted analogs are of the same order of magnitude [49]. Consequently, we also designed the ring-contracted analog **6**, by removing a methylene group from **IIb** and bonding positions C7 and C9 (Scheme 1). The synthesis of amine **6** involved four steps: a) reaction of known alcohol **3** [50] with mesyl chloride; b) reaction of the corresponding mesylate with NaI in the presence of H_3PO_3 to furnish iodide **4**; c) radical photochemical carboxylation of **4** to carboxylic acid **5**; and, d) Curtius rearrangement of **5** to generate primary amine **6**.

We have previously synthesized and described several derivatives of **I** and **II**, but, so far, we have not explored the impact of introducing substituents on the aromatic ring of the benzohomoadamantane scaffold. Although **IIb** (IC_{50} = 0.70 ± 0.12 μM), **IIc** (IC_{50} = 1.93 ± 0.21 μM) and **2** (IC_{50} = 1.2 ± 0.1 μM) are more potent NMDAR antagonists than **IIa** (IC_{50} = 13.6 ± 3.40 μM, see below), we

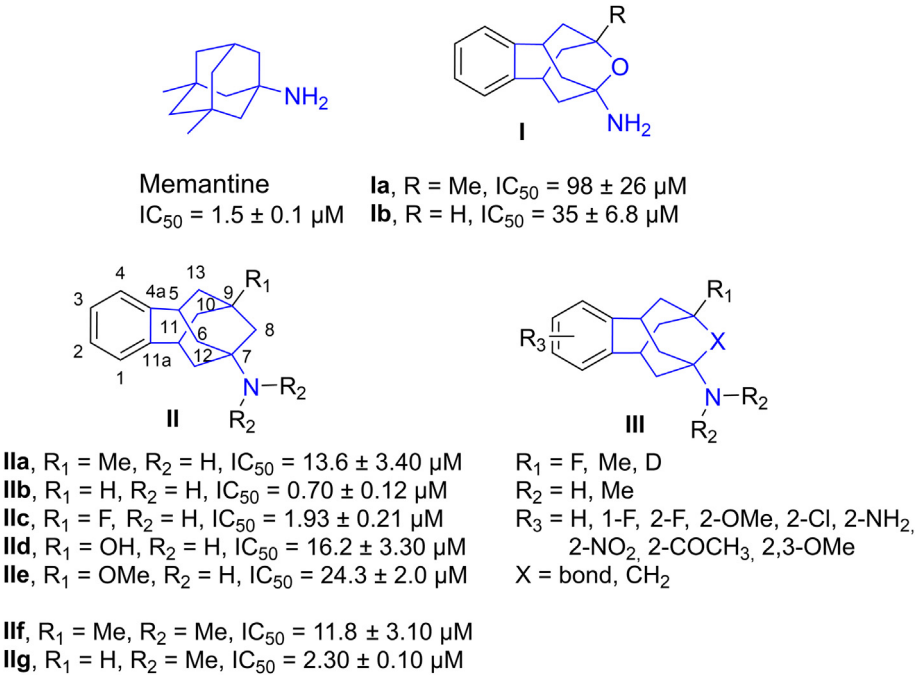

Fig. 1. Structures of memantine, previously studied polycycles Ia-b and IIa-g, and the new series III. IC_{50} values for memantine and polycycles **Ia-b** and **IIa-g** are provided under each structure.

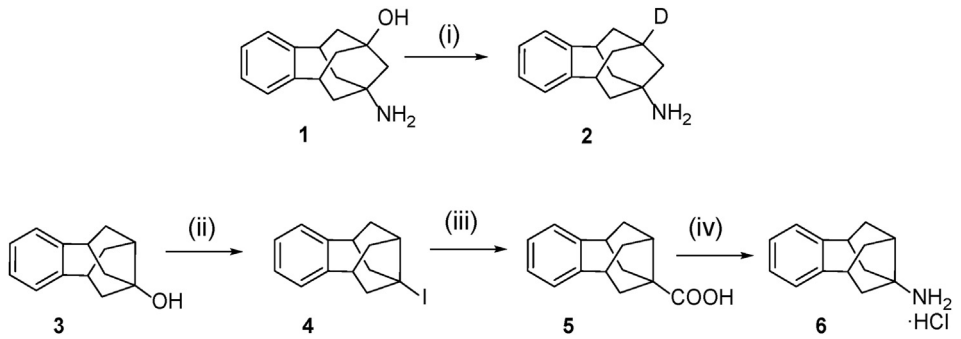

Scheme 1. Synthesis of series **III** amines **2** (R_1 = D, X = CH_2) and **6** (R_1 = H, X = bond). Reagent and conditions: (i) 1) $SOBr_2$, toluene, rt, 1.5 h; 2) Bu_3SnD, AIBN, anh toluene, 95 °C, 4 h, 40% overall yield. (ii) 1) Methanesulfonyl chloride, pyridine, 120 °C, 5 h; 2) H_3PO_3, NaI, 150 °C, 6 h, 76% overall yield. (iii) 1) bis(tributyltin), methyl oxalyl chloride, anh toluene, hν, 20 h; 2) MeOH, Et_3N; 3) KOH/MeOH 40%, 2 h; 4) H_2O, reflux, 3 h, 37% overall yield. (iv) DPPA, Et_3N, toluene, reflux, 3 h; 2) HCl 6 N, reflux, 24 h; 3) HCl/MeOH, 39% overall yield.

first decided to screen the NMDAR blocking activity of benzene-substituted derivatives based on **IIa**, because this amine shows an excellent compromise between acceptable potency as NMDAR channel blocker and better synthetic availability. Therefore, we prepared a series of ten derivatives of general structure **III** (R_1 = Me, X = CH_2) which are analogs of **IIa**, by introducing a variety of electron-withdrawing and electron-donating group on the aromatic ring. The key introduction of the substituents in the aromatic ring was accomplished using two alternative procedures (Schemes 2–4).

In the first approach, electrophilic aromatic substitution reactions on known chloroacetamide **7** [43] or acetamide **16** [51] were carried out for the synthesis of **9**, **10**, **12**, **14**, **15** and **20**. Thus, from the known chloroacetamide **7**, following a classical approach that involved aromatic nitration and cleavage of the chloroacetyl group, amine **9** was obtained. Catalytic hydrogenation of **9** furnished aniline **10**. Additionally, Friedel–Crafts acylation of **7**, followed by deprotection afforded amine **12** in good yield. A Friedel–Crafts reaction of the known **13** [43] led to amine **14** and a reductive alkylation of **9** provided amine **15** (Scheme 2).

A first attempt to obtain amine **20**, through catalytic hydrogenation of **8** followed by a classical Sandmeyer reaction and removal of the chloroacetamide group, met with failure. Thus, **20** was prepared from the known acetamide **16** [51] through a four-step process that involved aromatic nitration, catalytic hydrogenation, Sandmeyer reaction, and hydrolysis (Scheme 3).

A different synthetic strategy was undertaken for the synthesis of the aromatic substituted compounds **37**–**40**, which involved the construction of the benzohomoadamantane scaffold starting from a suitably mono- or disubstituted *o*-phthaldialdehyde (Scheme 4). Thus, once the substituted *o*-phthaldialdehydes **21** [52], **22** [53], **23** [54], and **24** [55] were obtained via procedures previously reported, a synthetic route that included a Weiss-Cook condensation [56], hydrolysis, decarboxylation, and dehydration led to the corresponding diketones **25**–**28**. Subsequently, the treatment of these ketones under Wittig olefination and Ritter-type transannular cyclization conditions furnished the chloroacetamides **33**–**36** that after deprotection provided the desired amines **37**–**40**.

In order to determine the effects of different aromatic substituents on NMDAR block, the potency of the new benzo-substituted amines **9**–**10**, **12**, **14**–**15**, **20** and **37**–**40** was tested (see below) and compared with that of the unsubstituted **IIa** (Table 1). Briefly, the introduction of substituents in the aromatic ring resulted in a decrease in the potency as NMDAR blockers for the majority of compounds regardless of the position, size or electronic character of the substituent (**9**, IC_{50} = 164 μM; **10**,

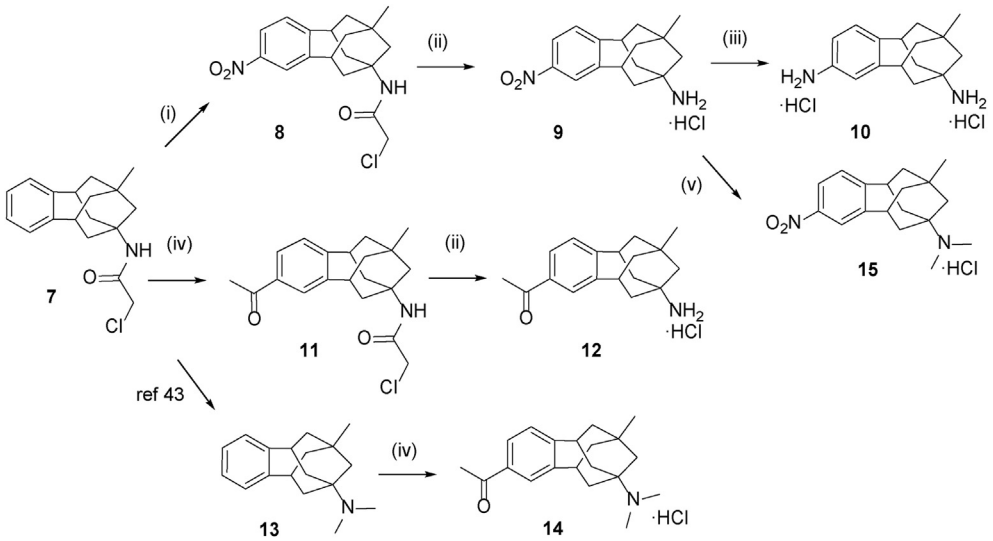

Scheme 2. Synthesis of amines **9**, **10**, **12**, **14** and **15** (compounds from series **III** with R_1 = Me and X = CH_2). Reagent and conditions: (i) fuming HNO_3, Ac_2O, AcOH, 0 °C to rt, overnight, 85% yield. (ii) 1) thiourea, glacial AcOH, abs. ethanol, reflux, overnight; 2) HCl/Et_2O, 74% overall yield for **9** and 52% overall yield for **12**. (iii) 1) H_2, Pd/C, MeOH, 1 atm, rt, 48 h; 2) HCl/MeOH, quant. overall yield. (iv) CH_3COCl, $AlCl_3$, DCM, rt, 1 h, 54% yield for **11** and 40% yield for **14** as hydrochloride salt obtained with HCl/Et_2O. (v) 1) formalin 37%, $NaBH_3CN$, glacial AcOH, MeOH, rt, overnight; 2) HCl/Et_2O, 74% overall yield.

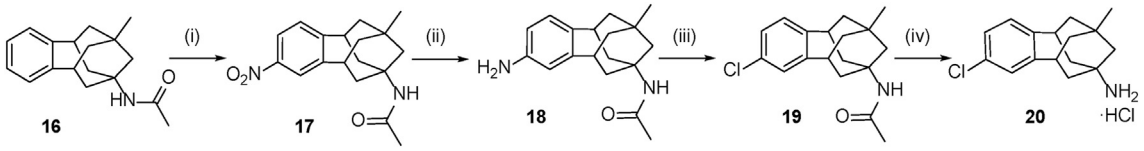

Scheme 3. Synthesis of amine **20** (compound from series **III** with R_1 = Me and X = CH_2). Reagent and conditions: (i) fuming HNO_3, Ac_2O, AcOH, 0 °C to rt, overnight, 60% yield. (ii) H_2, PtO_2, EtOH, 1 atm, rt, 4 h, 68% yield. (iii) 1) $NaNO_2$/conc. HCl, <5 °C; 2) CuCl/conc. HCl, 60 °C, 90 min, 21% overall yield. (iv) 1) conc. HCl/2-propanol, 6 days, reflux; 2) HCl/Et_2O, 19% overall yield.

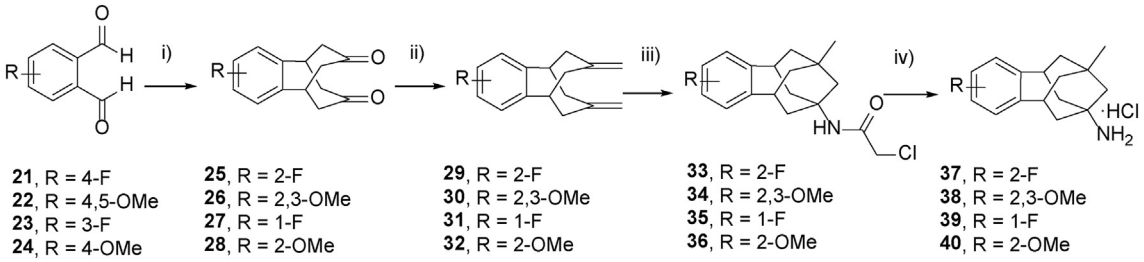

Scheme 4. Synthesis of amines **37**–**40** (compounds from series **III** with R_1 = Me and X = CH_2). Reagent and conditions: (i) 1) dimethyl-1,3-acetonedicarboxylate, Et_2NH, MeOH, reflux, 1.5 h; 2) glacial AcOH, conc. HCl, reflux, 12 h; 3) Toluene, reflux, 13% overall yield for **25**, 30% for **26**, 51% for **27**, 65% for **28**. (ii) Ph_3PCH_3I, NaH, anh DMSO, 90 °C, overnight, 60% yield for **29**, 23% for **30**, 69% for **31**, 38% for **32**. (iii) $ClCH_2CN$, conc. H_2SO_4, AcOH, 0 °C to rt, overnight, 48% yield for **33**, 75% yield for **34**, 68% yield for **35**, 57% for **36**. (iv) 1) thiourea, glacial AcOH, abs. ethanol, reflux, overnight; 2) HCl/Et_2O, 36% overall yield for **37**, 81% for **38**, 84% for **39**, 81% for **40**.

Table 1
IC_{50} values (μM) of the new series III of benzohomoadamantane derivatives as NMDAR channel blockers and of references IIa-c and memantine.[a]

Comp.	IC_{50} (μM)
2	1.16 ± 0.07
6	111 ± 18.8
9	164 ± 4.48
10	NA[b]
12	323 ± 89.2
14	566 ± 186
15	309 ± 120
20	34.7 ± 5.98
37	30.9 ± 4.70
38	517 ± 54.7
39	13.2 ± 1.07
40	77.4 ± 13.5
44	29.0 ± 11.9
IIa[c]	13.6 ± 3.40
IIb[d]	0.70 ± 0.12
IIc[d]	1.93 ± 0.21
Memantine	1.5 ± 0.1

[a] Functional data were obtained from primary cultures of cerebellar granule neurons using the method described in the experimental section by measuring the intracellular calcium concentration. Cells were challenged with NMDA as indicated. Data shown are means ± SEM of at least three separate experiments carried out on three different batches of cultured cells.
[b] NA, non-active.
[c] See ref. 43.
[d] See ref. 44.

IC_{50} = not active; **12**, IC_{50} = 323 μM; **14**, IC_{50} = 566 μM; **15**, IC_{50} = 309 μM; **20**, IC_{50} = 34.7 μM; **37**, IC_{50} = 30.9 μM; **38**, IC_{50} = 517 μM; **39**, IC_{50} = 13.2 μM; **40**, IC_{50} = 77.4 μM) (see below and Table 1). An exception to this trend is amine **39**, with a fluorine atom at the C1 position, the potency of which (IC_{50} = 13.2 μM) was similar to that of **IIa** (IC_{50} = 13.6 μM). Thus, once this screening was completed with derivatives of **IIa**, and considering the electrophysiological studies carried out with **IIb**, **IIc** and **2** (see below), amine **44** was envisaged as a promising compound. **44** contains two fluorine atoms at C1 and C9 and was synthesized starting from the diketone **27**, through a four-step sequence that involved a selective mono-Wittig olefination, followed by a Ritter-type transannular cyclization, substitution of the hydroxyl group by a fluorine atom and final removal of the chloroacetamide group (Scheme 5).

The new amines, **2**, **6**, **9**–**10**, **12**, **14**–**15**, **20**, **37**–**40**, and **44**, were fully characterized as hydrochlorides through their spectroscopic data and elemental analyses or HPLC/UV (see Experimental Section and supporting information for further details).

2.2. NMDAR blockers activities and SAR

To evaluate whether the synthesized compounds were able to block NMDARs, we measured their effect on increases in intracellular calcium evoked by 100 μM NMDA (in the presence of 10 μM of glycine) on rat cultured cerebellar granule neurons using a previously reported Fura 2 assay (Table 1) [57].

As expected, the substitution of the hydrogen atom at C9 in **IIb** by a deuterium atom did not affect the biological potency of **2** (IC_{50} = 0.70 ± 0.12 μM for **IIb** *vs* IC_{50} = 1.16 ± 0.07 μM for **2**). However, the ring contraction from **IIb** to **6** resulted in a dramatic drop in potency (IC_{50} = 0.70 ± 0.12 μM for **IIb** *vs* IC_{50} = 111 ± 18.8 μM for **6**).

Regarding the aromatic substitution, it can be concluded that the functionalization of the aromatic ring is highly deleterious for the compound's NMDAR channel blocking potency (Table 1), regardless of the electron donor or acceptor character of the substituent (compare **IIa** *vs* **9**, **10**, **12**, **20**, **37**–**40**). However, size and substitution position exerted a certain influence on potency. Small size substituents such as chlorine (**20**) and fluorine (**37**) at C2 were less deleterious for potency than bigger substituents such as a nitro (**9**) or an acetyl (**12**) group. More importantly, the introduction of a fluorine atom at C1, as in **39** (IC_{50} = 13.2 ± 1.07 μM) does not alter the IC_{50} value in respect to the unsubstituted **IIa** (IC_{50} = 13.6 ± 3.4 μM), unlike **37** (IC_{50} = 30.9 ± 4.70 μM) which possesses the fluorine atom at C2. Overall, within this series of new amines featuring a methyl group at C9, **39**, with its fluorine atom at C1, emerged as the most interesting derivative. Due to the effect of the C1 fluorine atom and our finding that the replacement of **IIa**'s methyl group at C9 with a fluorine atom, as in **IIc**, resulted in a

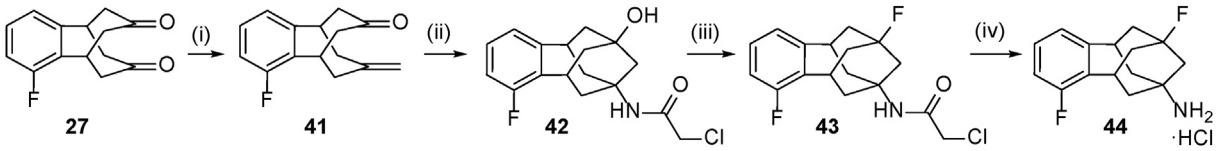

Scheme 5. Synthesis of amine **44** (compound from series **III** with R_1 = F and X = CH_2). Reagent and conditions: (i) Ph_3PCH_3I, NaH, anh DMSO, 90 °C, overnight, 46% yield. (ii) $ClCH_2CN$, conc. H_2SO_4, DCM, 0 °C to rt, overnight, 32% yield. (iii) diethylaminosulfur trifluoride (DAST), DCM, −30 °C to rt, overnight, 69% yield. (iv) 1) thiourea, glacial AcOH, abs. ethanol, reflux, overnight; 2) HCl/Et_2O, 79% yield.

remarkable increase of potency, we synthesized amine **44**. Unexpectedly, **44** (IC_{50} = 29.0 ± 11.9 μM) was a less potent NMDAR channel blocker than **IIc** (IC_{50} = 1.93 ± 0.21 μM).

Finally, within this new series of benzohomoadamantane derivatives, tertiary amines were clearly less potent than the corresponding primary amines (**9** *vs* **15** and **12** *vs* **14**), in contrast to the trend observed in reference compounds **IIa** and **IIb**.

Overall, with the sole exception of the deuterated amine **2** (IC_{50} = 1.16 ± 0.07 μM), all the amines herein reported were less potent as NMDAR channel blockers than the previously described amines **IIb** (IC_{50} = 0.70 ± 0.12 μM) and **IIc** (IC_{50} = 1.93 ± 0.21 μM). Particularly striking is the marked decrease in potency when going from **IIb** to its ring-contracted analog **6** (IC_{50} = 111 ± 18.8 μM).

2.3. Molecular dynamics (MD) simulations

Electrophysiological studies (see discussion below in electrophysiology section) confirmed NMDAR channel blocking ability for compounds investigated in this study. However, to better understand molecular mechanisms of how these channel blockers occlude ion permeation and to rationalize the differential binding affinities of these benzohomoadamantane derivatives caused by ring contraction, the exchange of substituent at the C9 position, or introduction of different groups on the aromatic ring, we used molecular dynamic (MD) simulations. We have developed a computational structural model of the NMDAR (GluN1/2A) transmembrane domain with a closed gate. We selected four compounds, **IIa**, **IIb**, **IIc** and **6**, to generate initial docking-based protein-ligand complex structures for NMDAR-**IIa**, NMDAR-**IIb**, NMDAR-**IIc** and NMDAR-**6**. The complexes then were embedded in a POPC lipid bilayer and solvated in water and 0.15 M NaCl solution. 200 ns molecular dynamics simulations were carried out for each of the structures to allow for equilibration of the ligand in the channel in native-like conditions. From these simulations we obtained atomic level insights on binding modes and their stabilities to analyze how their structural and dynamic features correlate with the reported difference in the binding affinities of these compounds.

During MD simulations, all compounds showed stable binding in a "flipped down" conformation (Fig. 2) with the NH_3^+ groups facing the intracellular side of the membrane. In this flipped down conformation the NH_3^+ groups formed H-bond interactions with the asparagine (ASN) clusters at the tips of the M2 helices of GluN1 (N616) and GluN2A (N614) subunits. The hydrophobic aromatic core of the compounds stabilized between the protein channel sub-pockets created by the hydrophobic side chains of L642 and A643 of GluN2A, and V644, A645 and M641 of GluN1 inside the channel (Fig. 2A–C). Similar flipped down binding modes were reported for memantine and MK-801 in the GluN1/2B NMDAR channel [58].

For all compounds that stabilized in flipped down conformations, we observed mobility of the blocker's hydrophobic core in the plane of its phenyl ring. This mobility allowed for different binding pose occupancies within the sub-pockets created between M3 helices of GluN1 and GluN2A (Fig. 3). Similar flexible orientations were reported in MD simulations of MK-801 in the GluN1/2B NMDAR channel [58]. Orientationally different poses are indeed stable in flipped down binding conformations (Fig. S1) and could easily block ion conduction by physical occlusion of the permeation pathway.

Comparing MD simulation results provided further insights into binding differences among **IIa**, **IIb** and **IIc**. For example, very close contact of the methyl at C9 in **IIa** (Fig. 2A) with the side chain hydroxyl groups of the threonines (T648 − GluN1 and T647 − GluN2A) inside the channel cavity may cause an energetic penalty on binding, which could explain the reduced binding affinity of **IIa** in comparison to **IIb** (Fig. 2B). In contrast, due to the smaller size of the fluorine at this position in **IIc**, there is no steric clash with threonine side chains, which may explain the more similar potencies of **IIb** and **IIc** (Fig. 2C). These observations also suggest that any substitution larger than hydrogen or fluorine will result in a steric clash with the hydrophobic wall and would require a wider channel opening to accommodate such a compound. Furthermore, the simulations showed that heavy atoms of the protein side chains are within 4 Å of the phenyl ring (Fig. 2). This suggests that any substitution on the aromatic ring will negatively affect binding since it will clash with the hydrophobic wall. Indeed, consistent with simulations, only unsubstituted derivatives of the phenyl ring (**IIa-g** and **2**) and their fluorinated analogs (**37**, **39** and **44**) showed acceptable potency (Fig. 1 and Table 1).

Finally, MD simulations performed with **6** showed a flipped down binding mode similar to **IIa**, **IIb** and **IIc** where the NH_3^+ of **6** maintains H-bonding interaction to ASN cluster through the majority of the MD simulation time (Fig. 2D). However, we observed a slight instability of the flipped down conformation. This could be explained by the presence of water molecules in the channel cavity between the hydrophobic core of compound **6** and the hydrophobic residues of the channel, which is likely due to the smaller size of the ring-contracted **6** (Fig. 2D). Considering that hydrophobic residues in the NMDAR channel cavity play an important role in the binding of channel blockers [59], the loss of the interaction between **6** and hydrophobic channel residues provides an explanation for the reduction of the potency of this amine.

2.4. Functional block of NMDAR by benzohomoadamantane derivatives *IIb*, *IIc*, and *2* compared with memantine

We next selected compounds with similar potency to memantine (**IIb**, **IIc** and **2**) and measured functional block of NMDAR. To measure the properties of the newly synthesized amines, we performed whole-cell patch-clamp recordings from tsA201 cells transfected with expression plasmids codifying for rat GluN1 and GluN2A subunits [28,60].

Fig. 4A shows representative current traces obtained using a protocol that allowed us to quickly screen NMDAR inhibition by the compounds of interest at two membrane potentials. While clamping the cell at −60 mV, NMDAR currents were elicited with 100 μM NMDA plus 10 μM glycine. After NMDA-mediated currents had reached a steady state, a blocking compound (either memantine, **IIb**, **IIc** or **2**) was applied for 40 s in the presence of agonist.

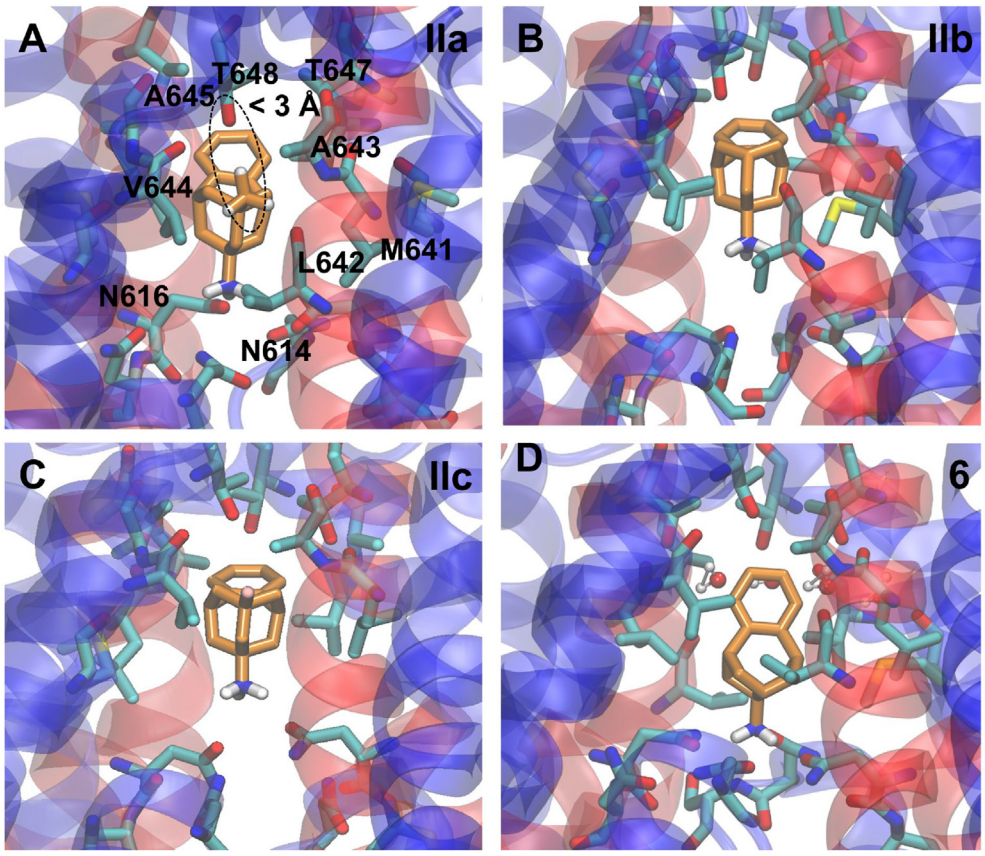

Fig. 2. Representative conformational orientation of IIa (A), IIb (B), IIc (C), and 6 (D). A. IIa shown with hydrophobic channel residues and ASN cluster residues also the methyl of **IIa** showed a minor clash (dotted circle) with threonine side chains from the cavity that may decrease its potency. **B. IIb** shows similar interactions as **IIa** but no clash with threonine. **C. IIc** shows similar interactions as **IIa D. 6** is shown surrounded by water molecules that may prevent it from interacting with the receptor biding pocket in the NMDA channel during MD simulations. In all panels GluN1 subunit is depicted as blue ribbons; GluN2A subunit is depicted as red ribbons; side chains of channel residues within 4 Å of compounds are shown in stick representations.

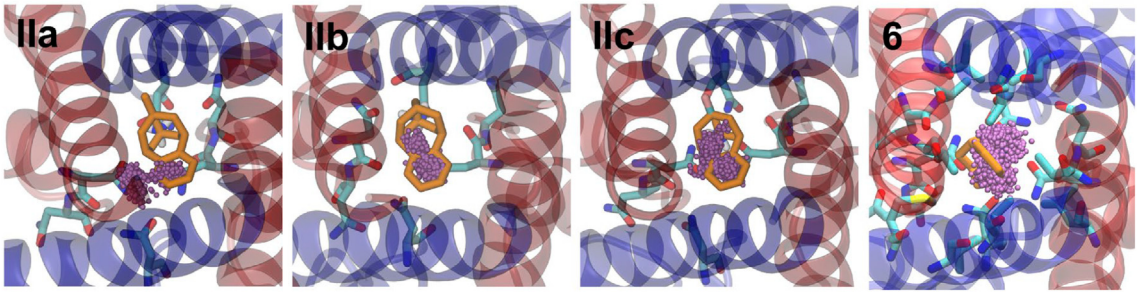

Fig. 3. Top view of the hydrophobic core orientation flexibility for IIa, IIb, IIc and 6 in XY plane with respect to phenyl ring inside the channel. Center of mass occupancies of phenyl rings are shown as purple balls.

During blocker application, the membrane voltage was jumped to +60 mV for 5 s and returned to −60 mV. Blocker then was removed to allow blocker unbinding and recovery of the current from inhibition, during which another 5 s jump to +60 mV was performed before returning to −60 mV and subsequent removal of agonists.

Although memantine, **IIb**, and **2** show a similar degree of NMDAR inhibition, inhibition by **IIc** was noticeably weaker (69.1 ± 1.2% for **IIc** *vs*. 86.2 ± 1.4% for memantine $p < 0.0001$; one-way ANOVA with Bonferroni's multiple comparison test; Fig. 4B). While no differences were observed in percentage of block for **2** in comparison to memantine (89.3 ± 3.1%; $p > 0.05$), **IIb** appeared to block slightly more efficiently than memantine (94.1 ± 1.4%; $p < 0.05$). Regarding blocking kinetics (measured as the time needed to reach approximately 2/3 of the maximal block; $\tau_{weighted}$ (weighted time constant) in seconds; see experimental section), all compounds tested presented values similar to memantine (around 1 s), although development of block by **IIc** was faintly slower (Fig. 4C).

Inhibition by all known NMDAR channel blockers depends on membrane voltage, with potency increasing as membrane voltage is hyperpolarized. We assessed the voltage dependence of the compounds tested by applying two positive voltage steps to +60 mV in the presence of the blocker or after blocker washout

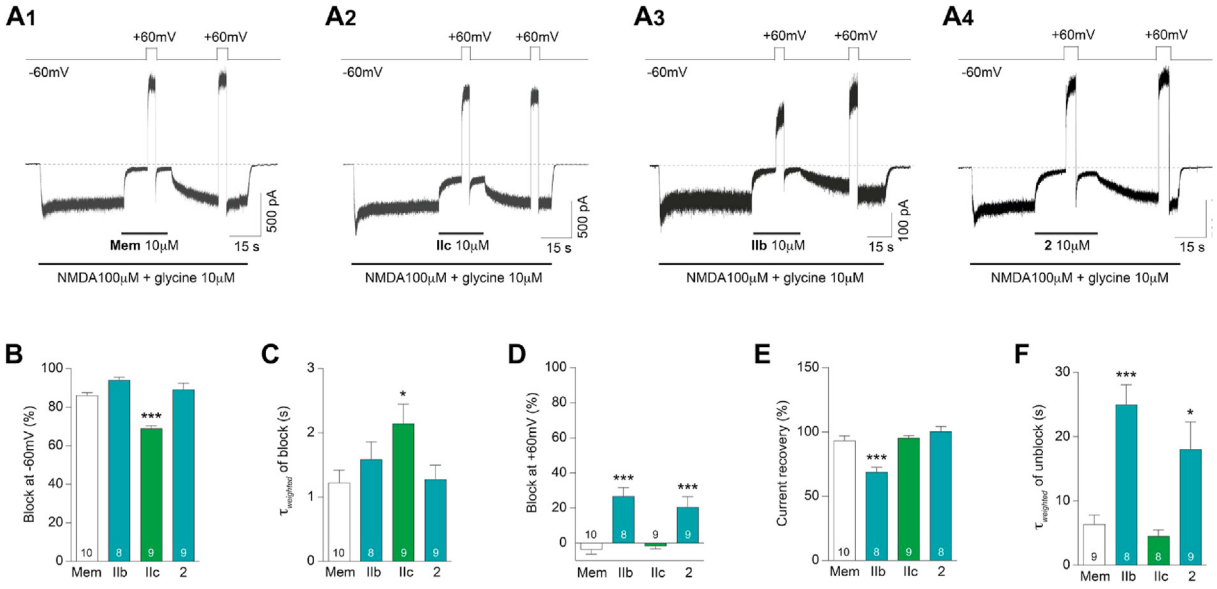

Fig. 4. Block, unbinding, voltage dependence, and blocking and unblocking kinetics of memantine (Mem), IIb, IIc and 2. A. Examples of whole-cell currents evoked by bath application of 100 μM NMDA plus 10 μM glycine onto tsA201 cells expressing GluN1/2A NMDARs. Compounds were rapidly applied with a piezoelectric device at 10 μM in the presence of the agonists. **B.** Blocking percentage at the holding potential of −60 mV. Numbers inside bars denote the number of experiments. **C.** Blocking kinetics expressed in time constant (s). Numbers inside bars denote the number of experiments. **D.** Percentage of block at +60 mV (n = 10, 8, 9 and 9 for memantine, **IIb**, **IIc** and **2**, respectively. **E.** Degree of unbinding, measured as the percentage of current recovery after removal of the blocker. Numbers inside bars denote the number of experiments. **F.** Unblocking kinetics expressed in time constant (s). Numbers inside bars denote the number of experiments. Asterisks identify mean values with statistically significant differences from the value for memantine: ****p < 0.0001, ***p < 0.001, **p < 0.01, *p < 0.05.

(Equation (1)). We observed that **IIc** showed strong voltage dependent block similar to that of memantine (Fig. 4D). **IIb** and **2** showed weaker apparent voltage dependence of block: % block at +60 mV was 26.9 ± 4.7% for **IIb** and 20.6 ± 5.9% for **2** compared to −3.9 ± 2.5% for memantine ($p < 0.001$ for both compounds *vs.* memantine). It is likely that these results reveal that **IIb** and **2** exhibit both weaker voltage dependence, and slower unblocking kinetics (Fig. 4F), than memantine or **IIc**.

Importantly, a potential memantine-like compound should have similar unbinding kinetics. Therefore, we calculated the percentage of current recovery 40 s after removal of the blocker for the selected compounds and we compared it with that of memantine (93.6 ± 3.3% recovery of current). Note that, because of the interposed depolarization, current recovery will depend on the drugs' unblocking kinetics both at −60 and at +60 mV. **IIb** showed less current recovery than memantine (69.0 ± 3.6% recovery; $p < 0.0001$ *vs.* memantine), whereas current recovery for **IIc** and **2** was similar to memantine (Fig. 4E). The lower current recovery after 40 s observed for **IIb** suggested that its unbinding kinetics are slower than memantine's, a conclusion supported by the observed unblocking kinetics (quantified as $\tau_{weighted}$; see experimental section; $\tau_{weighted}$ = 18.1 ± 4.2 s for **IIb** *vs.* 6.4 ± 1.4 s for memantine; $p > 0.001$; Fig. 4F).

Since our main aim was to select the best memantine analog for an *in vivo* study, **IIb** and **2** were discarded as candidates due to their relatively weak voltage dependence, despite their high potency. Although **IIc** did not block to the same degree as memantine, it showed a similar electrophysiological profile and IC_{50} value, making it a suitable candidate for additional *in vitro* experiments and a subsequent *in vivo* study.

2.5. Characteristics of NMDAR inhibition by *IIc*

We next further quantified the potency and voltage dependence of NMDAR inhibition by **IIc** using whole-cell patch-clamp recordings from tsA201 cells expressing GluN1/2A receptors. Inhibition by **IIc** was measured as a function of drug concentration (Fig. 5A) and used to calculate the **IIc** IC_{50} in cells held at −65 mV. The IC_{50} of **IIc** was found to be 4.40 ± 0.15 μM (Fig. 5B and C), well within the range of therapeutically beneficial NMDAR antagonists (e.g. ketamine IC_{50} ~ 1 μM; memantine IC_{50} ~ 1–2 μM; amantadine IC_{50} ~ 40–75 μM) [28,61–68]. This IC_{50} value slightly differs from the **IIc** IC_{50} measured using intracellular Ca^{2+} measurements from cerebellar granule neurons (1.93 ± 0.21 μM; Table 1), consistent with previous similar comparisons of NMDAR channel blocker IC_{50}s [28]. The discrepancy may result from differences in recording technique and/or from expression of GluN2 subunits other than GluN2A by cerebellar granule neurons [69–71].

NMDAR channel blockers share overlapping binding sites in the NMDAR channel [72–75]. Thus, many organic NMDAR channel blockers (e.g. amantadine, memantine, and ketamine) show competitive binding with the endogenous blocker Mg^{2+} [68,74,76–78]. To ascertain whether **IIc** inhibits NMDARs via channel block, we tested the effect of extracellular Mg^{2+} on **IIc** potency. As predicted, the inclusion of 0.2 mM Mg^{2+} in the recording solution led to a substantial rightward shift in the **IIc** IC_{50} curve and a significant increase in **IIc** IC_{50} (IC_{50} = 4.40 ± 0.15 μM in 0 Mg $^{2+}$ *vs* 21.41 ± 0.56 μM in 0.2 mM Mg^{2+}; $p < 0.0001$, two-sample Student t-test, n = 10 and 6, respectively; Fig. 5B and C). This roughly 5-fold decrease in **IIc** potency suggests a competitive interaction between Mg^{2+} and **IIc** in the NMDAR channel.

We next determined the voltage dependence of inhibition by 10 μM (~2-fold IC_{50} at −65 mV) **IIc**. As predicted of a positively charged channel blocker, inhibition by **IIc** was markedly weaker at depolarized potentials (Fig. 5D–F). Equations (3) and (4) were used to quantify V_0, the change in voltage (in mV) that results in an e-fold change in the IC_{50} of a drug, and δ, an estimate of the fraction of the total transmembrane voltage field felt by the blocker at its binding site [79]. Inhibition of GluN1/2A receptors by **IIc** is strongly voltage-dependent, as reflected by the drug's small V_0 (25.43 ± 0.54 mV) and large δ (1.01 ± 0.02). The **IIc** V_0 and δ values are similar to previously reported values for monovalent organic channel

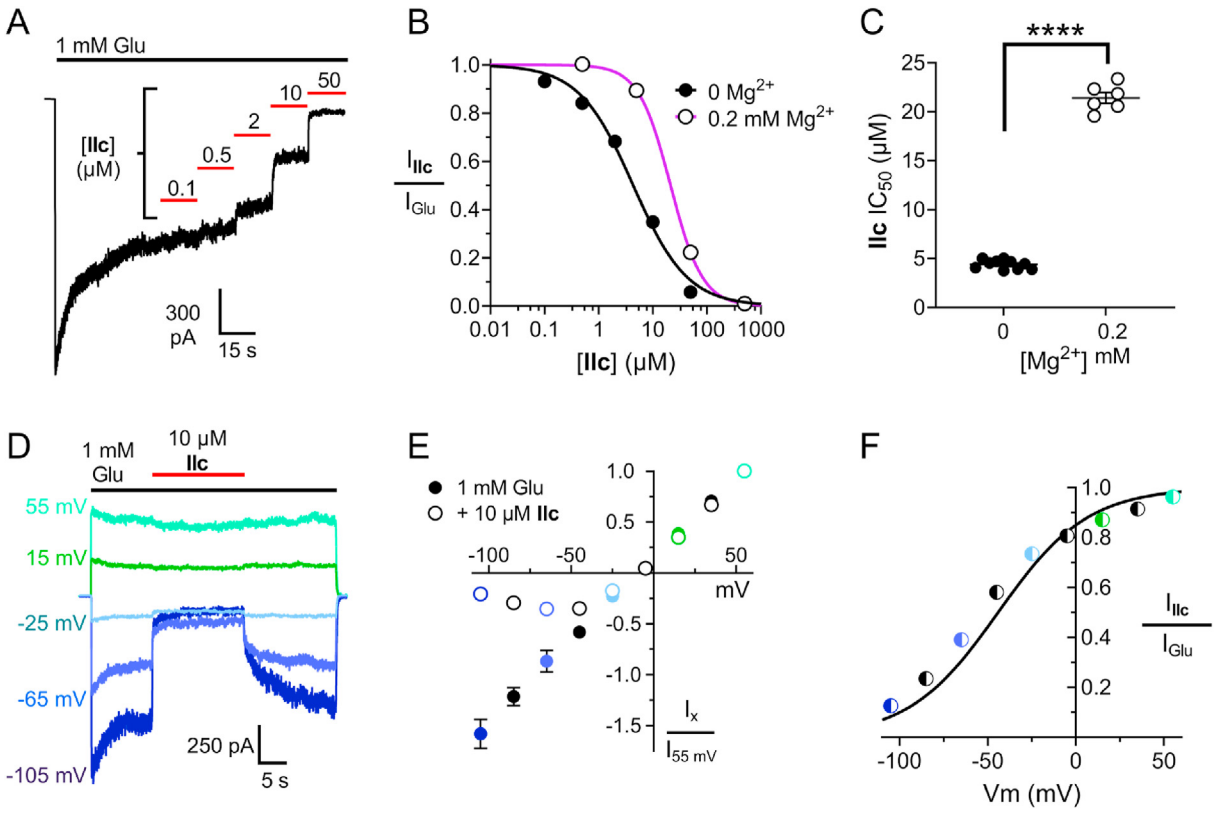

Fig. 5. Characteristics of GluN1/2A receptor channel block by IIc. **A.** Representative current trace from one cell depicting inhibition of GluN1/2A receptors by **IIc** at −65 mV. Current evoked by application of 1 mM glutamate (Glu; black bars) was reduced as concentration of **IIc** (red bars) increased. **B.** Concentration-inhibition relation for **IIc** in 0 Mg^{2+} (black line, filled symbols) and in 0.2 mM Mg^{2+} (purple line, open symbols). Symbols represent means, error bar are smaller than symbols. Lines show best fits of Equation (2) to data. **C.** Comparison of IC_{50} values in 0 and 0.2 mM Mg^{2+}. 0.2 mM Mg^{2+} greatly reduces **IIc** potency ($p < 0.0001$, two-sample Student t-test, $n = 10$ and 6, respectively). Data shown as individual values, line and error bars depict mean ± SEM. **D.** Representative current traces from one cell depicting the voltage dependence of inhibition by 10 μM **IIc**. For clarity, traces from only five of the tested membrane potentials are displayed. **E.** Current-voltage relation for GluN1/2A receptors in 1 mM Glu (filled symbols) and 1 mM Glu + 10 μM **IIc** (open symbols). Current at each voltage (I_X) was normalized to current at 55 mV (I_{55} mV) for each cell. Symbols represent means, error bars represent SEM; some error bars are smaller than symbols. **F.** Mean current-voltage relation data replotted as fractional current in the presence of 10 μM **IIc**. Solid line shows best fit of Equation (3) to estimate V_0 (25.43 ± 0.54 mV; $n = 7$). V_0 was subsequently used to calculate δ (1.01 ± 0.02; $n = 7$) with Equation (4). Error bars in F are smaller than symbols. Colored symbols in E and F correspond to example traces in D; black symbols represent measurements at voltages not shown in D.

blockers (e.g. V_0 ~ 26−30 mV, δ ~0.8−1.0 for memantine, ketamine, and recently synthesized polycyclic amines) [28,63,68,80,81]. The profound dependence of **IIc** inhibition on [Mg^{2+}] and on membrane potential strongly supports the conclusion that **IIc** inhibits NMDARs by binding in and blocking the NMDAR channel.

2.6. *In vitro DMPK profile, hERG safety and cytotoxicity of **IIc***

This compound was characterized in terms of microsomal stability (human and mouse species), hERG (human ether-a-go-go-related gene) inhibition, cytochrome P450 (CYP) inhibition, Caco-2 and predicted brain permeability (PAMPA-BBB assay), to confirm its suitability as a candidate for *in vivo* studies in *Caenorhabditis elegans* (*C. elegans*) and in the 5XFAD mouse model. Results from these measurements are given in Table 2.

IIc showed high metabolic stability in human and mice liver microsomes, which are widely used to determine the likely degree of primary metabolic clearance in the liver. Next, cytochrome P450 (CYP) inhibition was evaluated through a fluorescence-detection method using human recombinant cytochrome P450 enzymes CYP1A2, CYP2C19, CYP2C9, CYP2D6, and CYP3A4. Pleasantly, the compound did not significantly inhibit the evaluated cytochromes. hERG channel is an ion channel which is commonly used as an important toxicology screen because of its known association with cardiotoxicity. Interestingly, **IIc**, at 10 μM, did not significantly inhibit hERG. The Caco-2 cell permeability model was used to evaluate the permeability of the compound. Apparent permeability values (P_{app}) were determined from the amount permeated through the Caco-2 cell membranes in both apical-basolateral (A-B) and basolateral-apical (B-A) directions. Satisfactorily, **IIc** showed good permeability. Any AD drug should cross the blood-brain-barrier (BBB), so we used the PAMPA-BBB assay to predict the ability of **IIc** to permeate BBB. **IIc** had a positive predicted BBB permeability. Next, the cytotoxicity of **IIc** was tested using the MTT assay in Neuro2a cells. Interestingly, the selected compounds did not show cytotoxic at the highest concentration tested (100 μM) (see section 4.7. for further details).

Overall, **IIc** has low micromolar activity, an excellent electrophysiological profile as a NMDA receptor blocker, favorable DMPK properties, and non-cytotoxicity. Thus, **IIc** was deemed a suitable candidate for the *in vivo* studies [82].

2.7. *In vivo efficacy studies*

To evaluate the effectivity of **IIc** to ameliorate cognitive impairment through the modulation of NMDAR-mediated neurodegenerative pathways, we performed a series of *in vivo* studies in *C. elegans* and in the 5XFAD mouse model.

It has been reported that memory in *C. elegans* is mediated by NMDA-type ionotropic glutamate receptors [83]. This nematode

Table 2
Microsomal stability, cytochrome and hERG inhibition, Caco-2 and PAMPA-BBB of **IIc**.

Microsomal stability[a]		CYP inhibition[b]						hERG	Caco-2			PAMPA-BBB
								inhibition[b]	Papp (nm/s)[c]			
h	m	1A2	2C19	2C9	2D6	3A4[d]	3A4[e]		A - B	B - A	ER	
96	77	9 ± 2	21 ± 2	9 ± 3	15 ± 1	4 ± 2	10 ± 2	13 ± 1	310 ± 41	208 ± 12	0.7 ± 0.1	CNS+

[a] Percentage of remaining compound after 60 min of incubation with human (h) and mouse (m) microsomes in the presence of NADPH at 37 °C.
[b] Percentage of inhibition at 10 μM.
[c] The efflux ratio (ER) was calculated as ER = (Papp B→A)/(Papp A→B).
[d] Using benzyloxytrifluoromethylcoumarin (BFC) as substrate.
[e] Using dibenzylfluorescein (DBF) as substrate. See methods for further details.

expresses two NMDA-type subunits, NMR-1 and NMR-2, homologous to mammalian GluN1 and GluN2A subunits, respectively [84]. Thus, *C. elegans* has been described as a suitable model for the study of NMDAR-mediated neurotoxicity [85,86]. The 5XFAD mouse model, which displays altered NMDAR function [87], is one of the most used AD mouse models to evaluate pharmacological interventions [88].

Considering that **IIc** has proven to be a memantine analog in terms of potency and electrophysiological behavior, we incorporated memantine as a standard to analyze if these analogies persist in the *in vivo* efficacy studies. Of note, just a single study has been published on the effects of memantine in *C. elegans*, using the transgenic strain CL2006 [84], and only two studies have been published describing effects of memantine on 5XFAD mice [89,90].

2.7.1. Concentration-response effect of memantine and **IIc** on paralysis induced by Aβ expression in CL2006

The analysis of locomotor deficits has been traditionally used to discriminate between N2 wild-type (WT) and CL2006 mutant *C. elegans*. Herein, the N2 WT strain was used as a positive control and CL2006 worms, which constitutively expresses human $A\beta_{1\text{-}42}$, served as an AD model [91]. As expected, CL2006 worms presented paralysis (measured as defective locomotion) compared to N2 WT, which exhibited a significantly lower percentage of defective locomotion (Fig. 6A). After treatments, we found that memantine and **IIc** reduced defective locomotion over a range of concentrations (0.1–10 μM) in CL2006 nematodes (Fig. 6A–B). These initial results in nematodes showed the capability of **IIc**, as well as memantine, to rescue the motor deficits in an AD model.

2.7.2. Treatment with NMDAR channel blockers rescues chemotaxis behavior of CL2355 nematodes disrupted by Aβ expression

The impressive chemotaxis behavior of *C. elegans* is well known as a suitable model to evaluate the neuroprotective effects of new compounds. To evaluate the effect of NMDAR antagonists on the chemotaxis behavior of *C. elegans*, the transgenic strain CL2355, which shows Aβ aggregates as well as deficits in chemotaxis, and CL2122, a positive control strain, were used [91]. Therefore, we performed a chemotaxis assay as previously described [92]. As expected, CL2355 showed disrupted chemotaxis behavior and a reduced chemotaxis index (CI) in comparison to CL2122. Interestingly, both memantine and **IIc** treatments significantly reversed the disrupted chemotaxis behavior, suggesting that **IIc** might protect against Aβ toxicity-related neuronal dysfunction in a fashion similar to memantine (Fig. 6C).

2.7.3. NMDA channel blockers memantine and **IIc** rescue working memory impairment in 5XFAD

To determine the effects of the administration of memantine and **IIc** on AD-like symptoms, 5XFAD mice, a model of familial AD, were treated with either memantine or **IIc** at 5 mg/day for 4 weeks. A novel object recognition test (NORT) was used to evaluate short- and long-term working memories in 5XFAD mice. As described previously [88,93], 6-month-old 5XFAD mice presented robust cognitive deficits compared to WT (Fig. 7). We found that memantine treatment resulted in the recovery of cognitive function by increasing the discrimination index (DI) in both short-term (Fig. 7A) and long-term (Fig. 7B) memory tests. Importantly, **IIc** also enhanced working memory function in 5XFAD mice, with treated mice showing a significant DI increase at both tests (Fig. 7).

2.7.4. NMDAR molecular alterations in 5XFAD mouse model after **IIc** treatment

NMDARs are heterotetramers composed of two GluN1 subunits and typically two GluN2 subunits, of which there are four subtypes (GluN2A-D). In the adult forebrain, GluN2A and GluN2B are the two predominant subtypes. GluN2A subunits, incorporated into synaptic NMDARs, mediate long-term synaptic plasticity and their activation is associated with neuroprotective pathways. Therefore, selective activation of NMDARs containing GluN2A subunits would have a beneficial effect on AD pathology [94,95].

Western-blot analysis showed that 5XFAD mice exhibit less GluN2A protein levels than control mice, and interestingly, **IIc** treatment was able to rescue GluN2A to control levels (Fig. 8A–B).

Extrasynaptic NMDARs are enriched in GluN2B subunits and are believed to promote neuronal death, as occurring in neurodegenerative diseases. The activation of NDMARs containing the GluN2B subunit may be increased by Aβ, contributing to neurodegenerative and apoptotic pathways [96]. Memantine preferentially blocks extrasynaptic NMDARs over those located at the synaptic cleft, contributing to the clinical tolerability of this drug [21,97,98]. Additionally, GluN2B-subunit-containing NMDARs may induce synaptic NMDAR internalization after dephosphorylation, disrupting normal synaptic function [99]. Furthermore, phosphorylated Fyn kinase (p-Fyn) is responsible for phosphorylation of GluN2B at tyrosine 1472, which prevents GluN2B endocytosis and maintains NMDARs at the synaptic surface, preventing neuronal death [100]. To evaluate GluN2B subunit and Fyn kinase phosphorylation in control mice and the effects of memantine and **IIc** on 5XFAD mice, the p-GluN2B(Tyr1472)/GluN2B and p-Fyn/Fyn ratios (Figures 8A, 8C-D) were determined. Of note, we found that treatment of 5XFAD mice with memantine or **IIc** increased Fyn phosphorylated levels and correspondingly elevated GluN2B phosphorylation at Tyr1472. These findings support the literature relating GluN2B -subunit phosphorylation at Tyr1472 and the prevention of NMDAR internalization, which may prevent synaptic dysfunction [101,102].

2.7.5. **IIc** treatment modifies CREB pathways leading to synaptic improvements

Fyn activity is related to proteins implicated in cell-survival, such as cAMP response element binding protein (CREB) [103]. Therefore, we evaluated p-CREB protein levels in cytosol and nuclei.

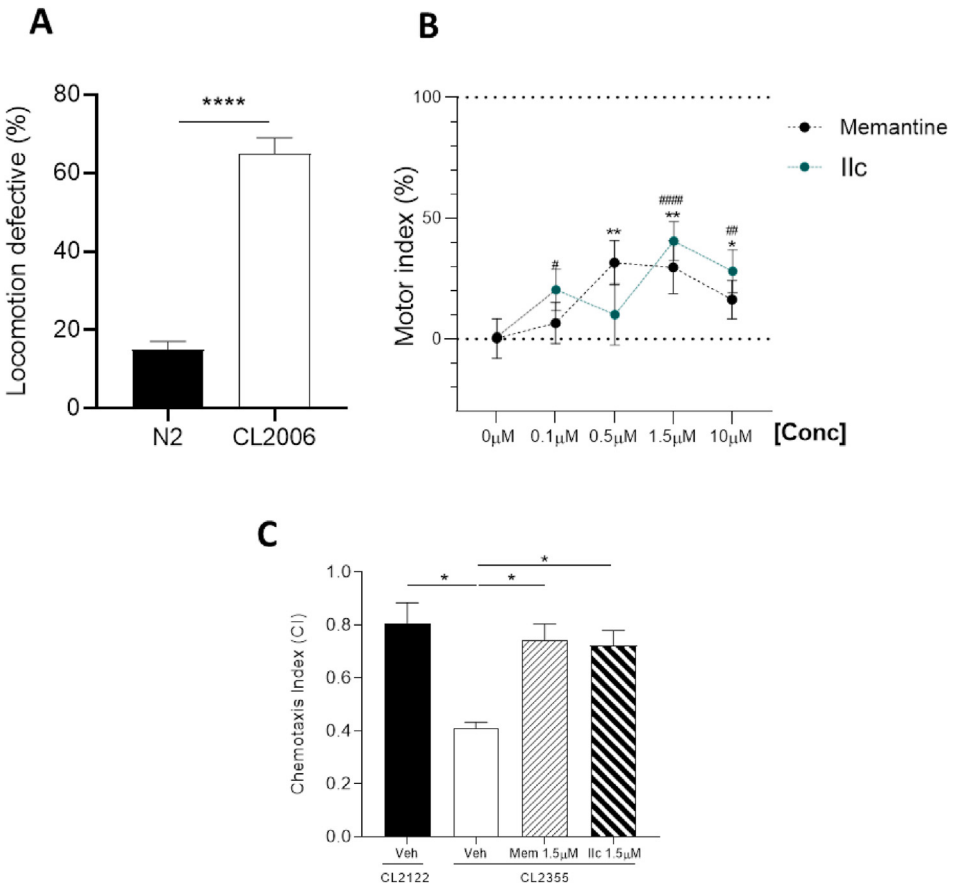

Fig. 6. A. Locomotion defective (%) of N2 WT *vs* CL2006 strains. **B**. Motor index (%) calculated in CL2006 worms treated with the indicated memantine or **IIc** concentrations. **C**. Chemotaxis index (CI) for CL2122 and CL2355 worms treated with vehicle (Veh), memantine (Mem) and **IIc**. Values are depicted as mean ± Standard error of the mean (SEM). ****p < 0.0001 for N2 *vs* CL2006; *p < 0.05, **p < 0.01 for memantine 0.5 μM, 1.5 μM and 10 μM *vs* memantine 0 μM; #p < 0.05, ##p < 0.01, ####p < 0.0001 for **IIc** 0.5 μM, 1.5 μM and 10 μM *vs* **IIc** 0 μM; *p < 0.05 for CL2355 Veh *vs* other groups.

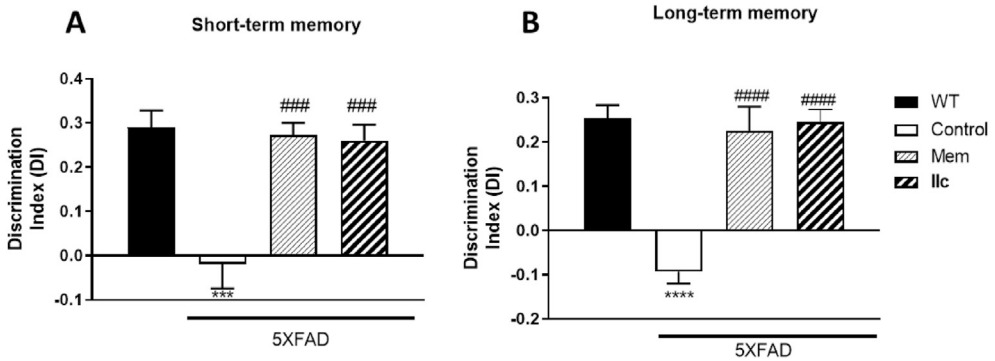

Fig. 7. A. Discrimination index (DI) calculated by using exploration time for novel and familiar object in the short-term (2 h) memory test. **B**. DI in the long-term memory test session (24 h). Values are the mean ± Standard error of the mean (SEM); (n = 14 for WT, n = 8 for 5XFAD control groups, n = 11 for memantine (Mem, 5 mg/kg) and n = 10 for **IIc** (5 mg/kg) groups). ***p < 0.001; ****p < 0.0001 for WT *vs* 5XFAD control. ###p < 0.001; ####p < 0.0001 for memantine (Mem, 5 mg/kg) or **IIc** (5 mg/kg) *vs* 5XFAD control.

p-CREB levels were found to be dysregulated in 5XFAD compared to WT. p-CREB protein in the nucleus was reduced in 5XFAD mice compared to the WT group, whereas treatment with memantine or **IIc** significantly increased p-CREB protein levels in the nucleus compared to untreated 5XFAD mice. The enhanced p-CREB translocation to the nucleus of the treated groups (Fig. 9A and B) indicated a beneficial effect of NMDAR antagonists by modulating signaling pathways involved in cell survival.

To further evaluate the effect of memantine and **IIc** on AD-related proteins, the calcium-dependent protein calbindin was evaluated. Calbindin D-28K is a Ca^{2+} binding protein and an important regulator of Ca^{2+} homeostasis found to be dysregulated in AD animal models [104]. Remarkably, we found a significant, unprecedented dysregulation of calbindin protein levels in 5XFAD mice (Fig. 9A and C), suggesting the important role of calbindin in the Aβ pathology presented by this transgenic mouse model. We also demonstrated that treatment with memantine or **IIc** reverts calbindin D-28K protein levels to WT levels (Fig. 9A and C).

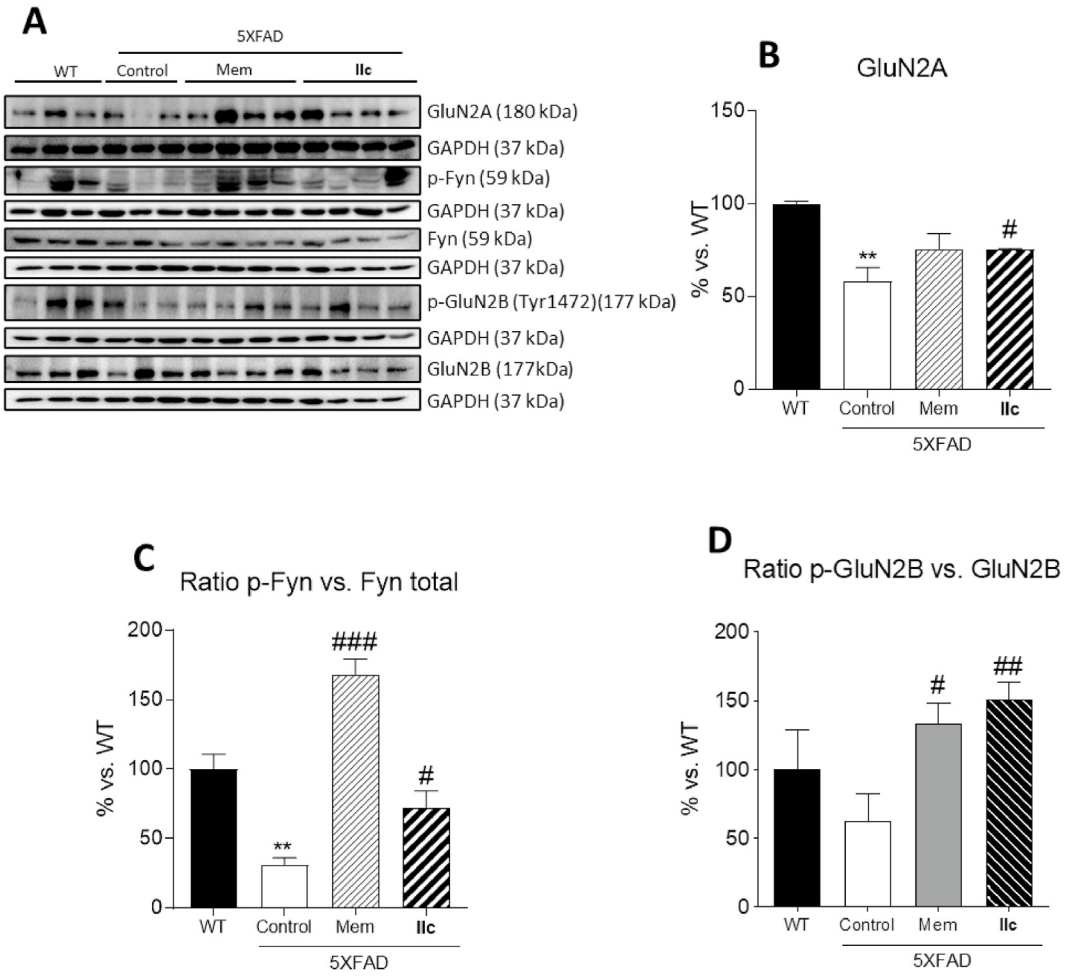

Fig. 8. A. Representative Western Blots and quantification. **B.** GluN2A. **C**. Ratio p-Fyn/Fyn. **D.** Ratio p-GluN2B (Tyr1472)/GluN2B. Values plotted in bar graphs are adjusted to 100% for protein levels of wild type (WT). Values are the mean ± Standard error of the mean (SEM); (n = 3 for WT and 5XFAD Control groups and n = 4 for memantine (Mem, 5 mg/kg) and **IIc** (5 mg/kg) groups. **p < 0.01 for WT *vs* 5XFAD Control. #p < 0.05; ##p < 0.01; ###p < 0.001 for memantine (Mem, 5 mg/kg) or **IIc** (5 mg/kg) *vs* 5XFAD Control.

It is noteworthy that p-CREB is a transcription factor that increases the expression of several proteins implicated in neuroprotection and neuronal signaling [105]. Interestingly, we found that treatment with memantine or **IIc** rescues expression of postsynaptic density protein (PSD) 95 in 5XFAD mice (Fig. 9D). Together, these data may explain the improvement in working memory observed in 5XFAD after treatment with NMDAR channel blockers.

Overall, we provide promising evidence that **IIc** treatment rescues Fyn-GluN2B-CREB signaling and PSD95 expression in 5XFAD mice. Our results suggest a mechanism by which **IIc** may improve cell survival and synaptic function in AD through increasing the activity of cell-survival signaling pathways and preventing internalization of synaptic NMDARs. Thus, **IIc** could be a feasible candidate for further testing as a new clinically therapeutic NMDAR channel blocker.

3. Conclusions

Despite scientific efforts to develop new clinically useful NMDAR blockers, memantine remains the only noncholinergic drug approved for symptomatic AD treatment. Therefore, we further explored the benzohomoadamantane scaffold with the main aim to develop new memantine analogs. Although most of the changes in the chemical structure of benzohomoadamantane negatively impact potency at NMDARs, **2**, **IIa** and **IIc** showed low micromolar potencies. Furthermore, these results were rationalized and strongly supported by MD simulations. Subsequently, of the most active derivatives, **IIc** was found to possess electrophysiological characteristics similar to memantine, including similar potencies, voltage dependencies, and blocking sites. Additionally, our DMPK studies (microsomal stability, cytochrome and hERG inhibition, Caco-2 and PAMPA assays) revealed that **IIc** was a good candidate for *in vivo* studies. The administration of **IIc** to both *C. elegans* and the 5XFAD mouse model of AD reverted the condition of the animals to that of controls, both at the behavioral and the biochemical levels. The effect observed was comparable with that produced by memantine, demonstrating that **IIc** could be a feasible and promising candidate for a new clinically therapeutic NMDAR blocker.

4. Experimental part

4.1. Chemistry. General methods

Commercially available reagents and solvents were used without further purification unless stated otherwise. Preparative normal phase chromatography was performed on a CombiFlash Rf 150 (Teledyne Isco) with pre-packed RediSep Rf silica gel cartridges. Thin-layer chromatography was performed with aluminum-backed sheets with silica gel 60 F254 (Merck, ref 1.05554), and spots were visualized with UV light and 1% aqueous solution of $KMnO_4$.

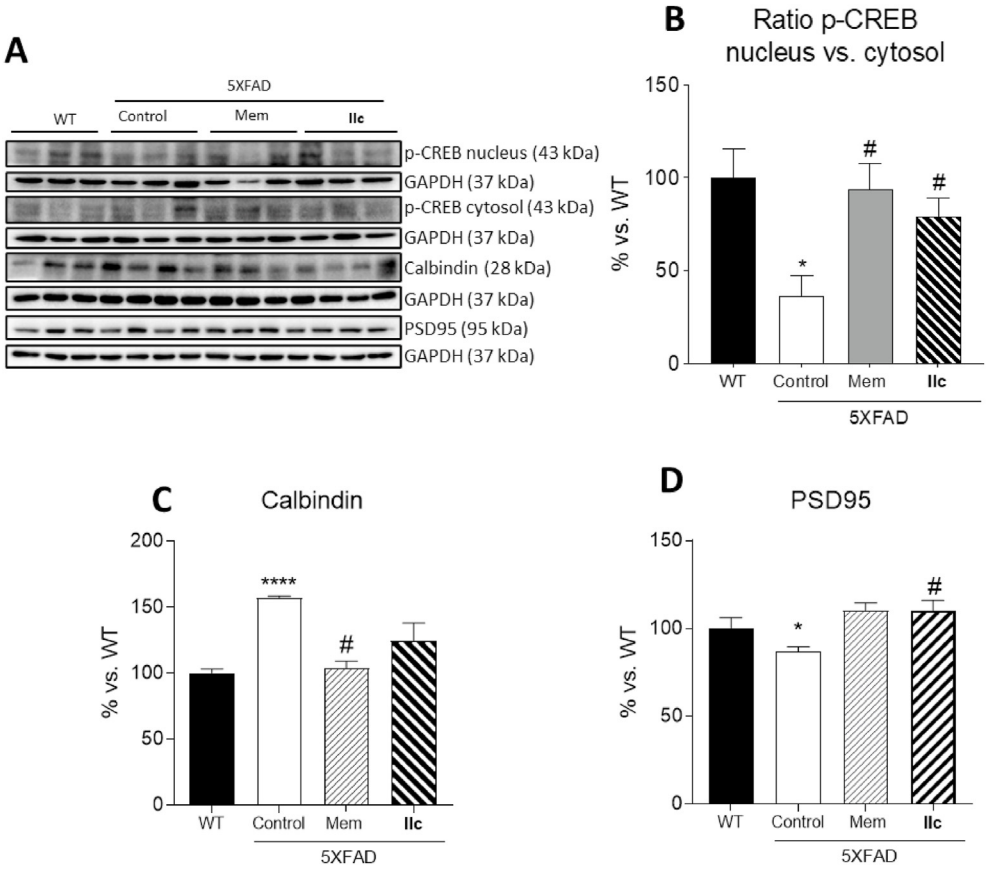

Fig. 9. A. Representative Western Blot and quantifications for **B**. Ratio of p-CREB in the nucleus *vs* in the cytosol **C**. Calbindin **D**. PSD95. Values in bar graphs are adjusted to 100% for protein levels of the wild type (WT). Values are the mean ± Standard error of the mean (SEM); (n = 3 for WT and 5XFAD Control groups and n = 4 for memantine (Mem, 5 mg/kg) and **IIc** (5 mg/kg) groups. *p < 0.05; ****p < 0.0001 for WT *vs* 5XFAD Control. #p < 0.05; ##p < 0.01 for memantine (Mem, 5 mg/kg) or **IIc** (5 mg/kg) *vs* 5XFAD Control.

Melting points were determined in open capillary tubes with a MFB 595010 M Gallenkamp. 400 MHz ^{1}H and 100.6 MHz ^{13}C NMR spectra were recorded on a Varian Mercury 400 or on a Bruker 400 Avance III spectrometers. The chemical shifts are reported in ppm (δ scale) relative to internal tetramethylsilane, and coupling constants are reported in Hertz (Hz). Assignments given for the NMR spectra of selected new compounds have been carried out on the basis of COSY $^{1}H/^{13}C$ (gHSQC) experiments. IR spectra were run on Perkin-Elmer Spectrum RX I, Perkin-Elmer Spectrum TWO or Nicolet Avatar 320 FT-IR spectrophotometers. Absorption values are expressed as wavenumbers (cm^{-1}); only significant absorption bands are given. High-resolution mass spectrometry (HRMS) analyses were performed with an LC/MSD TOF Agilent Technologies spectrometer. The elemental analyses were carried out in a Flash 1112 series Thermofinnigan elemental microanalyzator (A5) to determine C, H, N. HPLC/MS were determined with a HPLC Agilent 1260 Infinity II LC/MSD coupled to a photodiode array and mass spectrometer. 5 μL of sample 0.5 mg/mL in methanol: acetonitrile were injected, using an Agilent Poroshell 120 EC-C18, 2.7 μm, 50 mm × 4.6 mm column at 40 °C. The mobile phase was a mixture of A = water with 0.05% formic acid and B = acetonitrile with 0.05% formic acid, with the method described as follows: flow 0.6 mL/min, 5% B-95% A 3 min, 100% B 4 min, 95% B-5% A 1 min. Purity is given as % of absorbance at 210 or 275 nm. The structure of all new compounds was confirmed by elemental analysis and/or accurate mass measurement, IR, ^{1}H NMR and ^{13}C NMR. The analytical samples of all the new compounds, which were subjected to pharmacological evaluation, possessed purity >95% as evidenced by their elemental analyses or HPLC-UV.

*4.1.1. 5,6,8,9,10,11-Hexahydro-7H-5,9:7,11-dimethanobenzo[9]annulen-9-d-7-amine (**2**)*

a) 9-bromo-6,7,8,9,10,11-hexahydro-9-methyl-5,7:9,11-dimethano-*5H*-benzocyclononen-7-amine hydrochloride. Thionyl bromide (6.5 mL, δ = 2.68, 83.8 mmol) was added to a solution of amine **1** (500 mg, 2.81 mmol) in toluene (17 mL) containing a few drops of DMF. The resulting red solution was stirred at rt for 1.5 h. The reaction mixture was concentrated to dryness *in vacuo*. Toluene (50 mL) was added, and the resulting solution concentrated *in vacuo*. The procedure was repeated five times more until an orange solid was obtained. The crude was partitioned between DCM (15 mL) and saturated aq $NaHCO_3$ solution (15 mL) and the phases were separated. The aq layer was extracted with further dichloromethane (100 mL) and the combined organic extracts were dried over anh Na_2SO_4, filtered and concentrated *in vacuo* to give a colourless oil (530 mg, 83% yield) that was used in the next step without further purification.

b) 5,6,8,9,10,11-hexahydro-7*H*-5,9:7,11-dimethanobenzo[9]annulen-9-*d*-7-amine. To a suspension of 9-bromo-6,7,8,9,10,11-hexahydro-9-methyl-5,7:9,11-dimethano-5*H*-benzocyclononen-7-amine hydrochloride (prepared from the addition of an excess of HCl/Et_2O to the compound) (250 mg, 0.76 mmol) in anh and deoxygenated toluene (3 mL) under Ar atmosphere were added tributylstannane-*d* (372 μL, 1.37 mmol) and AIBN (16 mg, 0.10 mmol). The resulting solution was heated to 95 °C for 4 h adding more AIBN (16 mg, 0.10 mmol) each 60 min. Saturated aq Na_2CO_3 solution was added until pH = 12 and then

the aq layer was extracted with 10% MeOH/EtOAc (3 × 15 mL). All organic layers were joined, dried over anh Na_2SO_4, filtered and concentrated *in vacuo*. The resulting crude was purified by Biotage® purification system in silica gel using a MeOH/NH_3 0.7 M in DCM mixture (0.4/9.6) to obtain **2** as a pale-yellow solid (100 mg, 61% yield). Its hydrochloride was obtained by adding an excess of HCl/Et_2O in DCM, followed by filtration of the resulting white precipitate. mp 72–73 °C. IR (ATR) ν: 2906, 2838, 1653, 1560, 1490, 1439, 1352, 1115, 1047, 990, 933, 914, 874, 826, 755, 702, 610 cm^{-1}. ^1H NMR (400 MHz, CD_3OD) δ: 1.66–1.72 [complex signal, 6H, 6(12)-H_a, 10(13)-H_a and 8-H_2], 1.85 [m, 2H, 6(12)-H_b], 1.92 [dd, J = 12.8 Hz, J' = 6.0 Hz, 2H, 10(13)-H_b], 3.03 [tt, J = 6.0, J' = 1.5 Hz, 2H, 5(11)-H], 7.02 (br s, 4H, Ar–H). ^{13}C NMR (100.6 MHz, CD_3OD) δ: 32.7 (t, $J_{C\text{-}D}$ = 20.0 Hz, C9), 35.4 [CH_2, C10(13)], 42.9 [CH, C5(11)], 44.1 [CH_2, C6(12)], 45.0 (CH_2, C8), 48.8 (C, C7), 127.3 [CH, C2(C3)], 129.0 [CH, C1(C4)], 148.0 [C, C4a(C11a)]. HRMS-ESI + *m/z* $[M+H]^+$ calcd for $[C_{15}H_{19}DN]^+$: 215.1658, found: 215.1653.

4.1.2. 7-Iodo-5,6,7,8,9,10-hexahydro-5,8:7,10-dimethanobenzo[8]annulene (**4**)

a) 5,8,9,10-tetrahydro-5,8:7,10-dimethanobenzo[8]annulen-7(*6H*)-yl methanesulfonate. To a solution of 5,8,9,10-tetrahydro-5,8:7,10-dimethanobenzo[8]annulen-7(*6H*)-ol (1.19 g, 5.40 mmol) in pyridine (9 mL), methanesulfonyl chloride (2.32 mL, δ = 1.48, 29.9 mmol) was added slowly with stirring at rt. The mixture was then heated at 120 °C for 5 h. After cooling, crushed ice (100 g) was added and the mixture was extracted with DCM (5 × 40 mL). The combined organic phase was washed with 2 N HCl solution (2 × 40 mL), H_2O (2 × 40 mL), saturated aq $NaHCO_3$ solution (2 × 40 mL) and dried over anh Na_2SO_4. The crude mesylate was obtained after filtration and removal of the solvent under reduced pressure as a dark oil that was used in the next step without further purification (1.32 g, 80% yield). HRMS-ESI + *m/z* $[M+H]^+$ calcd for $[C_{15}H_{18}O_3S + NH_4]^+$: 296.1315, found: 296.1318.

b) 7-iodo-5,6,7,8,9,10-hexahydro-5,8:7,10-dimethanobenzo[8]annulene. In an RBF equipped with a reflux condenser, H_3PO_3 (99%, 135 g), mesylate (1.32 g, 4.75 mmol) and NaI (63 g, 42.0 mmol) were added. The mixture was stirred at 150 °C for 6 h. After cooling, H_2O (150 mL) was added slowly to the mixture. The resulting red solution was extracted with DCM (4 × 80 mL) and the combined organic phase was washed with saturated aq sodium thiosulfate solution (1 × 100 mL), dried over anh Na_2SO_4, then filtered and concentrated under vacuum to give **4** as a white solid (1.39 g, 95% yield). mp 132–133 °C (dec.). IR (NaCl disk) ν: 3052, 3013, 2950, 2892, 2852, 1490, 1447, 1304, 1278, 1232, 1215, 1095, 1046, 1032, 967, 830, 778, 755 cm^{-1}. ^1H NMR (400 MHz, $CDCl_3$) δ: 1.59 [dd, J = 12.4 Hz, J' = 2.4 Hz, 2H, 9(12)-H_a], 2.01 [dd, J = 11.6 Hz, J' = 2.4 Hz, 2H, 6(11)-H_a], 2.24 [m, 2H, 6(11)-H_b], 2.39 [m, 2H, 9(12)-H_b], 2.55 (t, J = 8.8 Hz, 1H, 8-H), 3.23 [t, J = 6.0 Hz, 2H, 5(10)-H], 7.08 [m, 2H, 1(4)-H or 2(3)-H], 7.13 [m, 2H, 2(3)-H or 1(4)-H]. ^{13}C NMR (100.6 MHz, $CDCl_3$) δ: 42.8 [CH_2, C9(12)], 48.3 [CH, C5(10)], 49.6 (CH, C8), 51.0 [CH_2, C6(11)], 90.5 (C, C7), 126.2 [CH, C1(4) or C2(3)], 129.5 [CH, C2(3) or C1(4)], 145.3 [C, C4a(10a)]. GC-MS (EI), t_r = 17.8 min: 310 [$(M)^{\cdot+}$, 2], 183 [$(M-I)^+$, 100], 141 (73), 129 (23), 128 (15).

4.1.3. 5,8,9,10-Tetrahydro-5,8:7,10-dimethanobenzo[8]annulene-7(6H)-carboxylic acid (**5**)

To a solution of 7-iodo-5,6,7,8,9,10-hexahydro-5,8:7,10-dimethanobenzo[8]annulene (2.03 g, 6.54 mmol) in dry and degassed toluene (20 mL), methyl oxalyl chloride (1.8 mL, δ = 1.33, 19.5 mmol) and bis(tributyltin) (4.55 g, 7.85 mmol) were added. The mixture was irradiated in a quartz reactor under argon atmosphere with a 125 W Hg lamp for 20 h. Then, DCM (15 mL), methanol (0.6 mL) and triethylamine (1.2 mL) were successively added to the reaction mixture at 0 °C and it was concentrated under vacuum to give a dark oil (3.99 g). A solution of this oil in a 40% methanol solution of KOH (50 mL) was heated to reflux for 2 h. H_2O (50 mL) was added, and the reaction was refluxed for 3 h. The reaction mixture was allowed to cool to rt and the methanol was removed under vacuum. H_2O (40 mL) was added to the residue and the aq layer was washed with DCM (4 × 50 mL). After that, the aq phase was acidified with conc. HCl until pH = 1 and extracted with DCM (4 × 50 mL). The organic extracts were dried over anh Na_2SO_4, filtered and concentrated under reduced pressure to give the acid as a brown solid (555 mg, 37% overall yield). An analytical sample of the acid was obtained by crystallization from DCM/Pentane, mp 188–189 °C. IR (NaCl disk) ν: 3300–2800 (3065, 3011, 2946, 2858), 1690, 1488, 1450, 1410, 1318, 1290, 1231, 1218, 1092, 1052, 1038, 941 cm^{-1}. ^1H NMR (400 MHz, $CDCl_3$) δ: 1.71 [dd, J = 12.8 Hz, J' = 2.4 Hz, 2H, 9(12)-H_a], 1.89 [dd, J = 12.4 Hz, J' = 2.4 Hz, 2H, 6(11)-H_a], 2.23 [m, 2H, 9(12)-H_b], 2.57 [dm, J = 12.4 Hz, 2H, 6(11)-H_b], 3.20 (t, J = 8.8 Hz, 1H, 8-H), 3.27 [t, J = 6 Hz, 2H, 5(10)-H], 7.08 [m, 2H, 1(4)-H or 2(3)-H], 7.15 [m, 2H, 2(3)-H or 1(4)-H]. ^{13}C NMR (100.6 MHz, $CDCl_3$) δ: 43.3 [CH_2, C9(12)], 46.4 [CH_2, C6(11)], 49.4 [CH, C5(10)], 49.9 (CH, C8), 59.9 (C, C7), 126.2 [CH, C1(4) or C2(3)], 129.5 [CH, C2(3) or C1(4)], 145.4 [C, C4a(10a)], 184.1 (C, C7–COOH). HRMS-ESI + *m/z* $[M-H]^-$ calcd for $[C_{15}H_{15}O_2]^-$: 227.1078, found: 227.1078.

4.1.4. 5,8,9,10-Tetrahydro-5,8:7,10-dimethanobenzo[8]annulen-7(6H)-amine hydrochloride (**6**)

To a solution of 5,8,9,10-tetrahydro-5,8:7,10-dimethano-benzo[8]annulene-7(*6H*)-carboxylic acid (90 mg, 0.39 mmol) in toluene (1.2 mL), Et_3N (73 μL, 0.53 mmol) and diphenylphosphoryl azide (159 mg, 0.58 mmol) were added and the mixture was heated at reflux for 3 h. The mixture was cooled and washed with 1 N HCl solution (2 × 10 mL). Thereafter, to the organic layer was added 6 N HCl solution (1.6 mL) and the suspension was heated at reflux for 24 h. The reaction mixture was then cooled to rt and the two phases were separated. The aq phase was extracted with ethyl acetate (3 × 3 mL). The combined organic phases were washed with 5 N NaOH solution (3 × 10 mL), dried over anh Na_2SO_4, filtered and concentrated under vacuum to give **6**. Its hydrochloride was obtained by adding an excess of HCl/methanol to a solution of the amine in methanol. The methanol was removed under reduced pressure yielding **6** as a brown solid (35 mg, 38% yield). An analytical sample was obtained by crystallization from MeOH/Et_2O, mp > 250 °C. IR (KBr disk) ν: 3100–2500 (2943, 2881, 2665), 2043, 1622, 1598, 1501, 1448, 1336, 1246, 1175, 1089, 1057, 1028, 952, 769, 749, 614 cm^{-1}. ^1H NMR (400 MHz, MeOD) δ: 1.67 [dd, J = 12.4 Hz, J' = 2.4 Hz, 2H, 9(12)-H_a], 2.02 [dd, J = 12.0 Hz, J' = 2.4 Hz, 2H, 6(11)-H_a], 2.30 [m, 2H, 6(11)-H_b], 2.42 [m, 2H, 9(12)-H_b], 2.80 (t, J = 8.8 Hz, 1H, 8-H), 3.33 [t, J = 6.0 Hz, 2H, 5(10)-H], 7.08 [m, 2H, 1(4)-H or 2(3)-H], 7.15 [m, 2H, 2(3)-H or 1(4)-H]. ^{13}C NMR (100.6 MHz, MeOD) δ: 43.4 [CH_2, C9(12)], 48.2 [CH_2, C6(11)], 49.1 (CH, C8), 49.4 [CH, C5(10)], 70.6 (C, C7), 127.6 [CH, C1(4) or C2(3)], 130.5 [CH, C2(3) or C1(4)], 145.3 [C, C4a(10a)]. HRMS-ESI + *m/z* $[M+H]^+$ calcd for $[C_{14}H_{18}N]^+$: 200.1434, found: 200.1432.

4.1.5. 2-Chloro-N-(9-methyl-2-nitro-5,6,8,9,10,11-hexahydro-7H-5,9:7,11-dimethanobenzo[9]annulen-7-yl)acetamide (**8**)

To a cold (0 °C) solution of chloroacetamide **7** (3.0 g, 9.87 mmol) in acetic anhydride (10 mL), glacial acetic acid (1.6 mL) and fuming nitric acid (1.9 mL) were carefully added. The mixture was allowed

to reach rt and left stirring overnight. The obtained yellow solution was then poured into ice–water (20 mL) and extracted with DCM (3 × 40 mL). The combined organic extracts were washed with 2 N NaOH solution (1 × 40 mL), H_2O (1 × 40 mL) and brine (1 × 40 mL). The organic layer was dried over anh Na_2SO_4, filtered and concentrated under vacuum to give a yellow residue. Purification by Combiflash® in silica gel using as eluent a gradient from hexane to ethyl acetate/hexane mixture (1/9) gave **8** as a white solid (2.92 g, 85% yield), mp 174–176 °C. IR (ATR) ν: 3269, 3233, 3080, 2951, 2922, 2903, 2846, 1670, 1563, 1518, 1460, 1405, 1362, 1346, 1336, 1303, 1279, 1226, 1166, 1138, 1083, 884, 839, 794, 739, 708, 667 cm^{-1}. ^1H NMR (400 MHz, $CDCl_3$) δ: 0.96 (s, 3H, 9-CH_3), 1.50–1.58 [complex signal, 2H, 10(13)-H_a], 1.67–1.76 [complex signal, 2 H, 10(13)-H_b], 1.81 (dm, J = 12.0 Hz, 1H, 8-H_a), 1.87 (dm, J = 12.0 Hz, 1H, 8-H_b), 2.10–2.23 [complex signal, 4H, 6(12)-H_2], 3.19–3.25 [complex signal, 2H, 5(11)-H], 3.93 (s, 2H, CH_2Cl), 6.34 (broad s., 1H, NH), 7.21 (d, J = 8.8 Hz, 1 H, 4-H), 7.94 (dd, J = 8.8 Hz, J' = 2.4 Hz, 1 H, 3-H), 7.95 (d, J = 2.4 Hz, 1H, 1-H). ^{13}C NMR (100.6 MHz, $CDCl_3$) δ: 32.1 (CH_3, C9–$\underline{C}H_3$), 33.8 (C, C9), 38.0 (CH_2) and 38.3 (CH_2) (C6 and C12), 40.5 (CH_2) and 40.7 (CH_2) (C10 and C13), 40.88 (CH) and 40.90 (CH) (C5 and C11), 43.0 (CH_2, CH_2Cl), 46.9 (CH_2, C8), 54.6 (C, C7), 121.9 (CH) and 123.1 (CH) (C1 and C3), 129.2 (CH, C4), 146.6 (C, C11a), 147.6 (C, C2), 153.8 (C, C4a), 164.9 (C, CO). HRMS-ESI + m/z $[M+H]^+$ calcd for $[C_{18}H_{22}ClN_2O_3]^+$: 349.1313, found: 349.1313.

4.1.6. 9-Methyl-2-nitro-5,6,8,9,10,11-hexahydro-7H-5,9:7,11-dimethanobenzo[9]annulen-7-amine hydrochloride (**9**)

Thiourea (177 mg, 2.33 mmol) and glacial acetic acid (1 mL) were added to a solution of chloroacetamide **8** (677 mg, 1.94 mmol) in abs. ethanol (33 mL) and the mixture was heated at reflux overnight. The resulting suspension was then tempered to rt, H_2O (20 mL) was added and the pH adjusted to 12 with 5 N NaOH solution. DCM (40 mL) was added, the phases were separated, and the aqueous phase was extracted with further DCM (2 × 40 mL). The combined organic layers were dried over anh Na_2SO_4, then filtered and concentrated *in vacuo* to give **9** as a light brown solid. Its hydrochloride was obtained by adding an excess of HCl/Et_2O to a solution of the amine in ethyl acetate, followed by filtration of the resulting white precipitate (443 mg, 74% yield), mp > 225 °C (dec). IR (ATR) ν: 3381, 3100–2800 (2997, 2927, 2856), 2065, 1613, 1520, 1486, 1350, 1329, 1305, 1286, 1138, 1033, 896, 837, 801, 762, 736 cm^{-1}. ^1H NMR (400 MHz, MeOD) δ: 1.02 (s, 3H, CH_3), 1.55–1.63 [complex signal, 2H, 10(13)-H_a], 1.71–1.75 (complex signal, 1H, 8-H_2), 1.73–1.81 [complex signal, 2 H, 10(13)-H_b], 1.85–1.94 [complex signal, 2H, 6(12)-H_a), 2.07–2.14 [complex signal, 2H, 6(12)-H_b], 3.36–3.42 [complex signal, 2H, 5(11)-H], 7.37 (d, J = 8.4 Hz, 1H, 4-H), 7.99 (dd, J = 8.2 Hz, J' = 2.4 Hz, 1H, 3-H), 8.02 (d, J = 2.4 Hz, 1H, 1-H). ^{13}C NMR (100.6 MHz, MeOD) δ: 32.0 (CH_3, C9–$\underline{C}H_3$), 34.7 (C, C9), 38.5 (CH_2) and 38.7 (CH_2) (C6 and C12), 40.8 (CH_2) and 41.0 (CH_2) (C10 and C13), 41.3 (CH) and 41.4 (CH) (C5 and C11), 46.8 (CH_2, C8), 55.2 (C, C7), 123.0 (CH, C3), 124.0 (CH, C1), 130.6 (CH, C4), 148.1 (C, C11a), 148.3 (C, C2), 154.2 (C, C4a). HRMS-ESI+ m/z $[M+H]^+$ calcd for $[C_{16}H_{21}N_2O_2]^+$: 273.1598, found: 273.1604.

4.1.7. 9-Methyl-5,6,8,9,10,11-hexahydro-7H-5,9:7,11-dimethanobenzo[9]annulene-2,7-diamine dihydrochloride (**10**)

To a solution of amine **9·HCl** (200 mg, 0.65 mmol) in methanol (25 mL), Pd on charcoal (20 mg, ca. 10% Pd) was added and the resulting suspension was hydrogenated at 1 atm of H_2 at rt for 48 h. The black suspension was filtered, and the solvent removed by concentration *in vacuo* to give **10** as a brown solid. Its hydrochloride was obtained by addition of an excess of HCl/MeOH to a solution of the amine in methanol followed by evaporation to obtain a brown solid (204 mg, quant. yield), mp 294–295 °C. IR (KBr disk) ν: 3200–2500 (3024, 2912, 2847, 2588), 1994, 1598, 1502, 1454, 1381, 1365, 1303, 1261, 1173, 1131, 1021, 957, 877, 827, 576, 473 cm^{-1}. ^1H NMR (400 MHz, MeOD) δ: 1.01 (s, 3H, CH_3), 1.50–1.60 [complex signal, 2H, 10(13)-H_a], 1.68–1.80 [complex signal, 2H, 10(13)-H_b], 1.72 (broad s., 2H, 8-H_2), 1.84–1.94 (complex signal, 2H, 6-H_a, 12-H_a), 2.03–2.14 (complex signal, 2H, 6-H_b, 12-H_b), 3.26–3.29 [complex signal, 5(11)-H], 7.16 (m, 1H, 3-H), 7.18 (d, J = 2.0 Hz, 1H, 1-H), 7.29 (m, 1H, 4-H). ^{13}C NMR (100.6 MHz, MeOD) δ: 32.1 (CH_3, C9–$\underline{C}H_3$), 34.7 (C, C9), 38.7 (CH_2) and 38.8 (CH_2) (C6 and C12), 41.1 (CH_2) and 41.15 (CH_2) (C10 and C13), 41.21 (CH_2) and 41.4 (CH_2) (C5 and C11), 46.8 (CH_2, C8), 55.3 (C, C7), 122.2 (CH) and 123.7 (CH) (C1 and C3), 130.4 (C, C4a), 131.1 (CH, C4), 147.1 (C) and 148.9 (C) (C2 and C11a). HRMS-ESI + m/z $[M+H]^+$ calcd for $[C_{16}H_{23}N_2]^+$: 243.1856, found: 243.1856.

4.1.8. N-(2-acetyl-9-methyl-5,6,8,9,10,11-hexahydro-7H-5,9:7,11-dimethanobenzo[9]annulen-7-yl)-2-chloroacetamide (**11**)

A solution of **7** (557 mg, 1.83 mmol) and acetyl chloride (1.31 mL, 18.4 mmol) were dissolved in DCM (14 mL) and treated with aluminium trichloride (1.22 g, 9.15 mmol). The resulting black mixture was stirred for 60 min then poured over a mixture of ice and saturated aq Na_2CO_3 solution (10 mL). After stirring 20 min the mixture was extracted with DCM (3 × 30 ml). The organic layer was dried over anh Na_2SO_4, filtered and concentrated *in vacuo* to give a yellow solid. Purification by Combiflash® in silica gel using as eluent a gradient from hexane to ethyl acetate/hexane mixture (2/8) gave **11** as a white solid (340 mg, 54% yield), mp 186–187 °C. IR (ATR) ν: 3276, 3083, 2959, 2916, 2845, 1670, 1603, 1562, 1456, 1419, 1405, 1364, 1336, 1281, 1271, 1249, 1238, 1228, 1166, 1108, 1051, 1013, 966, 948, 842, 795, 704, 689, 643 cm^{-1}. ^1H NMR (400 MHz, $CDCl_3$) δ: 0.95 (s, 3H, CH_3), 1.50–1.58 [complex signal, 2H, 10(13)-H_a], 1.66–1.74 [complex signal, 2H, 10(13)-H_b], 1.82 (dm, J = 12.0 Hz, 1H, 8-H_a), 1.87 (dm, J = 12.0 Hz, 1H, 8-H_b), 2.08–2.22 [complex signal, 4H, 6(12)-H_2], 2.57 (s, 3H, $COCH_3$), 3.13–3.23 [complex signal, 2H, 5-(11)-H], 3.92 (s, 2H, CH_2Cl), 6.32 (broad s., 1H, NH), 7.15 (d, J = 7.8 Hz, 1H, 4-H), 7.67 (m, 1H, 3-H), 7.69 (d, J = 1.6 Hz, 1H, 1-H). ^{13}C NMR (100.6 MHz, $CDCl_3$) δ: 26.7 (CH_3, $\underline{C}H_3CO$), 32.2 (CH_3, C9–$\underline{C}H_3$), 33.8 (C, C9), 38.3 (CH_2) and 38.6 (CH_2) (C6 and C12), 40.8 (CH_2) and 40.97 (CH_2) (C10 and C13), 41.0 (CH) (C5 and C11), 43.1 (CH_2, $\underline{C}H_2Cl$), 46.9 (CH_2, C8), 54.8 (C, C7), 127.1 (CH, C1), 128.0 (CH, C3), 128.6 (CH, C4), 135.7 (C) and 146.5 (C) (C2 and C11a), 151.9 (C, C4a), 164.8 (C, NHCO), 198.1 (C, $\underline{C}OCH_3$). HRMS-ESI + m/z $[M+H]^+$ calcd for $[C_{20}H_{25}ClNO_2]^+$: 346.1568, found: 346.1570.

4.1.9. 1-(7-Amino-9-methyl-6,7,8,9,10,11-hexahydro-5H-5,9:7,11-dimethanobenzo[9]annulen-2-yl)ethan-1-one hydrochloride (**12**)

Thiourea (233 mg, 3.06 mmol) and glacial acetic acid (1.6 mL) were added to a solution of chloroacetamide **11** (845 mg, 2.44 mmol) in abs. ethanol (42 mL) and the mixture was heated at reflux overnight. The resulting suspension was then tempered to rt, then H_2O (20 mL) was added and the pH was adjusted to 12 with 5 N NaOH solution. DCM (40 mL) was added, the phases were separated, and the aq phase was extracted with further dichloromethane (2 × 40 mL). The combined organic layers were dried over anh Na_2SO_4, filtered and concentrated *in vacuo* to give a light brown solid. Purification by Combiflash® in silica gel using as eluent a gradient from hexane to ethyl acetate/hexane mixture (3/7) gave **12** as a white solid. Its hydrochloride was obtained by adding an excess of HCl/Et_2O to a solution of the amine in ethyl acetate, followed by filtration of the resulting white precipitate (385 mg, 52% yield), mp > 200 °C (dec.). IR (ATR) ν: 3000–2400 (2988, 2904, 2858), 1678, 1603, 1508, 1451, 1428, 1362, 1272, 1256, 1207, 1135, 1115, 1031, 1002, 949, 912, 835, 827, 649, 640 cm^{-1}. ^1H NMR (400 MHz, MeOD) δ: 1.01 (s, 3H, CH_3), 1.53–1.61 [complex signal, 2H, 10(13)-H_a], 1.70 (broad s., 2H, 8-H_2), 1.70–1.80 [complex signal, 2 H, 10(13)-H_b], 1.82–1.92 [complex signal, 2H, 6(12)-H_a], 2.03–2.12 [complex

signal, 2H, 6(12)-H_b], 2.57 (s, 3H, $COCH_3$), 3.33–3.35 [complex signal, 2H, 5(11)-H], 7.26 [d, $J = 7.6$ Hz, 1H, 4-H), 7.75–7.78 (complex signal, 2H, 1-H, 3-H). ^{13}C NMR (100.6 MHz, MeOD) δ: 26.7 (CH_3, $\underline{C}H_3CO$), 32.1 (CH_3, C9–$\underline{C}H_3$), 34.7 (C, C9), 38.8 (CH_2) and 39.1 (CH_2) (C6 and C12), 41.1 (CH_2) and 41.4 (CH_2) (C10 and C13), 41.5 (CH) and 41.6 (CH) (C5 and C11), 47.0 (CH_2, C8), 55.3 (C, C7), 128.5 (CH) and 129.2 (CH) (C1 and C3), 129.8 (CH, C4), 137.2 (C) and 147.0 (C) (C2 and C11a), 152.3 (C, C4a), 200.2 (C, CO). HRMS-ESI + *m/z* $[M+H]^+$ calcd for $[C_{18}H_{24}NO]^+$: 270.1852, found: 270.1858.

4.1.10. 1-(7-(dimethylamino)-9-methyl-6,7,8,9,10,11-hexahydro-5H-5,9:7,11-dimethanobenzo[9]annulen-2-yl)ethan-1-one hydrochloride (**14**)

$AlCl_3$ (419 mg, 3.14 mmol) was added to a solution of **13** (161 mg, 0.63 mmol) and AcCl (0.45 mL, 6.31 mmol) in DCM (5 mL). The resulting mixture was stirred for 60 min and then poured over a mixture of ice and saturated aq Na_2CO_3 solution (10 mL). After stirring 20 min the mixture was extracted with DCM (3 × 10 mL). The organic layer was dried over anh Na_2SO_4, filtered and concentrated *in vacuo* to give **14** as a yellow solid. Its hydrochloride was obtained by adding an excess of HCl/Et_2O to a solution of the amine in ethyl acetate, followed by filtration of the resulting light brown precipitate (83 mg, 44% yield), mp 180–181 °C. IR (ATR) ν: 3300–2400 (3221, 2947, 2928, 2903, 2850), 1666, 1657, 1651, 1646, 1518, 1505, 1460, 1399, 1363, 1355, 1285, 1277, 1258, 1245, 1211, 1190, 1158, 1133, 1124, 1091, 1082, 1025, 1006, 960, 900, 864, 813, 803, 740, 708, 689 cm^{-1}. ^{1}H NMR (400 MHz, MeOD) δ: 1.04 (s, 3H, CH_3), 1.52–1.61 [complex signal, 2H, 10(13)-H_a], 1.71–1.81 [complex signal, 2 H, 10(13)-H_b], 1.81 (broad s., 2H, 8-H_2), 1.97–2.07 [complex signal, 2H, 6(12)-H_a], 2.10–2.21 [complex signal, 2H, 6(12)-H_b], 2.57 (s, 3H, $COCH_3$), 2.83 [s, 6H, $N(CH_3)_2$], 3.41 [complex signal, 2H, 5(11)-H], 7.27 (d, $J = 8.0$ Hz, 1H, 4-H), 7.75–7.80 (complex signal, 1-H, 3-H). ^{13}C NMR (100.6 MHz, MeOD) δ: 26.7 (CH_3, $\underline{C}H_3CO$), 32.3 (CH_3, C9–$\underline{C}H_3$), 34.0 (CH_2) and 34.2 (CH_2) (C6 and C12), 35.5 (C, C9), 37.3 [CH_3, $N(\underline{C}H_3)_2$], 40.9 (CH_2) and 41.2 (CH_2) (C10 and C13), 41.5 (CH) and 41.6 (CH) (C5 and C11), 44.2 (CH_2, C8), 67.0 (C, C7), 128.6 (CH) and 129.2 (CH) (C1 and C3), 129.8 (CH, C4), 137.2 (C, C2), 146.9 (C, C11a), 152.2 (C, C4a), 200.1 (C,CO). HRMS-ESI + *m/z* $[M+H]^+$ calcd for $[C_{20}H_{28}NO]^+$: 298.2165, found: 298.2176.

4.1.11. N,N,9-trimethyl-2-nitro-5,6,8,9,10,11-hexahydro-7H-5,9:7,11-dimethanobenzo[9]annulen-7-amine hydrochloride (**15**)

To a solution of **9·HCl** (222 mg, 0.72 mmol) in MeOH (7 mL), $NaBH_3CN$ (129 mg, 2.05 mmol), AcOH (0.3 mL) and formaldehyde (0.22 mL, 37% in H_2O solution, 2.16 mmol) were added and the mixture was stirred at rt for 8 h. An additional portion of $NaBH_3CN$ (129 mg, 2.05 mmol) and formaldehyde (0.22 mL, 37% in H_2O solution, 2.16 mmol) were added, then the mixture was stirred at rt for 18 h and subsequently was concentrated *in vacuo* to dryness. H_2O (20 mL) was added to the residue, then the suspension was basified with 1 N NaOH solution (10 mL) and was extracted with ethyl acetate (4 × 15 mL). The combined organic extracts were washed with brine (2 × 10 mL), dried with anh Na_2SO_4, then filtered and concentrated *in vacuo* to give **15** as a yellow oil. Its hydrochloride was obtained by adding an excess of HCl/Et_2O to a solution of the amine in ethyl acetate, followed by filtration of the white solid precipitate (180 mg, 74% yield), mp 168–169 °C. IR (ATR) ν: 3452, 3411, 2947, 2906, 2860, 2655, 2631, 2601, 1514, 1484, 1460, 1445, 1348, 1309, 1281, 1174, 1123, 1108, 1088, 1000, 982, 905, 896, 833, 801, 766, 736 cm^{-1}. ^{1}H NMR (400 MHz, MeOD) δ: 1.05 (s, 3H, CH_3), 1.55–1.62 [complex signal, 2H, 10(13)-H_a], 1.75–1.82 [complex signal, 2 H, 10(13)-H_b], 1.82–1.85 (complex signal, 2H, 8-H_2), 2.01–2.11 [complex signal, 2H, 6(12)-H_a], 2.14–2.22 [complex signal, 2H, 6(12)-H_b], 2.84 [s, 6H, $N(CH_3)_2$], 3.44–3.50 [complex signal, 2H, 5(11)-H], 7.39 (d, $J = 8.0$ Hz, 1H, 4-H), 8.00 (dd, $J = 8.0$ Hz, $J' = 2.4$ Hz, 1H, 3-H), 8.04 (d, $J = 2.4$ Hz, 1H, 1-H). ^{13}C NMR (100.6 MHz, MeOD) δ: 32.2 (CH_3, C9–$\underline{C}H_3$), 33.6 (CH_2) and 33.9 (CH_2) (C6 and C12), 35.5 (C, C9), 37.3 [CH_3, $N(CH_3)_2$], 40.6 (CH_2) and 40.8 (CH_2), (C10 and C13), 41.3 (CH) and 41.4 (CH) (C5 and C11), 44.0 (CH_2, C8), 66.8 (C, C7), 123.0 (CH, C3), 124.0 (CH, C1), 130.6 (CH, C4), 148.1 (C) and 148.2 (C) (C2 and C11a), 154.1 (C, C4a). HRMS-ESI + *m/z* $[M+H]^+$ calcd for $[C_{18}H_{25}N_2O_2]^+$: 301.1911, found: 301.1916.

4.1.12. N-(9-methyl-2-nitro-5,6,8,9,10,11-hexahydro-7H-5,9:7,11-dimethanobenzo[9]annulen-7-yl)acetamide (**17**)

To a cold (0 °C) solution of **16** (2.68 g, 9.95 mmol) in acetic anhydride (10.6 mL), glacial acetic acid (1.6 mL) and fuming nitric acid (1.9 mL) were carefully added. The mixture was allowed to reach rt and left stirring overnight. The obtained yellow solution was then poured into ice–water (20 mL) and extracted with DCM (3 × 40 mL). The combined organic extracts were washed with 2 N NaOH solution (1 × 40 mL), H_2O (1 × 40 mL) and brine (1 × 40 mL). The organic layer was dried over anh Na_2SO_4, filtered and concentrated *in vacuo* to give a yellow residue. Purification by Combiflash® in silica gel using as eluent a gradient from hexane to ethyl acetate/hexane mixture (3/7) gave **17** as a white solid (1.87 g, 60% yield), mp 174–176 °C. IR (NaCl disk) ν: 3398, 3307, 3201, 3063, 2943, 2917, 2863, 1653, 1588, 1523, 1455, 1346, 1322, 1304, 1268, 1245, 1214, 1166, 1141, 1124, 1081, 1037, 1010, 945, 893, 865, 838, 798, 763, 740, 701, 645 cm^{-1}. ^{1}H NMR (400 MHz, $CDCl_3$) δ: 0.93 (s, 3H, C$\underline{H}_3$), 1.52 [complex signal, 2H, 10(13)-H_a], 1.67–1.73 [complex signal, 2H, 10(13)-H_b], 1.76 (dt, $J = 12.0$ Hz, $J' = 2.0$ Hz, 2H, 8-H_a), 1.84 (dt, $J = 12.0$ Hz, $J' = 2.0$ Hz, 2H, 8-H_b), 1.90 (s, CH_3, C$\underline{H}_3$CO), 2.06–2.19 [complex signal, 4H, 6(12)-H_2], 3.17–3.21 [complex signal, 2H, 5(11)-H], 5.27 (broad s, 1H, NH), 7.20 (d, $J = 8.8$ Hz, 1H, 4-H), 7.91–7.94 (complex signal, 2H, 1-H, 3-H). ^{13}C NMR (100.6 MHz, $CDCl_3$) δ: 24.8 (CH_3, $\underline{C}H_3CO$), 32.2 (CH_3, C9–$\underline{C}H_3$), 33.7 (C, C9), 38.2 (CH_2, C6 or C12), 38.7 (CH_2, C12 or C6), 40.6 (CH_2, C10 or C13), 40.8 (CH_2, C13 or C10), 40.98 (CH, C5 or C11) and 41.00 (CH, C11 or C5), 47.2 (CH_2, C8), 54.1 (C, C7), 121.8 (CH, C1 or C3), 123.1 (CH, C3 or C1), 129.2 (CH, C4), 146.5 (C2 or C11a), 147.8 (C, C11a or C2), 154.1 (C, C4a), 169.5 (C, NHCO). HRMS-ESI + *m/z* $[M - H]^+$ calcd for $[C_{18}H_{23}N_2O_3]^+$: 315.1703, found: 315.1714.

4.1.13. N-(2-amino-9-methyl-5,6,8,9,10,11-hexahydro-7H-5,9:7,11-dimethanobenzo[9]annulen-7-yl)acetamide (**18**)

To a solution of acetamide (2.65 g, 8.43 mmol) in abs. ethanol (140 mL), PtO_2 (190 mg, 0.84 mmol) was added, and the resulting suspension was hydrogenated at 1 atm of H_2 at rt for 4 h. The black suspension was filtered, and the solvent removed by concentration *in vacuo* to give a dark solid. Purification by Combiflash® in silica gel using as eluent a gradient from hexane to ethyl acetate/hexane mixture (5/5) gave **18** as a white solid (1.63 g, 68% yield), mp 113 °C. IR (NaCl disk) ν: 3432, 3324, 3224, 3056, 3004, 2938, 2903, 2856, 2835, 1651, 1618, 1546, 1507, 1447,1362, 1344, 1300, 1262, 1194, 1164, 1136, 1065, 862, 818, 735, 701 cm^{-1}. ^{1}H-RMN (400 MHz, $CDCl_3$) δ: 0.89 (s, 3H, C$\underline{H}_3$), 1.45–1.54 [complex signal, 2H, 10(13)-H_a], 1.59–1.65 [complex signal, 2H, 10(13)-H_b], 1.76 (dm, $J = 12.0$ Hz, 1H, 8-H_a), 1.85 (dm, $J = 12.0$ Hz, 1H, 8-H_b), 1.89 (s, 3H, C$\underline{H}_3$CO), 1.90 (m, 1 H, 6-H_a or 12-H_a), 1.96 (broad d, $J = 12.0$ Hz, 1 H, 12-H_a or 6-H_a), 2.09 (ddd, $J = 12.8$ Hz, $J' = 6.4$ Hz, $J'' = 2.4$ Hz, 2H, 6-H_b or 12-H_b), 2.17 (ddd, $J = 12.8$ Hz, $J' = 6.4$ Hz, $J'' = 2.4$ Hz, 2H, 12-H_b or 6-H_b), 2.90 (t, $J = 6.0$ Hz, 1H, 5-H or 11-H), 2.96 (t, $J = 6.0$ Hz, 1H, 11-H or 5-H), 5.21 (broad s., 1H, NH), 6.40 (dd, $J = 8.0$ Hz, $J' = 2.2$ Hz, 1H, 3-H), 6.42 (d, $J = 2.2$ Hz, 1H, 1-H), 6.83 (d, $J = 8.0$ Hz, 1H, 4-H). ^{13}C NMR (100.6 MHz, $CDCl_3$) δ: 25.0 (CH_3, $\underline{C}H_3CO$), 32.4 (CH_3, C9–$\underline{C}H_3$), 33.6 (C, C9), 39.1 (CH_2, C12 or C6), 39.9 (CH_2, C6 or C12), 40.2 (CH, C11 or C5), 41.2 (CH, C5 or C11), 41.3 (CH_2, C10 or C13), 41.9 (CH_2, C13 or C10), 47.3 (CH_2, C8), 54.6 (C, C7), 112.6 (CH, C3), 115.4 (CH, C1), 129.1 (CH, C4), 136.9 (C, C4a), 144.6 (C, C11a), 147.5 (C, C2), 169.3 (C,

NHCO). HRMS-ESI + *m/z* $[M - H]^+$ calcd for $[C_{18}H_{25}N_2O]^+$:285.1961, found: 285.1972.

4.1.14. N-(2-chloro-9-methyl-5,6,8,9,10,11-hexahydro-7H-5,9:7,11-dimethanobenzo[9]annulen-7-yl)acetamide (**19**)

18·HCl (1.04 g, 3.24 mmol) was dissolved in H_2O (6 mL) and conc. HCl solution (6 mL) then cooled to 0 °C and treated with a solution of sodium nitrite (448 mg, 6.49 mmol) in H_2O (2 mL) dropwise. To the resulting solution was added a CuCl (691 mg, 6.98 mmol) in conc. HCl solution (3 mL) and over 10 min gas was observed. The resulting solution was warmed to 60 °C for 90 min, then was cooled to rt, diluted in H_2O (60 mL) and extracted with DCM (4 × 90 mL). The combined organic extracts were washed with saturated aq $NaHCO_3$ solution, brine and were dried over anh Na_2SO_4, filtered and concentrated *in vacuo* to give a dark green solid. Purification by Combiflash® in silica gel using as eluent a gradient from hexane to ethyl acetate/hexane mixture (1/9) gave **19** as a white solid (210 mg, 21% yield), mp 190–191 °C. IR (NaCl disk) *ν*: 3301, 3196, 3071, 2921, 2855, 1651, 1594, 1549, 1487, 1454, 1414, 1364, 1343, 1308, 1281, 1263, 1211, 1139, 1109, 1012, 950, 875, 820 cm^{-1}. ^1H NMR (400 MHz, $CDCl_3$) *δ*: 0.91 (s, 3H, CH_3), 1.46–1.54 [complex signal, 2H, 10(13)-H_a] 1.60–1.68 [complex signal, 2H, 10(13)-H_b], 1.78–1.81 (complex signal, 2H, 8-H_2), 1.90 (s, 3H, CH_3CO), 1.98–2.06 [complex signal, 2H, 6(12)-H_a], 2.09–2.16 [complex signal, 2H, 6(12)-H_b] 3.00 (tm, $J = 6.0$ Hz, 1H, 5-H or 11-H], 3.04 (tm, $J = 6.0$ Hz, 1H, 11-H or 5-H], 5.19 (broad s., 1H, NH), 6.97 (dd, $J = 7.2$ Hz, $J' = 1.6$ Hz, 1H, 3-H), 7.02–7.04 [complex signal, 2H, 1(4)-H]. ^{13}C NMR (100.6 MHz, $CDCl_3$) *δ*: 24.9 (CH_3, $\underline{C}H_3CO$), 32.3 (CH_3, C9–$\underline{C}H_3$), 33.7 (C, C9), 38.9 (CH_2, C12 or C6), 39.0 (CH_2, C6 or C12), 40.5 (CH, C11 or C5), 40.9 (CH, C5 or C11), 41.1 (CH_2, C10 or C13), 41.2 (CH_2, C13 or C10), 47.3 (CH_2, C8), 54.4 (C, C7), 126.2 (CH, C1 or C4), 128.1 (CH, C4 or C1), 129.6 (CH, C3), 131.6 (C, C2), 144.6 (C, C4a), 148.2 (C, C11a), 169.3 (C, NH$\underline{C}$O). HRMS-ESI + *m/z* $[M - H]^+$ calcd for $[C_{18}H_{23}ClNO]^+$: 304.1463, found: 304.1460.

4.1.15. 2-Chloro-9-methyl-5,6,8,9,10,11-hexahydro-7H-5,9:7,11-dimethanobenzo[9]annulen-7-amine hydrochloride (**20**)

To a solution of acetamide **19** (190 mg, 0.63 mmol) in 2-propanol (6 mL), H_2O (8 mL) and conc. HCl (4 mL) were added, and the mixture was stirred under reflux for 6 days. The solution was cooled and washed with ethyl acetate (3 × 4 mL). The aq phase was basified with 1 N NaOH solution (10 mL) and extracted with ethyl acetate (4 × 15 mL). The combined organic layers were dried over anh Na_2SO_4, filtered and concentrated *in vacuo* to give **20** as a light brown solid. Its hydrochloride was obtained by adding an excess of HCl/Et_2O to a solution of the amine in ethyl acetate, followed by filtration of the resulting white precipitate (36 mg, 19% yield). The analytical sample was obtained by crystallization from $MeOH/Et_2O$, mp > 250 °C. IR (KBr disk) *ν*: 3200–2500 (2990, 2950, 2916, 2861), 2058, 1597, 1570, 1509, 1488, 1454, 1416, 1380, 1365, 1302, 1256, 1217, 1155, 1133, 1110, 1093, 1032, 1000, 948, 875, 820, 771, 673 cm^{-1}. ^1H NMR (400 MHz, MeOD) *δ*: 1.00 (s, 3H, CH_3), 1.52–1.60 [complex signal, 2H, 10(13)-H_a], 1.65–1.68 (complex signal, 2H, 8-H_2), 1.68–1.74 [complex signal, 2H, 10(13)-H_b], 1.82–1.90 [complex signal, 2H, 6(12)-H_a], 1.99–2.07 [complex signal, 2H, 6(12)-H_b], 3.18 (tm, $J = 6.0$ Hz, 1H, 5-H or 11-H], 3.22 (tm, $J = 6.0$ Hz, 1H, 11-H or 5-H], 7.09–7.102 [complex signal, 2 H, 3(4)-H], 7.14 (broad signal, 1H, 1-H). ^{13}C NMR (100.6 MHz, MeOD) *δ*: 32.2 (CH_3, C9–$\underline{C}H_3$), 34.7 (C, C9), 39.0 (CH_2, C12 or C6), 39.1 (CH_2, C6 or C12), 41.0 (CH, C11 or C5), 41.3 (CH, C5 or C11 and CH_2, C10 or C13), 41.4 (CH_2, C13 or C10), 47.0 (CH_2, C8), 55.3 (C, C7), 127.7 (CH, C3 or C4), 129.1 (CH, C1), 130.9 (CH, C4 or C3), 133.2 (C, C2), 145.2 (C, C4a), 148.5 (C, C11a). HRMS-ESI + *m/z* $[M+]^+$ calcd for $[C_{16}H_{21}ClN]^+$: 262.1357, found: 262.1359.

4.1.16. 2-Fluoro-5,6,8,9-tetrahydro-7H-5,9-propanobenzo[7]annulene-7,11-dione (**25**)

a) 4-fluorophthalaldehyde (1 g, 6.57 mmol) was dissolved in methanol (18 mL) then dimethyl-1,3-acetonedicarboxylate (2.33 g, 13.4 mmol) and diethylamine (2 drops) were added. The yellow solution was brought to reflux for 1.5 h. The solution was allowed to cool to rt and more diethylamine (2 drops) was added. The solution was left at 4 °C overnight and then the solid was filtered off, obtaining the tetraester as a white solid (675 mg, 22% yield). Crude was used in the next step without further purification.
b) The aforementioned tetraester (675 mg, 1.45 mmol) was mixed with conc. HCl (1 mL) and glacial acetic acid (4 mL). The yellow solution was heated to reflux for 12 h. The solvent was removed under vacuum and the solid residue was diluted with hot diethyl ether (10 mL) over 15 min and the solution was stored at 4 °C overnight. The residue was filtered off obtaining a white solid (250 mg) that was constituted by a mixture of diketone **25** and its hydrate in an approximate ratio of 1:2. The pure diketone was obtained as a white solid using 7 mL of toluene as a solvent in a Dean-Stark apparatus for 24 h (200 mg, 59% yield), mp 105–107 °C. IR (NaCl disk) *ν*: 2923, 2848, 1710, 1607, 1593, 1490, 1428, 1380, 1346, 1253, 1208, 1153, 1119, 1074, 985, 944, 865, 806 cm^{-1}. ^1H NMR (400 MHz, $CDCl_3$) *δ*: 2.68–2.78 [complex signal, 4H, 6(12)-H_a, 8(10)-H_a], 2.84–2.93 [complex signal, 4H, 6(12)-H_b, 8(10)-H_b], 3.31 (tt, $J = J' = 4.4$ Hz, 1H, 5-H or 9-H), 3.37 (tt, $J = J' = 4.4$ Hz, 1H, 9-H or 5-H), 7.01 (td, $J = 8.0$ Hz, $J' = 2.8$ Hz, 1H, 3-H), 7.06 (dd, $J = 9.2$ Hz, $J' = 2.8$ Hz, 1H, 1-H), 7.29 (dd, $J = 8.0$ Hz, $J' = 5.6$ Hz, 1H, 4-H). ^{13}C NMR (100.6 MHz, $CDCl_3$) *δ*: 37.3 (CH) and 38.1 (CH), (C5 and C9), 49.0 (CH_2) and 49.3 (CH_2) [C6(12) and C8(10)], 115.0 (CH, d, $J_{C\text{-}F} = 21$ Hz, C3), 115.8 (CH, d, $J_{C\text{-}F} = 22$ Hz, C1), 130.7 (CH, d, $J_{C\text{-}F} = 8.0$ Hz, C4), 138.9 (C, C4a), 145.2 (C, d, $J_{C\text{-}F} = 7.1$ Hz, C9a), 162.4 (C, d, $J_{C\text{-}F} = 247.3$ Hz, C2), 208.4 [C, C7(11)-$\underline{C}$O]. HRMS-ESI + *m/z* $[M+]^+$ calcd for $[C_{14}H_{14}FO_2]^+$: 233.0972, found: 233.0967.

4.1.17. 2,3-Dimethoxy-5,6,8,9-tetrahydro-7H-5,9-propanobenzo[7]annulene-7,11-dione (**26**)

a) 4,5-dimethoxyphthalaldehyde (6.54 g, 33.7 mmol) was dissolved in methanol (130 mL) then dimethyl-1,3-acetonedicarboxylate (11.7 g, 67.4 mmol) and diethylamine (19 drops) were added. The brown solution was brought to reflux for 1.5 h. The brown suspension was allowed to cool to rt and more diethylamine (19 drops) was added. The suspension was left at 4 °C over the weekend and was then filtered under vacuum. The white residue was dried under vacuum (6.84 g, 40% yield) and was used in the next step without further purification.
b) The aforementioned tetraester (6.84 g, 13.5 mmol) was mixed with conc. HCl (10 mL) and glacial acetic acid (35 mL). The yellow paste was heated to reflux for 24 h. The resulting orange suspension was allowed to cool to rt and was then concentrated under vacuum. The brown solid was dissolved in toluene and the brown solution was heated to reflux in a Dean-Stark set up for 24 h. The yellow solution was allowed to cool to rt and was then concentrated under vacuum. The resulting brown solid was washed twice with hot methanol and was dried again to obtain diketone **26** as a brown solid (2.80 g, 76% yield), mp 236–237 °C. IR (NaCl disk) *ν*: 2952, 2840, 1698, 1605, 1516, 1467, 1451, 1416, 1355, 1336, 1254, 1221, 1192, 1162, 1025, 1002, 880, 811 cm^{-1}. ^1H NMR (400 MHz, $CDCl_3$) *δ*: 2.73 [dd, $J = 15.2$ Hz, $J' = 4.0$ Hz, 4H, 6(8,10,12)-H_a], 2.85 [dd, $J = 15.2$ Hz, $J' = 4.4$ Hz, 4H, 6(8,10,12)-

H_b], 3.27 [tt, J = 4.8 Hz, J' = 3.6 Hz, 2H, 5(9)-H], 3.90 (s, 6H, OCH_3), 6.82 [s, 2H, 1(4)-H]. ^{13}C NMR (100.6 MHz, $CDCl_3$) δ: 37.7 [CH, C5(9)], 49.4 [CH_2, C6(8,10,12)], 56.3 [CH_3, O$\underline{C}H_3$], 112.4 [CH, C1(4)], 135.2 [C, C4a(9a)], 148.5 [C, C2(3)], 209.1 [C, C7(11)]. HRMS-ESI + m/z $[M+H]^+$ calcd for $[C_{16}H_{19}O_4]^+$: 275.1278, found: 275.1279.

4.1.18. 1-Fluoro-5,6,8,9-tetrahydro-7H-5,9-propanobenzo[7]annulene-7,11-dione (**27**)

a) 3-fluorophthalaldehyde (11.2 g, 73.6 mmol) was dissolved in methanol (220 mL) then dimethyl-1,3-acetonedicarboxylate (25.6 g, 147 mmol) and diethylamine (33 drops) were added. The yellow solution was brought to reflux for 1.5 h. The solution was allowed to cool to rt and more diethylamine (33 drops) was added. The solution was left at 4 °C overnight and was then filtered under vacuum. The white crystals were dried under vacuum and the tetraester was used in the next step without further purification (18.5 g, 54% yield).
b) The aforementioned tetraester (18.5, 39.9 mmol) was mixed with conc. HCl (31 mL) and glacial acetic acid (103 mL). The yellow solution was heated to reflux for 24 h. The pale-yellow solution was allowed to cool to rt and was then concentrated under vacuum. The off-white solid was dissolved in toluene and the yellow solution was heated to reflux in a Dean-Stark set up for 24 h. The yellow solution was allowed to cool to rt and was then concentrated under vacuum to give **27** as a an off-white solid (8.73 g, 94% yield), mp > 150 °C. IR (NaCl disk) ν: 2940, 2908, 1701, 1619, 1585, 1468, 1421, 1370, 1304, 1245, 1222, 1203, 1072, 1052, 988, 931, 897, 789, 746 cm^{-1}. ^{1}H NMR (400 MHz, $CDCl_3$) δ: 2.69 [dd, J = 15.6 Hz, J' = 3.6 Hz, 2H, 8(10)-H_a], 2.75 [dd, J = 15.6 Hz, J' = 4.0 Hz, 2H, 6(12)-H_a], 2.90 [dd, J = 15.6 Hz, J' = 4.8 Hz, 4H, 6(12)-H_b, 8(10)-H_b], 3.42 (m, 1H, 5-H), 4.00 (tt, J = 4.4 Hz, J' = 4.0 Hz, 1H, 9-H), 7.08–7.15 [complex signal, 2H, 2(4)-H], 7.29 (m, 1H, 3-H). ^{19}F NMR (376 MHz, $CDCl_3$) δ: 117.3 (t, J = 7.52 Hz). ^{13}C NMR (100.6 MHz, $CDCl_3$) δ: 26.4 (CH, d, $J_{C\text{-}F}$ = 6.4 Hz, C9), 37.9 (CH, d, $J_{C\text{-}F}$ = 2.5 Hz, C5), 48.6 [CH_2, C8(10)], 49.0 [CH_2, C6(12)], 115.1 (CH, d, $J_{C\text{-}F}$ = 24.1 Hz, C2), 124.3 (CH, d, $J_{C\text{-}F}$ = 3.2 Hz, C4), 129.3 (CH, d, $J_{C\text{-}F}$ = 9.2 Hz, C3), 130.0 (C, d, $J_{C\text{-}F}$ = 13.8 Hz, C9a), 146.0 (C, d, $J_{C\text{-}F}$ = 1.9 Hz, C4a), 159.5 (C, d, $J_{C\text{-}F}$ = 245.8 Hz, C1), 208.5 (C, $\underline{C}O$). HRMS-ESI + m/z $[M+H]^+$ calcd for $[C_{14}H_{14}FO_2]^+$: 233.0972, found: 233.0976.

4.1.19. 2-Methoxy-5,6,8,9-tetrahydro-7H-5,9-propanobenzo[7]annulene-7,11-dione (**28**)

a) 4-methoxyphthalaldehyde (10.2 g, 62.1 mmol) was dissolved in methanol (380 mL) then dimethyl-1,3-acetonedicarboxylate (21.6 g, 124 mmol) and diethylamine (28 drops) were added. The dark red solution was brought to reflux for 1.5 h. The solution was allowed to cool to rt and more diethylamine (22 drops) was added. The solution was left at 4 °C over 5 days and was then filtered under vacuum. The red residue was dried under vacuum (19.4 g, 66% yield) and was used in the next step without further purification.
b) The aforementioned tetraester (250 mg, 0.53 mmol) was mixed with conc. HCl (0.4 mL) and glacial acetic acid (1.4 mL). The white suspension was heated to reflux for 24 h. The dark red solution was allowed to cool to rt and was then concentrated under vacuum. The red oil was dissolved in toluene and the red solution was heated to reflux in a Dean-Stark set up for 24 h. The red solution was allowed to cool to rt and was then concentrated under vacuum to give **28** as a red solid (125 mg, 98% yield), mp 157–158 °C. IR (NaCl disk) ν: 2941, 2910, 2837, 1701, 1610, 1585, 1504, 1431, 1414, 1370, 1321, 1300, 1266, 1166, 1094, 1033, 989 cm^{-1}. ^{1}H NMR (400 MHz, $CDCl_3$) δ: 2.68–2.78 [complex signal, 4H, 6(12)-H_a, 8(10)-H_a], 2.82–2.91 [complex signal, 4H, 6(12)-H_b, 8(10)-H_b], 3.27 (tt, J = 4.4 Hz, J' = 4.0 Hz, 1H, 9-H), 3.32 (tt, J = 4.4 Hz, J' = 4.0 Hz, 1H, 5-H), 3.84 (s, 3H, OCH_3), 6.83 (dd, J = 8.4 Hz, J' = 2.8 Hz, 1H, 3-H), 6.87 (d, J = 2.8 Hz, 1H, 1-H), 7.23 (d, J = 8.4 Hz, 1H, 4-H). ^{13}C NMR (100.6 MHz, $CDCl_3$) δ: 37.2 (CH, C5), 38.4 (CH, C9), 49.2 (CH_2) and 49.6 (CH_2), C6(12) and C8(10), 55.5 (CH_3, O$\underline{C}H_3$), 112.9 (CH, C3), 114.7 (CH, C1), 130.2 (CH, C4), 135.2 (C, C4a), 144.2 (C, C9a), 160.0 (C, C2), 209.1 [C, C7(11)-$\underline{C}O$]. HRMS-ESI + m/z $[M+H]^+$ calcd for $[C_{15}H_{17}O_3]^+$: 245.1172, found: 245.1180.

4.1.20. 2-Fluoro-7,11-dimethylene-6,7,8,9-tetrahydro-5H-5,9propanobenzo[7]annulene (**29**)

A suspension of sodium hydride, 60% dispersion in mineral oil (85 mg, 2.13 mmol), in anh DMSO (2 mL) was heated to 90 °C for 45 min under N_2 atmosphere. After the reaction mixture was tempered, a solution of triphenylmethylphophonium iodide (1.48 g, 3.66 mmol) in anh DMSO (3.5 mL) was added, and the resulting yellow solution was stirred at rt for 20 min. Then a suspension of diketone (200 mg, 0.86 mmol) in anh DMSO (2 mL) was added and the obtained solution was heated to 90 °C overnight. The resulting black solution was allowed to cool to rt and then poured into H_2O (20 mL). Hexane (20 mL) was added and the phases were separated. The aq phase was extracted with further hexane (4 × 20 mL) and the combined organic phases were washed with brine (20 mL), dried over anh Na_2SO_4, filtered and concentrated *in vacuo*. The crude was purified by Combiflash® in silica gel using 100% hexane to give diene **29** as a white solid (118 mg, 60% yield), mp 108–109 °C. IR (NaCl disk) ν: 3072, 2985, 2921, 2844, 1639, 1612, 1592, 1494, 1451, 1444, 1363, 1246, 1162, 1135, 1095, 1048, 974, 951, 930, 887, 820, 716, 658, 638, 598, 528 cm^{-1}. ^{1}H NMR (400 MHz, $CDCl_3$) δ: 2.41–2.51 [complex signal, 4H, 6(12)-H_a, 8(10)-H_a], 2.55–2.62 [complex signal, 4H, 6(12)-H_b, 8(10)-H_b], 3.04 (tt, J = J' = 4.4 Hz, 1H, 5-H or 9-H), 3.09 (tt, J = J' = 4.4 Hz, 1H, 9-H or 5-H), 4.68 [s, 4H, 7(11)-C$\underline{H}_2$], 6.75–6.82 [complex signal, 2H, 1(3)-H], 7.02 (m, 1H, 4-H). ^{13}C NMR (100.6 MHz, $CDCl_3$) δ: 40.7 (CH_2) and 40.9 (CH_2) [C6(12) and C8(10)], 40.9 (CH) and 41.6 (CH) (C5 and C9), 112.8 (CH, d, $J_{C\text{-}F}$ = 20 Hz, C1), 115.4 [complex signal, C7(11) = $\underline{C}H_2$, C3), 130.0 (CH, d, $J_{C\text{-}F}$ = 8.0 Hz, C4), 137.1 (C, C4a), 146.3 [C, C7(11)], 162.8 (C, C2). The signal from C9a was not observed.

4.1.21. 2,3-Dimethoxy-7,11-dimethylene-6,7,8,9-tetrahydro-5H-5,9-propanobenzo[7]annulene (**30**)

In a flame dried 3-necked round bottom flask, sodium hydride 60% in mineral oil (1.67 g, 41.8 mmol) was added under N_2 and was dissolved in anh DMSO (22 mL). The grey suspension was heated to 75 °C for 45 min and was then cooled to rt. Methyltriphenylphosphonium iodide (16.9 g, 41.8 mmol) dissolved in anh DMSO (36 mL) and diketone **29** (2.80 g, 10.2 mmol) dissolved in anh DMSO (23 mL) were sequentially added under N_2. The brown solution was stirred and heated to 90 °C overnight. The black solution was allowed to cool to rt and it was then poured into H_2O (200 mL). The H_2O was extracted with hexane (4 × 200 mL) and the organic layer was dried over anh Na_2SO_4, filtered and concentrated under vacuum. The crude was purified by Combiflash® in silica gel using a solvent system of 100% hexane. Diene **30** was isolated as a yellow solid (633 mg, 23% yield), mp 74–75 °C. IR (NaCl disk) ν: 3068, 2977, 2913, 2832, 1639, 1606, 1515, 1464, 1450, 1429, 1414, 1358, 1342, 1293, 1261, 1240, 1225, 1191, 1173, 1103, 1023, 956, 931, 889, 804, 656, 634 cm^{-1}. ^{1}H NMR (400 MHz, $CDCl_3$) δ: 2.48 [dd, J = 14.0 Hz, J' = 5.2 Hz, 4H, 6(8,10,12)-H_a], 2.59 [dd, J = 14.0 Hz, J' = 4.4 Hz, 4H,

6(8,10,12)-H_b], 3.00 [tt, J = 4.8 Hz, J' = 4.4 Hz, 2H, 5(9)-H], 3.86 (s, 6H, OCH_3), 4.67 (s, 4H, 7(11)-C=CH_2), 6.63 [s, 2H, 1(4)-H]. ^{13}C NMR (100.6 MHz, $CDCl_3$) δ: 41.1 [CH_2, C6(8,10,12)], 41.3 [CH, C5(9)], 56.1 [CH_3, OCH_3], 112.7 [CH, C1(4)], 115.1 [CH_2, C=CH_2], 136.8 [C, C4a(9a)], 146.8 [C, C7(11)], 148.5 [C, C2(3)]. HRMS-ESI + m/z $[M+H]^+$ calcd for $[C_{18}H_{23}O_2]^+$: 271.1693, found: 271.1688.

4.1.22. 1-Fluoro-7,11-dimethylene-6,7,8,9-tetrahydro-5H-5,9-propanobenzo[7]annulene (**31**)

In a flame dried 3-necked round bottom flask, sodium hydride 60% dispersion in mineral oil (2.82 g, 70.5 mmol) was added under N_2 and was dissolved in anh DMSO (34.8 mL). The grey suspension was heated to 75 °C for 45 min, yielding a green suspension, and was then cooled to rt. To the green suspension, methyltriphenylphosphonium iodide (28.5 g, 70.5 mmol) diluted in anh DMSO (75 mL) and the diketone **27** (4.00 g, 17.2 mmol) diluted in anh DMSO (38 mL) were added sequentially. The resulting mixture was heated at 90 °C overnight. The resulting black solution was allowed to cool to rt and it was then poured into H_2O (200 mL). The H_2O was extracted with hexane (4 × 200 mL) and the organic layer was dried over anh Na_2SO_4, filtered and concentrated under vacuum. The crude was purified by Combiflash® using as eluent a gradient from pure hexane to ethyl acetate/hexane mixture (1/9). Diene **31** was isolated as a colourless oil (2.69 g, 69% yield). IR (NaCl disk) ν: 3071, 3033, 2981, 2921, 2838, 1639, 1614, 1583, 1464, 1446, 1429, 1365, 1248, 1155, 1046, 991, 935, 919, 895 cm^{-1}. ^{1}H NMR (400 MHz, $CDCl_3$) δ: 2.43–2.56 [complex signal, 4H, 6(12)-H_a, 8(10)-H_a], 2.64 [dd, J = 14.4 Hz, J' = 4.2 Hz, 4H, 6(12)-H_b, 8(10)-H_b], 3.19 (m, 1H, 5-H), 3.79 (tt, $J = J'$ = 4.8 Hz, 1H, 9-H), 4.72 [d, J = 0.8 Hz, 4H, 7(11)-CH_2], 6.88–6.96 (complex signal, 2H, 2-H, 4-H), 7.08 (m, 1H, 3-H). ^{19}F NMR (376 MHz, $CDCl_3$) δ: −119.9 (t, J = 4.89 Hz). ^{13}C NMR (100.6 MHz, $CDCl_3$) δ: 29.5 (CH, d, $J_{C\text{-}F}$ = 5 Hz, C9), 40.2 (CH_2) and 40.6 (CH_2), C6(12) and C8(10), 41.7 (CH, d, $J_{C\text{-}F}$ = 2.0 Hz, C5), 113.7 (CH, d, $J_{C\text{-}F}$ = 24 Hz, C2), 115.5 [CH_2, C7(11)-CH_2], 124.1 (CH, d, $J_{C\text{-}F}$ = 3.0 Hz, C4), 127.4 (CH, d, $J_{C\text{-}F}$ = 9.1 Hz, C3), 131.0 (C, d, $J_{C\text{-}F}$ = 13.1 Hz, C9a), 146.2 [C, C7(11)], 147.6 (C, d, $J_{C\text{-}F}$ = 2.5 Hz, C4a), 159.7 (C, d, $J_{C\text{-}F}$ = 242.4 Hz, C1). HRMS-ESI + m/z $[M+H]^+$ calcd for $[C_{16}H_{18}F]^+$: 229.1387, found: 229.1392.

4.1.23. 2-Methoxy-7,11-dimethylene-6,7,8,9-tetrahydro-5H-5,9-propanobenzo[7]annulene (**32**)

In a flame dried 3-necked round bottom flask, sodium hydride 60% in mineral oil (2.68 g, 67.0 mmol) was added under N_2 and was dissolved in anh DMSO (35 mL). The grey suspension was heated to 75 °C for 45 min and was then cooled to rt. Methyltriphenylphosphonium iodide (27.1 g, 67.0 mmol) dissolved in anh DMSO (57 mL) and **28** (4.00 g, 16.4 mmol) dissolved in anh DMSO (38 mL) were sequentially added under N_2. The brown solution was stirred and heated to 90 °C overnight. The black solution was allowed to cool to rt and it was then poured into H_2O (200 mL). The H_2O was extracted with hexane (4 × 200 mL) and the organic layer was dried over anh Na_2SO_4, filtered and concentrated under vacuum. The crude was purified by Combiflash® in silica gel using a solvent system of 100% hexane. Diene **32** was isolated as a yellow waxy oil (1.50 g, 38% yield), mp 68–69 °C. IR (NaCl disk) ν: 3068, 2979, 2911, 2833, 1639, 1609, 1580, 1501, 1464, 1449, 1431, 1363, 1313, 1260, 1203, 1172, 1152, 1109, 1034, 955, 929, 889, 809, 661, 613 cm^{-1}. ^{1}H NMR (400 MHz, $CDCl_3$) δ: 2.43–2.53 [complex signal, 4H, 6(12)-H_a, 8(10)-H_a], 2.55–2.64 [complex signal, 4H, 6(12)-H_b, 8(10)-H_b], 3.03 (tt, J = 4.8 Hz, J' = 4.4 Hz, 1H, 5-H), 3.07 (tt, J = 4.8 Hz, J' = 4.4 Hz, 9-H), 3.79 (s, 3H, CH_3), 4.68 [s, 4H, 7(11)-CH_2], 6.65 (dd, J = 8.0 Hz, J' = 2.8 Hz, 1H, 3-H), 6.66 (d, J = 2.8 Hz, 1H, 1-H), 7.00 (d, J = 8.0 Hz, 1H, 4-H). ^{13}C NMR (100.6 MHz, $CDCl_3$) δ: 40.7 (CH, C9), 40.9 (CH_2) and 41.2 (CH_2) C6(8,10,12), 41.9 (CH, C5), 55.2 (CH_3, OCH_3), 110.8 (CH, C3), 114.9 (CH, C1), 115.1 [CH_2, C7(11)-CH_2], 129.6 (CH, C4), 136.9 (C, C4a), 146.0 (C, C9a), 146.7 [C, C7(11)], 158.3 (C, C2). HRMS-ESI + m/z $[M+H]^+$ calcd for $[C_{17}H_{21}O]^+$: 241.1587, found: 241.1588.

4.1.24. 2-Chloro-N-(2-fluoro-9-methyl-5,6,8,9,10,11-hexahydro-7H-5,9:7,11-dimethanobenzo[9]annulen-7-yl)acetamide (**33**)

Chloroacetonitrile (84 μL, δ = 1.19, 1.32 mmol) was added to a solution of 2-fluoro-7,11-dimethylene-6,7,8,9-tetrahydro-5*H*-5,9-propanobenzo[7]annulene (75 mg, 0.32 mmol) in acetic acid (0.25 mL) and the mixture was cooled to 0–5 °C with an ice bath. Conc. H_2SO_4 (0.11 mL, δ = 1.84, 1.97 mmol) was added dropwise (<10 °C). After the addition, the mixture was allowed to reach rt and was stirred overnight. The solution was added to ice (2 g) and the mixture was stirred at rt for a few minutes. DCM (5 mL) was added, the phases were separated, and the aq phase was extracted with further DCM (2 × 5 mL). The combined organic layers were dried over anh Na_2SO_4, then filtered and evaporated *in vacuo* to give **33** as a yellow solid (50 mg, 48% yield), mp 141–144 °C. IR (NaCl disk) ν: 3399, 3313, 3067, 2944, 2920, 2851, 1657, 1607, 1591, 1518, 1498, 1451, 1361, 1345, 1252, 1179, 1145, 1086, 1049, 1009, 966, 963, 863, 820 cm^{-1}. ^{1}H NMR (400 MHz, $CDCl_3$) δ: 0.94 (s, 3H, 9-CH_3), 1.49–1.59 [complex signal, 2H, 10(13)-H_a], 1.62–1.70 [complex signal, 2 H, 10(13)-H_b], 1.81 (m, 1H, 8-H_a), 1.84 (m, 1H, 8-H_b), 2.05–2.19 [complex signal, 4H, 6(12)-H_2], 3.03 (m, 1H, 5-H or 11-H), 3.09 (m, 1H, 11-H or 5-H), 3.93 (s, 2H, CH_2Cl), 6.30 (broad s, 1H, NH), 6.73 (dd, J = 8.4 Hz, J' = 2.8 Hz, 1H, 1-H), 6.76 (m, 1H, 3-H), 7.00 (dd, J = 8.0 Hz, J' = 6.0 Hz, 1 H, 4-H). ^{13}C NMR (100.6 MHz, $CDCl_3$) δ: 32.2 (CH_3, C9–CH_3), 33.7 (C, C9), 38.5 (CH_2) and 38.9 (CH_2) (C6 and C12), 40.3 (CH, C11), 40.93 (CH, C5), 40.97 (CH_2) and 41.26 (CH_2) (C10 and C13), 43.1 (CH_2, CH_2Cl), 47.0 (CH_2, C8), 55.0 (C, C7), 112.5 (CH, d, $J_{C\text{-}F}$ = 20 Hz, C1), 115.0 (CH, d, $J_{C\text{-}F}$ = 21 Hz, C3), 129.6 (CH, d, $J_{C\text{-}F}$ = 8 Hz, C4), 141.9 (C, d, $J_{C\text{-}F}$ = 3 Hz, C4a), 148.2 (C, d, $J_{C\text{-}F}$ = 6.9 Hz, C11a), 161.4 (C, d, $J_{C\text{-}F}$ = 244 Hz, C2), 164.7 (C, NHCO). HRMS-ESI + m/z $[M+H]^+$ calcd for $[C_{18}H_{22}ClFNO]^+$: 322.1368, found: 322.137.

4.1.25. 2-Chloro-N-(2,3-dimethoxy-9-methyl-5,6,8,9,10,11-hexahydro-7H-5,9:7,11-dimethanobenzo[9]annulen-7-yl)acetamide (**34**)

Diene **30** (498 mg, 1.84 mmol) was dissolved in glacial acetic acid (1.6 mL) and chloroacetonitrile (467 μL, δ = 1.19, 7.38 mmol) was added. The solution was cooled to 0 °C and conc. H_2SO_4 (601 μL, δ = 1.84, 11.0 mmol) was added dropwise with care not to raise above 10 °C. The solution was allowed to warm to rt and was left stirring overnight, then it was poured over ice (2 g) and extracted with DCM (3 × 10 mL). The organic layer was dried over anh Na_2SO_4, then filtered and concentrated under vacuum. The crude was crystallized from DCM to obtain **34** as a white solid (501 mg, 75% yield), mp 204–205 °C. IR (NaCl disk) ν: 3306, 2941, 2907, 2861, 2838, 1666, 1605, 1516, 1467, 1452, 1415, 1381, 1361, 1345, 1293, 1252, 1231, 1191, 1168, 1092, 1021, 948, 861, 802 cm^{-1}. ^{1}H NMR (400 MHz, $CDCl_3$) δ: 0.93 (s, 3H, 9-CH_3), 1.55 [d, J = 13.2 Hz, 2H, 10(13)-H_a], 1.65 [dd, J = 13.2 Hz, J' = 6 Hz, 2H, 10(13)-H_b], 1.83 (s, 2H, 8-H_2), 2.07 [d, J = 12.8 Hz, 2H, 6(12)-H_a], 2.15 [ddd, J = 12.8 Hz, J' = 6.4 Hz, J'' = 2.0 Hz, 2H, 6(12)-H_b], 3.00 [t, J = 6.4 Hz, 2H, 5(11)-H], 3.84 (s, 6H, OCH_3), 3.93 (s, 2H, CH_2–Cl), 6.29 (broad s., 1H, NH), 6.60 [s, 2H, 1(4)-H]. ^{13}C NMR (100.6 MHz, $CDCl_3$) δ: 32.3 (CH_3, C9–CH_3), 33.7 (C, C9), 39.0 [CH_2, C6(12)], 40.7 [CH, C5(11)], 41.4 [CH_2, C10(13)], 43.1 (CH_2, CH_2–Cl), 47.1 (CH_2, C8), 55.1 (C, C7), 56.2 (CH_3, OCH_3), 112.4 [CH, C1(4)], 138.4 [C, C4a(11a)], 146.8 [C, 2(3)], 164.7 (C, NHCO). HRMS-ESI + m/z $[M+H]^+$ calcd for $[C_{20}H_{27}ClNO_3]^+$: 364.1674, found: 364.1674.

*4.1.26. 2-Chloro-N-(1-fluoro-9-methyl-5,6,8,9,10,11-hexahydro-7H-5,9:7,11-dimethanobenzo[9]annulen-7-yl)acetamide (**35**)*

Chloroacetonitrile (2.7 mL, δ = 1.19, 42.7 mmol) was added to a solution of diene **31** (2.37 g, 10.4 mmol) in acetic acid (7 mL) and the mixture was cooled to 0–5 °C with an ice bath. Conc. H_2SO_4 (3.4 mL, δ = 1.84, 63.8 mmol) was added dropwise (<10 °C). After the addition, the mixture was allowed to reach rt and stirred overnight. The solution was added to ice (10 g) and the mixture was stirred at rt for few minutes. DCM (100 mL) was added, the phases were separated, and the aqueous phase was extracted with further DCM (2 × 100 mL). The combined organic layers were dried over anh Na_2SO_4, filtered and evaporated *in vacuo* to give **35** as a white solid (2.28 g, 68% yield), mp 154–155 °C. IR (NaCl disk) ν: 3402, 3308, 3073, 2947, 2911, 2863, 2840, 1660, 1613, 1583, 1529, 1463, 1363, 1348, 1312, 1242, 1186, 1155, 1069, 1053, 979, 875, 798, 748 cm^{-1}. ^{1}H-RMN (400 MHz, $CDCl_3$) δ: 0.93 (s, 3H, 9-CH_3), 1.45–1.61 (complex signal, 2H, 10-H_a, 13-H_a), 1.63–1.71 (complex signal, 2H, 10-H_b, 13-H_b), 1.80 (dt, J = 12.0 Hz, J' = 2.0 Hz, 1H, 8-H_a), 1.87 (dt, J = 12.0 Hz, J' = 2.0 Hz, 1H, 8-H_b), 2.08–2.11 (complex signal, 2H, 6-H_2 or 12-H_2), 2.14–2.17 (complex signal, 2H, 12-H_2, 6-H_2), 3.13 (m, 1H, 5-H), 3.73 (tm, J = 6.0 Hz, 1H, 11-H), 3.93 (s, 2H, CH_2Cl), 6.31 (broad s., 1H, NH), 6.84 (d, J = 8.0 Hz, 1H, 4-H), 6.86 (dd, J = 8.4 Hz, J' = 1.2 Hz, 1H, 2-H) 7.01 (m, 1 H, 3-H). ^{13}C NMR (100.6 MHz, $CDCl_3$) δ: 28.6 (CH, d, $J_{C\text{-}F}$ = 5.7 Hz, C11), 32.2 (CH_3, C9–$\underline{C}H_3$), 33.81 (C, C9), 38.3 (CH_2) and 38.4 (CH_2) (C6 and C12), 40.6 ($\underline{C}H_2$) and 40.96 (CH_2) (C10 and C13), 41.03 (CH, d, J = 2.3 Hz, C5), 43.1 (CH_2, $\underline{C}H_2Cl$), 47.0 (CH_2, C8), 55.0 (C, C7), 113.5 (CH, d, $J_{C\text{-}F}$ = 24.8 Hz, C2), 123.6 (CH, d, $J_{C\text{-}F}$ = 3.1 Hz, C4), 127.2 (CH, d, $J_{C\text{-}F}$ = 9.3 Hz, C3), 132.6 (CH, d, $J_{C\text{-}F}$ = 13.2 Hz, C11a), 149.3 (C, d, $J_{C\text{-}F}$ = 2.2 Hz, C4a), 159.3 (C, d, $J_{C\text{-}F}$ = 243.5 Hz, C1), 164.7 (C, NH$\underline{C}$O). HRMS-ESI + *m/z* $[M+H]^+$ calcd for $[C_{18}H_{22}ClFNO]^+$: 322.1368, found: 322.1374.

*4.1.27. 2-Chloro-N-(2-methoxy-9-methyl-5,6,8,9,10,11-hexahydro-7H-5,9:7,11-dimethanobenzo[9]annulen-7-yl)acetamide (**36**)*

Diene **32** (1.50 g, 6.24 mmol) was dissolved in glacial acetic acid (4.8 mL) and chloroacetonitrile (1.58 mL, δ = 1.19, 24.9 mmol) was added. The solution was cooled to 0 °C and conc. H_2SO_4 (2.00 mL, δ = 1.84, 37.5 mmol) was added dropwise with care not to raise above 10 °C. The dark red solution was allowed to warm to rt and was left stirring overnight. The dark red solution was poured over ice (5 g) and it was then extracted with DCM (3 × 20 mL). The organic layer was washed with 10 N NaOH solution (1 × 20 mL), dried over anh Na_2SO_4, then filtered and concentrated under vacuum to give a brown solid (1.18 g, 57% yield), mp 144–145 °C. IR (NaCl disk) ν: 3403, 3304, 3062, 2997, 2945, 2905, 2860, 2838, 1662, 1609, 1582, 1528, 1499, 1454, 1382, 1361, 1311, 1267, 1242, 1198, 1180, 1154, 1043, 1013, 955, 873 cm^{-1}. ^{1}H NMR (400 MHz, $CDCl_3$) δ: 0.93 (s, 3H, 9-CH_3), 1.48–1.59 [complex signal, 2H, 10(13)-H_a], 1.61–1.70 [complex signal, 2H, 10(13)-H_b], 1.82 (dm, J = 12.0 Hz, 1H, 8-H_a), 1.86 (dm, J = 12.0 Hz, 1H, 8-H_b), 2.00–2.10 [complex signal, 2H, 6(12)-H_a], 2.10–2.21 [complex signal, 2H, 6(12)-H_b), 2.99–3.09 [complex signal, 2H, 5(11)-H], 3.77 (s, 3H, OCH_3), 3.92 (s, 2H, CH_2–Cl), 6.60 (dd, J = 8.0 Hz, J' = 2.8 Hz, 1H, 3-H), 6.63 (d, J = 2.8 Hz, 1-H), 6.97 (d, J = 8.0 Hz, 1H, 4-H). ^{13}C NMR (100.6 MHz, $CDCl_3$) δ: 32.3 (CH_3, C9–$\underline{C}H_3$), 33.7 (C, C9), 38.8 (CH_2) and 39.2 (CH_2) (C6 and C12), 40.1 (CH) and 41.2 (CH) (C5 and C11), 41.2 (CH_2) and 41.6 (CH_2) (C10 and C13), 43.0 (CH_2, $\underline{C}H_2$–Cl), 47.0 (CH_2, C8), 54.8 (C, C7), 55.3 (CH_3, O$\underline{C}H_3$), 110.6 (CH, C3), 114.3 (CH, C1), 129.2 (CH, C4), 138.5 (C, C4a), 147.5 (C, C11a), 158.1 (C, C2), 164.6 (C, NH$\underline{C}$O). HRMS-ESI + *m/z* $[M+H]^+$ calcd for $[C_{19}H_{25}ClNO_2]^+$: 334.1568, found: 334.1569.

*4.1.28. 2-Fluoro-9-methyl-5,6,8,9,10,11-hexahydro-7H-5,9:7,11-dimethanobenzo[9]annulen-7-amine hydrochloride (**37**)*

Thiourea (15 mg, 0.20 mmol) and glacial acetic acid (0.1 mL) were added to a solution of **33** (50 mg, 0.16 mmol) in absolute ethanol (3 mL) and the mixture was heated at reflux overnight. The resulting suspension was then tempered to rt and concentrated under vacuum. Crude was partitioned in H_2O (2 mL) and DCM (3 mL) and the phases were separated. Then the pH of the aq phase was adjusted to 12 with 5 N NaOH solution and extracted with further DCM (3 × 3 mL). The combined organic layers were dried over anh Na_2SO_4, filtered and concentrated *in vacuo* to obtain amine **37**. Its hydrochloride was obtained by adding an excess of HCl/Et_2O to a solution of the amine in ethyl acetate, followed by filtration of the resulting white precipitate (16 mg, 36% yield), mp > 300 °C (dec.) IR (KBr disk) ν: 3200–2500 (2983, 2945, 2917, 2867), 2059, 1612, 1595, 1501, 1456, 1444, 1431, 1379, 1364, 1302, 1283, 1256, 1246, 1186, 1157, 1143, 1132, 1030, 1004, 962, 863, 814 cm^{-1}. ^{1}H NMR (400 MHz, MeOD) δ: 1.0 (s, 3H, 9-CH_3), 1.51–1.61 [complex signal, 2H, 10(13)H_a], 1.68 (s, 2H, 8-H_2), 1.68–1.75 [complex signal, 2H, 10(13)-H_b], 1.82–1.91 [complex signal, 2 H, 6(12)-H_a], 2.00–2.08 [complex signal, 4H, 6(12)-H_b], 3.18 (tm, J = 6.2 Hz, 1H, 5-H or 11-H), 3.23 (tm, J = 6.2 Hz, 1H, 11-H or 5-H), 6.81 (td, J = 8.4 Hz, J' = 2.8 Hz, 3-H), 6.87 (dd, J = 9.4 Hz, J' = 2.8 Hz, 1-H), 7.11 (dd, J = 8.4 Hz, J' = 5.6 Hz, 1 H, 4-H). ^{13}C NMR (100.6 MHz, MeOD) δ: 32.2 (CH_3, C9–$\underline{C}H_3$), 34.7 (C, C9), 39.0 (CH_2) and 39.3 (CH_2) (C6 and C12), 40.8 (CH) and 41.4 (CH) (C5 and C11), 41.3 (CH_2) and 41.6 (CH_2) (C10 and C13), 47.1 (CH_2, C8), 55.3 (C, C7), 113.8 (CH, d, $J_{C\text{-}F}$ = 20 Hz, C3), 115.9 (CH, d, $J_{C\text{-}F}$ = 22 Hz, C1), 131.0 (CH, d, $J_{C\text{-}F}$ = 8.1 Hz, C4), 142.5 (C, d, $J_{C\text{-}F}$ = 3 Hz, C4a), 148.8 (C, d, $J_{C\text{-}F}$ = 7.1 Hz, C11a), 162.9 (C, d, $J_{C\text{-}F}$ = 243 Hz, C2). HRMS-ESI + *m/z* $[M+H]^+$ calcd for $[C_{16}H_{21}FN]^+$: 246.1653, found: 246.1649.

*4.1.29. 2,3-Dimethoxy-9-methyl-5,6,8,9,10,11-hexahydro-7H-5,9:7,11-dimethanobenzo[9]annulen-7-amine hydrochloride (**38**)*

Chloroacetamide **34** (436 mg, 1.20 mmol) was dissolved in abs. ethanol (23 mL) and glacial acetic acid (0.75 mL). Thiourea (109 mg, 1.44 mmol) was added, and the solution was left stirring overnight at reflux. The yellow solution was concentrated under vacuum and the solid was dissolved in MeOH (10 mL). HCl/Et_2O was added, and the solution was concentrated to dryness. The off-white solid was washed with DCM (2 × 3 mL). The combined supernatants were concentrated under vacuum to obtain the hydrochloride of **38** as a white solid (315 mg, 81% yield), mp > 200 °C (dec.). IR (KBr disk) ν: 3200–2500 (2993, 2918, 2831), 2047, 1701, 1606, 1517, 1451, 1416, 1386, 1365, 1327, 1310, 1291, 1252, 1237, 1192, 1174, 1131, 1098, 1031, 973, 950, 863, 798, 586, 543 cm^{-1}. ^{1}H NMR (400 MHz, $CDCl_3$) δ: 0.95 (s, 3H, 9-CH_3), 1.55 [d, J = 13.6 Hz, 2H, 10(13)-H_a], 1.63 [dd, J = 13.6 Hz, J' = 6.0 Hz, 2H, 10(13)-H_b], 1.80 (s, 2H, 8-CH_2), 2.04 [d, J = 12.6 Hz, 2H, 6(12)-H_a], 2.15 [dd, J = 12.6 Hz, J' = 6.0 Hz, 2H, 6(12)-H_b], 3.01 [t, J = 5.2 Hz, 2H, 5(11)-H], 3.83 (s, 6H, OCH_3), 6.58 [s, 2H, 1(4)-H], 8.38 (broad s., 3H, 7C–N$\underline{H}_3^+$). ^{13}C NMR (100.6 MHz, $CDCl_3$) δ: 31.9 (CH_3, C9–$\underline{C}H_3$), 33.9 (C, C9), 38.6 [CH_2, C6(12)], 40.1 [CH, C5(11)], 40.7 [CH_2, C10(13)], 46.5 (CH_2, C8), 55.7 (C, C7), 56.2 (CH_3, O$\underline{C}H_3$), 112.5 [CH, C1(4)], 137.4 [C, C4a(11a)], 147.1 [C, 2(3)]. HRMS-ESI + *m/z* $[M+H]^+$ calcd for $[C_{18}H_{26}NO_2]^+$: 288.1958, found: 288.1954.

*4.1.30. 1-Fluoro-9-methyl-5,6,8,9,10,11-hexahydro-7H-5,9:7,11-dimethanobenzo[9]annulen-7-amine hydrochloride (**39**)*

Thiourea (284 mg, 3.73 mmol) and glacial acetic acid (2 mL) were added to a solution of **35** (1.00 g, 3.11 mmol) in abs. ethanol (54 mL) and the mixture was heated at reflux overnight. The resulting suspension was then tempered to rt and concentrated under vacuum. Crude was partitioned in H_2O (40 mL) and DCM (30 mL) and the phases were separated. Then the pH of the aq phase was adjusted to 12 with 5 N NaOH solution and extracted with further DCM (3 × 30 mL). The combined organic layers were dried over anh Na_2SO_4, then filtered and concentrated *in vacuo*. The hydrochloride of **39** was obtained by adding an excess of HCl/Et_2O

to a solution of the amine in ethyl acetate followed by filtration of the resulting white precipitate (732 mg, 84% yield). The analytical sample was obtained by crystallization from methanol, mp > 200 °C (dec.). IR (KBr disk) ν: 3200–2500 (2945, 2717, 2586), 2060, 1677, 1608, 1584, 1511, 1464, 1380, 1366, 1317, 1303, 1248, 1214, 1199, 1165, 1132, 1071, 1052, 1032, 1000, 977, 946, 885, 877, 854, 798, 747, 623 cm^{-1}. ^1H NMR (400 MHz, MeOD) δ: 1.0 (s, 3H, CH_3), 1.50 [d, J = 14.0 Hz, 1H, 10-H_a or13-H_a], 1.57 (d, J = 14.0 Hz, 1H, 13-H_a or 10-H_a), 1.72 (s, 2H, 8-H_2), 1.68–1.75 [complex signal, 2H, 10(13)-H_b], 1.79 (d, J = 12.8 Hz, 1H, 6-H_a or 12-H_a) 1.86 (d, J = 12.8 Hz, 1H, 12-H_a or 6-H_a), 2.00–2.08 (complex signal, 2H, 6-H_b, 12-H_b), 3.27 (m, 1H, 5-H), 3.80 (t, J = 6.2 Hz, 11-H), 6.90 (ddd, J = 8.4 Hz, J' = 8.0 Hz, J'' = 1.4 Hz, 1H, 2-H), 6.92 (m, 1H, 4-H), 7.09 (ddd, J = 8.4 Hz, J' = 7.6 Hz, J'' = 5.6 Hz, 1H, 3-H). ^{13}C NMR (100.6 MHz, MeOD) δ: 29.5 (CH, d, $J_{C\text{-}F}$ = 6 Hz, C11), 32.7 (CH_3, C9–$\underline{C}H_3$), 34.7 (C, C9), 38.6 (CH_2) and 39.0 (CH_2) (C6 and C12), 40.9 (CH_2) and 41.3 (CH_2) (C10 and C13), 41.6 (CH, d, $J_{C\text{-}F}$ = 3 Hz, C5), 47.0 (CH_2, C8), 55.3 (C, C7), 114.7 (CH, d, $J_{C\text{-}F}$ = 25 Hz, C2), 125.2 (CH, d, $J_{C\text{-}F}$ = 4 Hz, C4), 129.1 (CH, d, $J_{C\text{-}F}$ = 10 Hz, C3), 132.8 (CH, d, $J_{C\text{-}F}$ = 14.1 Hz, C11a), 149.7 (C, d, $J_{C\text{-}F}$ = 2 Hz, C4a), 160.4 (C, d, $J_{C\text{-}F}$ = 242.4 Hz, C1). HRMS-ESI + m/z $[M+H]^+$ calcd for $[C_{16}H_{21}FN]^+$: 246.1653, found: 246.1649.

4.1.31. 2-Methoxy-9-methyl-5,6,8,9,10,11-hexahydro-7H-5,9:7,11-dimethanobenzo[9]annulen-7-amine hydrochloride (**40**)

Chloroacetamide **36** (1.10 g, 3.29 mmol) was dissolved in abs. ethanol (60 mL) and glacial acetic acid (2.2 mL). Thiourea (300 mg, 3.94 mmol) was added and the orange solution was left stirring overnight. The orange solution was concentrated under vacuum and the solid was dissolved in MeOH (10 mL). HCl/Et_2O was added, the solution was concentrated, and the off-white solid was extracted with DCM (2 × 3 mL). The combined supernatants were concentrated under vacuum to obtain **40** as a brown solid that was crystallized from DCM/pentane (779 mg, 81% yield), mp > 200 °C (dec.). IR (KBr disk) ν: 3200–2500 (2985, 2942, 2908), 2056, 1735, 1609, 1582, 1499, 1449, 1379, 1364, 1334, 1305, 1268, 1252, 1205, 1170, 1132, 1103, 1040, 1001, 954, 869, 849, 815, 756, 692 cm^{-1}. ^1H NMR (400 MHz, CD_3OD) δ: 0.99 (s, 3H, 9-CH_3), 1.50–1.59 [complex signal, 2H, 10(13)-H_a], 1.65 (s, 2H, 8-CH_2), 1.65–1.73 [complex signal, 2H, 10(13)-H_b], 1.79–1.89 [complex signal, 2H, 6(12)-H_a], 1.97–2.06 [complex signal, 2H, 6(12)-H_b], 3.10–3.18 [complex signal, 2H, 5(11)-H], 3.74 (s, 3H, OCH_3), 6.64 (dd, J = 8.0 Hz, J' = 2.8 Hz, 1H, 3-H), 6.67 (d, J = 2.8 Hz, 1H, 1-H), 7.00 (d, J = 8.0 Hz, 4-H). ^{13}C NMR (100.6 MHz, CD_3OD) δ: 32.3 (CH_2, 9-$\underline{C}H_3$), 34.6 (C, C9), 39.3 (CH_2) and 39.6 (CH_2) (C6 and C12), 40.8 (CH) and 41.6 (CH) (C5 and C11), 41.7 (CH_2) and 42.0 (CH_2) (C10 and C13), 47.2 (CH_2, C8), 55.5 (C, C7), 55.7 (CH_3, O$\underline{C}H_3$) 112.1 (CH, C3), 115.2 (CH, C1), 130.3 (CH, C4), 138.6 (C, C4a), 147.7 (C, C11a), 159.9 (C, C2). HRMS-ESI + m/z $[M+H]^+$ calcd for $[C_{17}H_{24}NO]^+$: 258.1852, found: 258.1862.

4.1.32. 1-Fluoro-11-methylene-6,7,8,9-tetrahydro-5H-5,9-propanobenzo[7]annulen-7-one (**41**)

In a flame dried 3-necked round bottom flask, sodium hydride 60% dispersion in mineral oil (1.01 g, 25.2 mmol) was added under N_2 and was dissolved in anh DMSO (50 mL). The grey suspension was heated to 90 °C for 45 min and was then cooled to rt. After the reaction mixture was tempered, a solution of triphenylmethylphophonium iodide (10.6 g, 26.2 mmol) in anh DMSO (58 mL) was added and the resulting yellow solution was stirred at rt for 20 min. Then a suspension of diketone **27** (4.72 g, 20.3 mmol) in anh DMSO (50 mL) was added and the obtained solution was heated to 90 °C overnight. The resulting black solution was allowed to cool to rt and then poured into H_2O (200 mL). The H_2O was extracted with hexane (4 × 200 mL) and the organic layer was dried over anh Na_2SO_4, filtered and concentrated under vacuum. The crude was purified by Combiflash® using as eluent a gradient from pure hexane to an ethyl acetate/hexane mixture (2.5/7.5). The product **41** was isolated as a yellow solid (2.16 g, 46% yield), mp 96 °C. IR (ATR) ν: 2928, 2913, 2895, 2849, 1688, 1612, 1583, 1462, 1432, 1406, 1366, 1247, 1196, 1104, 1049, 1034, 1002, 970, 921, 911, 883, 819, 789, 749, 657 cm^{-1}. ^1H NMR (400 MHz, $CDCl_3$) δ: 2.39 (d, J = 13.2 Hz, 1H, 10-H_a or 12-H_a), 2.46 (d, J = 12.4 Hz, 1H, 10-H_a or 12-H_a), 2.48–2.62 [complex signal, 2H, 6(8)-H_a], 2.64–2.72 [complex signal, 2H, 10(12)-H_b], 2.83–2.91 [complex signal, 2H, 6(8)-H_b], 3.22 (m, 1H, 5-H), 3.80 (m, 1H, 9-H), 4.96 (complex signal, C=C$\underline{H}_2$), 6.97 (ddd, J = 8.4 Hz, J' = 1.6 Hz, 1H, 2-H), 6.99 (d, J = 8.0 Hz, 4-H), 7.15 (ddd, J = 8.4 Hz, J' = 7.6 Hz, J'' = 5.6 Hz, 1H, 3-H). ^{13}C NMR (100.6 MHz, $CDCl_3$) δ: 28.3 (CH, d, $J_{C\text{-}F}$ = 5 Hz, C9), 40.4 (CH, d, $J_{C\text{-}F}$ = 3 Hz, C5), 41.4 (CH_2) and 41.7 (CH_2) (C10 and C12), 48.1 (CH_2) and 48.5 (CH_2) (C6 and C8), 114.3 (CH, d, $J_{C\text{-}F}$ = 24 Hz, C2), 120.3 (CH_2, 11-$\underline{C}H_2$), 124.1 (CH, d, $J_{C\text{-}F}$ = 3 Hz, C4), 128.3 (CH, d, $J_{C\text{-}F}$ = 9 Hz, C3), 131.2 (C, d, $J_{C\text{-}F}$ = 14.1 Hz, C9a), 143.4 (C, C11), 147.5 (C, d, $J_{C\text{-}F}$ = 3 Hz, C4a), 159.5 (C, d, $J_{C\text{-}F}$ = 244.5 Hz, C1), 211.2 [C, C7–$\underline{C}O$]. HRMS-ESI + m/z $[M+H]^+$ calcd for $[C_{15}H_{16}FO]^+$: 231.1180, found: 231.1180.

4.1.33. 2-Chloro-N-(1-fluoro-9-hydroxy-5,6,8,9,10,11-hexahydro-7H-5,9:7,11-dimethanobenzo[9]annulen-7-yl)acetamide (**42**)

Chloroacetonitrile (0.62 mL, δ = 1.19, 9.77 mmol) was added to a solution of **41** (2.06 g, 8.94 mmol) in DCM (21 mL) and the mixture was cooled to 0–5 °C with an ice bath. Conc. H_2SO_4 (0.75 mL, δ = 1.84, 14.1 mmol) was added dropwise (<10 °C). After the addition, the mixture was allowed to reach rt and stirred overnight. The solution was added to ice (10 g) and the mixture was stirred at rt for a few minutes. DCM (15 mL) was added, the phases were separated, and the aq phase was extracted with further DCM (2 × 15 mL). The combined organic layers were dried over anh Na_2SO_4, then filtered and evaporated *in vacuo* to give **42** as a white solid (921 mg, 32% yield), mp 150 °C. IR (ATR) ν: 3406, 3272, 3217, 3075, 2926, 2905, 2850, 1661, 1585, 1561, 1466, 1443, 1428, 1409, 1362, 1341, 1311, 1298, 1243, 1218, 1158, 1105, 1037, 991, 974, 891, 884, 791, 744, 734, 679, 625 cm^{-1}. ^1H NMR (400 MHz, $CDCl_3$) δ: 1.67–1.80 [complex signal, 2H, 10(13)-H_a], 1.93–2.00 [complex signal, 2H, 10(13)-H_b], 2.02–2.22 [complex signal, 4H, 6(12)-H_2], 3.24 (m, 1H, 5-H), 3.84 (t, J = 6.8 Hz, 1H, 11-H), 3.93 (s, 2H, CH_2Cl), 6.38 (broad s., 1H, NH), 6.86–6.91 [complex signal, 2 H, 2(4)-H], 7.05 (ddd, J = 8.2 Hz, J' = 7.6 Hz, J'' = 5.6 Hz, 1H, 3-H). ^{13}C NMR (100.6 MHz, $CDCl_3$) δ: 27.8 (CH, d, $J_{C\text{-}F}$ = 6 Hz, C11), 37.9 (CH_2) and 38.0 (CH_2) (C6 and C12), 39.9 (CH, d, J = 3 Hz, C5), 41.9 (CH_2) and 42.2 (CH_2) (C10 and C13), 43.0 (CH_2, $\underline{C}H_2Cl$), 48.0 (CH_2, C8), 57.4 (C, C7), 70.8 (C, C9), 113.8 (CH, d, $J_{C\text{-}F}$ = 24 Hz, C2), 123.7 (CH, d, $J_{C\text{-}F}$ = 3 Hz, C4), 127.6 (CH, d, $J_{C\text{-}F}$ = 9 Hz, C3), 131.6 (CH, d, $J_{C\text{-}F}$ = 13.1 Hz, C11a), 148.2 (C, d, $J_{C\text{-}F}$ = 2 Hz, C4a), 159.2 (C, d, $J_{C\text{-}F}$ = 243.5 Hz, C1), 164.9 (C, N$\underline{H}\underline{C}O$). HRMS-ESI + m/z $[M+H]^+$ calcd for $[C_{17}H_{20}ClFNO_2]^+$: 324.1161, found: 324.1162.

4.1.34. 2-Chloro-N-(1,9-difluoro-5,6,8,9,10,11-hexahydro-7H-5,9:7,11-dimethanobenzo[9]annulen-7-yl)acetamide (**43**)

A solution of chloroacetamide **42** (611 mg, 1.89 mmol) in DCM (10 mL) was cooled to −30 °C. Then, DAST (2.8 mL, 1 M solution in DCM, 2.8 mmol) was added and the reaction mixture was stirred at rt overnight. To the resulting solution was added H_2O (10 mL) and the pH adjusted to 12 with 5 N NaOH solution. The phases were separated, and the aq phase was extracted with further DCM (3 × 10 mL), and the combined organic layers were dried over anh Na_2SO_4, then filtered and concentrated *in vacuo*. The crude was purified by Combiflash® in silica gel using as eluent a gradient from pure hexane to ethyl acetate/hexane mixture (6/4) to give **43** as a white solid (420 mg, 69% yield), mp 180 °C. IR (ATR) ν: 3276, 3075, 2964, 2940, 2901, 2858, 1671, 1650, 1584, 1552, 1463, 1442, 1360,

1337, 1331, 1317, 1282, 1242, 1219, 1175, 1143, 1104, 1018, 1066, 1018, 1004, 979, 901, 887, 865, 799, 746, 737, 696, 662 cm^{-1}. ^1H NMR (400 MHz, $CDCl_3$) δ: 1.85–1.92 [complex signal, 2H, 6(12)-H_a], 2.01–2.12 [complex signal, 2H, 10(13)-H_a], 2.13–2.24 [complex signal, 4H, 6(10,12,13)-H_b], 2.24–2.35 (complex signal, 2H, 8-H_2), 3.31 (m, 1H, 5-H), 3.90 (m, 1H, 11-H), 3.94 (s, 2H, CH_2Cl), 6.40 (broad s., 1H, NH), 6.88 (m, 1H, 4-H), 6.93 (ddd, J = 8.8 Hz, J' = 8.4 Hz, J'' = 1.6 Hz, 1H, 2-H), 7.07 (ddd, J = 8.4 Hz, J' = 7.2 Hz, J'' = 5.2 Hz, 1H, 3-H). ^{13}C NMR (100.6 MHz, $CDCl_3$) δ: 27.4 (CH, dd, $J_{C\text{-}F}$ = 13.6 Hz, J'_{C-F} = 6.4 Hz, C11), 37.8 (CH_2, d, $J_{C\text{-}F}$ = 1.1 Hz, C6 or C12), 37.9 (CH_2, d, $J_{C\text{-}F}$ = 1.0 Hz, C12 or C6), 39.4 (CH, dd, $J_{C\text{-}F}$ = 13.3 Hz, J'_{C-F} = 2.4 Hz, C5), 39.7 (CH_2, d, $J_{C\text{-}F}$ = 19.5 Hz, C10 or C13), 39.8 (CH_2, d, $J_{C\text{-}F}$ = 20.4 Hz, C13 or C10), 43.0 (CH_2, $\underline{C}H_2Cl$), 45.7 (CH_2, d, $J_{C\text{-}F}$ = 19 Hz, C8), 58.1 (C, d, $J_{C\text{-}F}$ = 11 Hz, C7), 93.0 (C, d, $J_{C\text{-}F}$ = 178.1 Hz, C9), 114.1 (CH, d, $J_{C\text{-}F}$ = 24.8 Hz, C2), 123.8 (CH, d, $J_{C\text{-}F}$ = 3.2 Hz, C4), 127.9 (CH, d, $J_{C\text{-}F}$ = 9.3 Hz, C3), 131.2 (CH, d, $J_{C\text{-}F}$ = 13.4 Hz, C11a), 147.7 (C, d, $J_{C\text{-}F}$ = 2.1 Hz, C4a), 159.2 (C, d, $J_{C\text{-}F}$ = 244.1 Hz, C1), 164.9 (C, NHCO). HRMS-ESI + *m/z* $[M+H]^+$ calcd for $[C_{17}H_{19}ClF_2NO]^+$: 326.1118, found: 326.1116.

4.1.35. 1,9-Difluoro-5,6,8,9,10,11-hexahydro-7H-5,9:7,11-dimethanobenzo[9]annulen-7-amine hydrochloride (**44**)

Thiourea (56 mg, 0.74 mmol) and glacial acetic acid (0.46 mL) were added to a solution of **43** (240 mg, 0.74 mmol) in absolute ethanol (14 mL) and the mixture was heated at reflux overnight. The resulting suspension was then tempered to rt and concentrated under vacuum. Crude was partitioned in H_2O (30 mL) and DCM (30 mL) and the phases were separated. Then the pH of the aq phase was adjusted to 12 with 5 N NaOH solution and extracted with further DCM (3 × 40 mL). The combined organic layers were dried over anh Na_2SO_4, then filtered and concentrated *in vacuo*. The hydrochloride of **44** was obtained by adding an excess of HCl/Et_2O to a solution of the amine in ethyl acetate, followed by filtration of the resulting white precipitate (167 mg, 79% yield). The analytical sample was obtained by crystallization from methanol, mp > 200 °C (dec.) IR (ATR) ν: 3000–2700 (2981, 2950, 2911, 2867, 2831), 2063, 1611, 1588, 1509, 1465, 1445, 1363, 1321, 1246, 1194, 1105, 1095, 1008, 1002, 988, 967, 903, 888, 860, 801, 743, 673 cm^{-1}. ^1H-RMN (400 MHz, MeOD) δ: 1.74–1.96 [complex signal, 4 H, 6(10,12,13)-H_a], 2.07–2.15 [complex signal, 4H, 6(12)-H_b and 8-H_2], 2.15–2.26 [complex signal, 2H, 10(13)-H_b], 3.48 (broad s, 1H, 5-H), 3.99 (t, J = 5.6 Hz, 1H, 11-H), 6.98 (ddd, J = 8.8 Hz, J' = 8.0 Hz, J'' = 1.2 Hz, 1H, 2-H), 7.00 (m, 1H, 4-H), 7.17 (ddd, J = 8.4 Hz, J' = 8.0 Hz, J'' = 5.6 Hz, 1H, 3-H). ^{13}C NMR (100.6 MHz, MeOD) δ: 28.4 (CH, dd, $J_{C\text{-}F}$ = 13.4 Hz, J'_{C-F} = 6.9 Hz, C11), 38.0 (CH_2, C6 or C12), 38.4 (CH_2, C12 or C6), 39.8 (CH_2, d, $J_{C\text{-}F}$ = 21.0 Hz, C10 or C13), 40.0 (CH, dd, $J_{C\text{-}F}$ = 13.1 Hz, J'_{C-F} = 2.1 Hz, C5), 40.2 (CH_2, d, $J_{C\text{-}F}$ = 20.8 Hz, C13 or C10), 45.8 (CH_2, d, $J_{C\text{-}F}$ = 20.6 Hz, C8), 58.0 (C, d, $J_{C\text{-}F}$ = 11.1 Hz, C7), 93.9 (C, d, $J_{C\text{-}F}$ = 179.9 Hz, C9), 115.2 (CH, d, $J_{C\text{-}F}$ = 25 Hz, C2), 125.2 (CH, d, $J_{C\text{-}F}$ = 4 Hz, C4), 129.6 (CH, d, $J_{C\text{-}F}$ = 9 Hz, C3), 131.7 (CH, d, $J_{C\text{-}F}$ = 13 Hz, C11a), 148.3 (C, C4a), 160.3 (C, d, $J_{C\text{-}F}$ = 243.4 Hz, C1). HRMS-ESI + *m/z* $[M+H]^+$ calcd for $[C_{15}H_{18}F_2N]^+$: 250.1402, found: 250.1401.

4.2. Intracellular calcium-based determination of IC_{50} of NMDAR channel blockers

A functional assay of antagonist activity at NMDA receptors was performed using primary cultures of rat cerebellar granule neurons that were prepared according to established protocols [49]. Cells were grown on 10 mm poly-L-lysine coated round glass cover slips and used for the experiments after 6–9 days *in vitro*. Cells were loaded with 6 μM Fura-2 AM (ThermoFisher) for 30 min. After loading, a coverslip was mounted on a quartz cuvette containing a Mg^{2+}-free Locke-HEPES buffer using a specialized holder. Measurements were performed using a PerkinElmer LS-55 fluorescence spectrometer equipped with a fast filter accessory, under mild agitation and at 37 °C. Analysis from each sample was recorded real-time over 1600 s. After stimulation with NMDA (100 μM, in the presence of 10 μM glycine), increasing concentrations of the compound to be tested were added after signal stabilization. The percentage of inhibition at every tested concentration was analyzed using non-linear regression curve fitting (variable slope) using the software Prism 5.04 (GraphPad Software Inc.).

4.3. Molecular docking and MD simulations

To understand structural aspects of ligand binding using molecular docking and MD simulations, we used an MD-refined computational structural model of the NMDAR (GluN1/2A) transmembrane domain with the channel gate closed. Simulations of receptor-bound **IIa**, **IIb**, **IIc** and **6** were initiated with the compounds in their protonated forms docked into the channel oriented in a "flipped down" conformation such that their amines were interacting with the asparagine (ASN) cluster on the tip of M2 helices. Docking was performed in AutoDock Vina [106], which predicts interactions between small molecules and proteins. Protein and ligand coordinate files were converted to pdbqt format using AutoDock Tools, where non-polar hydrogen atoms were merged to the bonded heavy atoms. The active site of the protein was designated as a box with size of 26 × 26 × 40 at 1 Å grid spacing.

Docked receptor-ligand complexes of NMDAR-**IIa**, NMDAR-**IIb**, NMDAR-**IIc** and NMDAR-**6** were built and assembled with POPC membrane using CHARMM-GUI *Membrane Builder* [107,108]. All systems were solvated with TIP3P water and neutralized by adding Na^+ and Cl^- ions to the bulk solution until the salt concentration was 0.15 M, leading to a total system size of approximately 169,070 atoms and box size of 127 × 127 × 101 Å. All initial membrane-protein-ligand complex model systems for MD equilibration simulations were built with tleap program in AMBERTOOLS18 [109]. FF14SB force field parameters were used for the protein [110]; Amber Lipid14 FF for POPC lipid [111] and general AMBER force field [112] (GAFF) was used for all four ligands. To confirm convergence in binding stability of ligands, we used two replicates for each of NMDAR-**IIa**, NMDAR-**IIb**, NMDAR-**IIc** and NMDAR-**6** systems.

All 8 initial membrane-protein-ligand complex model systems were energy minimized for 500 cycles of each steepest-descent and conjugate gradient algorithm while keeping restraints on the protein Cα atoms. Water and ions were equilibrated at constant volume as the temperature was gradually increased from 0 to 300K with restraints of 40 kcal/mol/Å on all protein and lipid heavy atoms. This was followed by equilibration for 20 ns at 1 atm and 300 K with a time step of 2 fs using the pmemd.cuda program of the AMBER18 molecular dynamics package [109]. The restraints on the protein residues were gradually reduced from 20 to 0.5 kcal/mol/Å. For each system, MD production runs without any restraints using AMBER18 were performed for 200 ns. The NPT equilibration and production MD simulations were performed with an integration time step of 2 fs while pressure and temperature of the simulated system were maintained at 1 bar and 300 K respectively. We used Langevin thermostat with damping coefficient of 1 ps^{-1} and a semi-isotropic pressure scaling algorithm as implemented in AMBER18, with pressure relaxation time of 5 ps. During whole simulations, hydrogen bonds were constrained via the SHAKE algorithm [113]. Periodic boundary conditions and all atom wrapping were employed in all simulations as implemented in AMBER18. Long range electrostatics were calculated using the Particle Mesh Ewald method [114] where Non-bonded Lennard-Jones and Coulombic interactions were truncated at 8 Å. Results were viewed and analyzed with VMD [115] and CPPTRAJ tools [116].

4.4. Cell culture, transfection, recording, and analysis for electrophysiology experiments

Electrophysiological characterization of memantine-like compounds for Fig. 4 was carried out using tsA201 cells transiently transfected with plasmids codifying for NMDAR subunits. tsA201 (Sigma catalog #85120602) is a cell line derived from HEK293 cells stably expressing the temperature sensitive gene for SV40 T-antigen to allow plasmid replication using the SV40 origin and thus enabling high levels of recombinant proteins. Cells were maintained in DMEM supplemented with 10% fetal bovine serum and 1% streptomycin/penicillin as described [60]. Prior to transfection, cells were plated at 1×10^6 cells/coverslip in glass coverslips previously coated with poly D-lysine (0.1 mg/ml). 24 h after plating, cells were transiently transfected with 1 μg total cDNAs using PEI transfection reagent (1 mg/ml) in a 3:1 ratio (PEI:DNA). Cells were transfected with plasmids encoding the rat GluN1 subunit, rat GluN2A subunit and enhanced green fluorescent protein (eGFP) for identification of transfected cells. cDNA ratios of 0.5 eGFP: 1 GluN1: 1 GluN2A were used. Culture medium was supplemented with the competitive NMDAR antagonist D,L-2-amino-5-phosphonopentanoate (dl-APV, Sigma, 200 μM) at the time of transfection to prevent NMDAR-mediated cell death.

Whole-cell voltage-clamp recordings were obtained on tsA201 cells 18–30 h after transfection. Pipettes were pulled from borosilicate capillary tubing (OD = 1.5 mm, ID = 0.86 mm; Harvard Apparatus) using a P-97 electrode puller (Sutter Instruments) and subsequently fire-polished to a resistance of 2–5 MΩ using a MF-830 forge (Narishige). Intracellular pipette solution contained (in mM): 140 CsCl, 10 HEPES, 5 EGTA, 4 Na_2ATP and 0.1 Na_3GTP with pH adjusted to 7.25 with CsOH. Extracellular recording solution contained (in mM): 140 NaCl, 5 KCl, 1 $CaCl_2$, 10 HEPES and 10 glucose, adjusted to pH 7.42 with NaOH.

Whole-cell currents were recorded using an Axopatch 200B patch-clamp amplifier (Molecular Devices). Current signal was low-pass filtered at 1 kHz, and sampled at 2 kHz in pClamp 10 (Molecular Devices). Solutions containing agonists (100 μM NMDA and 10 μM glycine) or blockers (10 μM) were applied by piezoelectric translation (P-601.30; Physik Instrumente) of a theta-barrel application tool made from borosilicate glass (1.5 mm o.d.; Sutter Instruments). All recordings were performed at rt.

The percentage of channel block, unblock, and recovery were measured with the following protocol: At a holding of −60 mV, NMDA (100 μM) and glycine (10 μM) were applied until current reached a clear steady-state. Then, **IIb**, **IIc** or **2** were rapidly applied by piezo control (1 ms solution exchange) for 30 s as described [28]. During the application of the blocker, a 5 s jump to +60 mV was performed to study the voltage dependence of channel block. Blockers were then removed in the presence of the agonists to allow recovery of the current. During this period (around 1 min) a second jump (5 s duration) to +60 mV was performed. Finally, agonists were removed. Percentage of block was calculated by dividing steady state current in the presence of the blocker by steady state current in the absence of the blocker. Percentage of unblock was calculated by dividing the steady state current after blocker removal by the steady state current before blocker application. Finally, the voltage dependence (% of block at +60 mV) was calculated by using Equation 1:

$$\%\ of\ block = 100\left(1 - \frac{I_{+60\ (Drug)}}{I_{+60\ (Agonist)}}\right)$$

where $I_{+60(Drug)}$ is the current after 5 s at the holding voltage of +60 mV in the presence of the blocker and $I_{+60(Agonist)}$ is the current after 5 s at +60 mV in the absence of the blocker. The kinetics of blocking and unblocking of NMDAR responses were fitted according to a double-exponential function to calculate the weighted time constant ($\tau_{weighted}$):

$$\tau_{weighted} = \tau_f\left(\frac{A_f}{A_f + A_s}\right) + \tau_s\left(\frac{A_s}{A_f + A_s}\right)$$

where A_f and τ_f are the amplitude and time constant of the fast component of recovery and A_s and τ_s are the amplitude and time constant of the slow component.

For Fig. 5, cells were maintained as previously described [117]. Briefly, tsA201 cells (European Collection of Authenticated Cell Cultures) were cultured and plated in DMEM supplemented with 10% fetal bovine serum and 1% GlutaMAX (Thermo Fisher Scientific). 18–24 h after plating, the cells were transfected using FuGENE 6 (Promega) with cDNA coding for enhanced green fluorescent protein (eGFP), WT rat GluN1-1a (GluN1; GenBank X63255), and GluN2A (GenBank M91561 in pcDNA1). GluN1-1a and eGFP were expressed using a plasmid containing cDNA encoding eGFP inserted between the promoter and the GluN1 open reading frame [118]. dl-APV was added to the medium at the time of transfection to prevent NMDAR-mediated cell death.

For Fig. 5, all whole-cell voltage-clamp recordings were performed at rt 18–30 h after transfection. Pipettes were fabricated from borosilicate capillary tubing (OD = 1.5 mm, ID = 0.86 mm) using a Flaming Brown P-97 electrode puller (Sutter Instruments) and fire-polished to a resistance of 3.0–4.0 MΩ. The intracellular pipette solution contained (in mM): 130 CsCl, 10 HEPES, 10 BAPTA, and 4 MgATP; adjusted to pH 7.2 ± 0.05 with CsOH. Pipette solution osmolality was 275 ± 10 mOsm. Extracellular recording solutions contained (in mM): 140 NaCl, 2.8 KCl, 1 $CaCl_2$, 10 HEPES, 0.01 EDTA, and 0.1 glycine; adjusted to pH 7.2 ± 0.05 with NaOH and to osmolality 290 ± 10 mOsm with sucrose. Concentrated stocks of glutamate, $MgCl_2$, and/or **IIc** were diluted in extracellular solution on the day of experiments (glutamate stock = 1 M; $MgCl_2$ stock = 1 M; **IIc** stock = 10 mM in 140 mM NaCl and 2% DMSO, maximum [DMSO] = 0.075%). Extracellular solutions were applied to the patched cell via an in-house built fast perfusion system [117]. Whole-cell currents were recorded and digitized using an Axopatch 200A patch-clamp amplifier and Digidata 1440A digitizer (Molecular Devices). The current signal was low-pass filtered at 5 kHz and sampled at 20 kHz using pClamp 10.7 (Molecular Devices). Series resistance was compensated 85–90% in all experiments. An empirically determined −6 mV liquid junction potential between the internal and external solutions was corrected in all experiments.

Concentration-inhibition relations were measured using the protocol shown in Fig. 5A. Glutamate (1 mM) was applied until current reached steady-state, then sequentially increasing concentrations of **IIc** were applied for 10 s in the presence of glutamate. Glutamate alone was reapplied for 80 s following **IIc** application to allow recovery from inhibition. Cells in which current did not recover to 90% of steady-state current during the initial glutamate application were excluded from analysis to prevent underestimation of potency. We estimated IC_{50} by fitting Equation 2 to concentration-inhibition data:

$$\frac{I_{\mathbf{IIc}}}{I_{Glu}} = \frac{1}{1 + \left(\frac{[\mathbf{IIc}]}{IC_{50}}\right)^{n_H}}$$

where $I_{\mathbf{IIc}}$ is mean current steady state current during application of **IIc**, I_{Glu} is the average of the mean steady state currents before and after application of **IIc** and n_H is the Hill coefficient. IC_{50} and n_H

were free parameters during fitting. I_{IIc} and I_{Glu} were measured as the mean current over the final 1 s of each application. Baseline current was subtracted from all current measurements. For Mg^{2+} competition experiments, **IIc** IC_{50}s were measured in the constant presence of extracellular 0.2 mM Mg^{2+}.

We measured the voltage dependence of block by **IIc** using the protocol shown in Fig. 5D. Inhibition by **IIc** was measured in each cell at nine voltages ranging from −105 to +55 mV. During each voltage step, the cell was exposed to: 5 s in extracellular solution following the voltage step; a 10 s application of 1 mM glutamate; a 15 s application of **IIc** with 1 mM glutamate; a second application of 1 mM glutamate for 15 s to allow drug unbinding; application of extracellular solution for 2 s to allow a return to baseline current. Voltage was then returned to −65 mV for 3 s before the next voltage jump was made. Voltage dependence of block was quantified using Equation 3:

$$\frac{I_{\mathbf{IIc}}}{I_{Glu}} = \frac{1}{1 + \frac{[\mathbf{IIc}]}{(IC_{50}^{-65\ mV})e^{\frac{V_m+65}{V_0}}}}$$

where $IC_{50}^{-65\ mV}$ is the IC_{50} at −65 mV (calculated from concentration-inhibition experiments), V_m represents the holding potential, and V_0 represents the change in voltage (in mV) that results in an e-fold change in the IC_{50} of the drug. $I_{\mathbf{IIc}}$ and I_{Glu} were measured as in analysis of concentration-inhibition data. V_0 was the only free parameter during fitting. The fraction of the total membrane voltage field felt by the blocker at its binding site (δ) [119] was estimated using Equation 4:

$$\delta = \frac{RT}{V_0 zF}$$

where R is the ideal gas constant, T is the absolute temperature, z represents the valence of the blocker, and F is the Faraday constant. Note that while δ is useful for comparing voltage dependence of blockers, permeant ions influence the voltage dependence of NMDAR channel block [120]. Therefore, δ only provides a rough estimate of the location of a channel blocker's binding site in the voltage field.

4.5. In vitro DMPK

4.5.1. Microsomal stability

The human, rat, and mouse pooled microsomes employed were purchased from Tebu-Xenotech. The compound was incubated at 37 °C with the microsomes in a 50 mM phosphate buffer (pH = 7.4) containing 3 mM $MgCl_2$, 1 mM NADP, 10 mM glucose-6-phosphate and 1 U/mL glucose-6-phosphate-dehydrogenase. Samples (75 μL) were taken from each well at 0, 10, 20, 40 and 60 min and transferred to 4 °C in a plate containing 75 μL acetonitrile and 30 μL of 0.5% formic acid in water, which were added to improve the chromatographic conditions. The plate was centrifuged (46000 g, 30 min) and supernatants were taken and analyzed in a UPLC-MS/MS (Xevo-TQD, Waters) using a BEH C18 column and an isocratic gradient of 0.1% formic acid in water: 0.1% formic acid acetonitrile (60:40). The metabolic stability of the compounds was calculated from the logarithm of the remaining compounds at each time point studied.

4.5.2. Permeability

The Caco-2 cells were cultured to confluency, trypsinized and seeded onto a 96-filter transwell insert (Corning) at a density of ~10,000 cells/well in DMEM cell culture medium supplemented with 10% fetal bovine serum, 2 mM L-Glutamine and 1% penicillin/streptomycin. Confluent Caco-2 cells were subcultured at passages 58−62 and grown in a humidified atmosphere of 5% CO_2 at 37 °C. Following an overnight attachment period (24 h after seeding), the cell medium was replaced with fresh medium in both the apical and basolateral compartments every other day. The cell monolayers were used for transport studies 21 days post seeding. The monolayer integrity was checked by measuring the transepithelial electrical resistance (TEER), obtaining values ≥ 500 Ω/cm^2. On the day of the study, after the TEER measurement, the medium was removed and the cells were washed twice with pre-warmed (37 °C) Hank's Balanced Salt Solution (HBSS) buffer to remove traces of medium. Stock solutions were made in DMSO, and further diluted in HBSS (final DMSO concentration 1%). Each compound and reference compounds (Colchicine, E3S) were tested at a final concentration of 10 μM. For A → B directional transport, the donor working solution was added to the apical (A) compartment and the transport media as receiver working solution was added to the basolateral (B) compartment. For B → A directional transport, the donor working was added to the basolateral (B) compartment and transport media as receiver working solution was added to the apical (A) compartment. The cells were incubated at 37 °C for 2 h with gentle stirring.

At the end of the incubation, samples were taken from both donor and receiver compartments and transferred into 384-well plates and analyzed by UPLC-MS/MS. Detection was performed using an ACQUITY UPLC/Xevo TQD system. After the assay, Lucifer yellow (LY) was used to further validate the cell monolayer integrity, cells were incubated with LY 10 μM in HBSS for 1 h at 37 °C, obtaining permeability (Papp) values for LY of ≤10 nm/s confirming the well-established Caco-2 monolayer.

4.5.3. Cytochrome P450 inhibition assay

The objective of this study was to screen the inhibition potential of the compound using recombinant human cytochrome P450 enzymes (CYP1A2, CYP2C9, CYP2C19, CYP2D6, CYP3A4 (BFC) and CYP3A4 (DBF)) and probe substrates with fluorescent detection. Incubations were conducted in a 200 μL volume in 96-well microtiter plates (COSTAR 3915). The addition of the mixture buffer-cofactor (KH_2PO_4 buffer, 1.3 mM NADP, 3.3 mM $MgCl_2$, 3.3 mM glucose-6-phosphate and 0.4 U/mL glucose-6-phosphate dehydrogenase), control supersomes, standard inhibitors (furafyline, tranylzypromine, ketoconazole, sulfaphenazole and quinidine; Sigma Aldrich), and previously diluted compound to plates was carried out by a liquid handling station (Zephyr Caliper). The plate was then preincubated at 37 °C for 5 min, and the reaction was initiated by the addition of prewarmed enzyme/substrate (E/S) mix. The E/S mix contained buffer (KH_2PO_4), c-DNA-expressed cytochrome P450 enzymes in insect cell microsomes, substrate (3-cyano-7-ethoxycoumarin, for CYP1A2 and CYP2C19; 7-methoxy-4-(trifluoromethyl)coumarin for CYP2C9; 3-[2-(*N*,*N*-diethyl-*N*-methylammonium)ethyl]-7-methoxy-4-methylcoumarin for CYP2D6; and 7-benzyloxytrifluoromethyl coumarin (7-BFC) and dibenzylfluorescein (DBF) for CYP3A4) in a reaction volume of 200 μL. Reactions were terminated after various times (a specific time for each cytochrome) by addition of STOP solution (ACN/TrisHCl 0.5 M 80:20 or 2 N NaOH). Fluorescence per well was measured using a fluorescence plate reader (Tecan Infinity M1000 pro) and percentage of inhibition was calculated.

4.5.4. hERG inhibition assay

The assay was carried out on a CHO cell line transfected with the hERG potassium channel. 72 h before the assay, 2500 cells were seeded on a 384 well black plate (Greiner 781091). Cells were maintained at 37 °C in a 5% CO_2 atmosphere for 24 h and at 30 °C in a 5% CO_2 atmosphere for 48 h plus. hERG activity was measured by

using the FluxorTM Potassium Ion Chanel Assay Kit (Thermo Fisher F10016). Medium was replaced for 20 μl Loading Buffer and the cells were incubated for 60 min at RT, protected from direct light. After incubation, Loading Buffer was replaced with Assay buffer and the compounds were incubated for 30 min at RT. 5 μl of Stimulus Buffer was added to each well and the fluorescence was read (λex = 490 nm, λem = 525 nm) using imaging plate reader system (FDSS7000EX, Hamamatsu®) every second after the establishment of a baseline line. Astemizole (IC_{50} = 152 nM) was used to validate the assay.

4.5.5. Parallel artificial membrane permeation assays-blood-brain barrier (PAMPA-BBB)

To evaluate the brain penetration of the compounds, a parallel artificial membrane permeation assay for blood-brain barrier was used, following the method described by Di et al. [121] The *in vitro* permeability (P_e) of fourteen commercial drugs through lipid extract of porcine brain membrane together with the test compounds were determined. Commercial drugs and assayed compounds were tested using a mixture of PBS:EtOH (70:30). The assay was validated by comparing experimental and reported P_e values of a set of fourteen commercial drugs (Table S2), and the following correlation was obtained: P_e (exp) = 1.6662 P_e (lit) − 1.4174 (R^2 = 0.9334). On the basis of this equation and the limits established for BBB permeation [119], the threshold for high BBB permeation (CNS+) was set at P_e (10^{-6} cm s^{-1}) > 5.247; low BBB permeation (CNS-) was set at P_e (10^{-6} cm s^{-1}) < 1.915; and the range for uncertain BBB permeation (CNS±) at 5.247 > *P*e (10^{-6} cm s^{-1}) > 1.915. Three different experiments, each performed in triplicate, were carried out for each compound.

4.6. In vivo evaluation of **IIc** and memantine

4.6.1. Worm strains, maintenance, and general methods

Strains used are listed in Table S3. Standard methods were used for culturing and examination *C. elegans* [92]. Wild-type strains were cultured at 20 °C, while transgenic strains were cultured at 16 °C in a temperature-controlled incubator on solid nematode growth medium (NGM) seeded with *Escherichia coli (E. coli)* OP50 strain as a food source. To collect age synchronized populations of eggs, adults were treated with alkaline hypochlorite solution (0.5 M NaOH, ~2.6% NaCl) for 5–7 min. Fertilized eggs were re-suspended in S-medium for 12 h, and L1 larvae were incubated to hatch overnight in the absence of food.

4.6.2. Compound preparation and treatment

The compounds were dissolved in 100% DMSO. Each concentration was then dissolved in MilliQ purified water to achieve a final concentration between 100 mg/L and 16 mg/L in 1% DMSO in well. For the locomotion assay, treatments were carried out in liquid culture for 4 days at 20 °C. Each well contained a final volume of 60 μL, consisting of 25–30 animals in the L1 stage, compounds under study at the appropriate doses, and OP50 inactivated by freeze-thaw cycles and incubated in S-medium complete to a final optical density of 595 (OD595) of 0.9–0.8 measured in the microplate reader. For the chemotaxis assay synchronized CL2355 and CL2122 strains were treated with DMSO or compounds on NGM plates seeded with inactivated *E. coli* (OP50). They were cultured at 16 °C for 36 h, and then at 23 °C for 36 h.

4.6.3. Locomotion assay

A locomotion assay of NMDA receptor channel blockers was run to obtain a dose-response profile and evaluate their effects on motor function of the CL2006 transgenic strain. The animals were synchronized by alkaline hypochlorite treatment, and the OP50 bacteria OD595 was adjusted to 0.9 to perform the assay. WT strain (N2), and the transgenic strain (CL2006) were treated in liquid media for 4 days at 20 °C with continuous shaking at 180 rpm, starting at the L1 stage. On day 5 of age, the nematodes were moved from the 96-well plates to an unseeded NGM plate for 45 min before starting the trial, allowing the plate to dry. Locomotion assays were conducted in 30 mm NGM plates, where the entire plate was covered by OP50. 5 to 10 adult nematodes were positioned in the center of a circle (1 cm diameter) in seeded 30 mm NGM plates. After 1 min, the number of animals remaining inside the circle were considered locomotor defective. A locomotor defective score (LD) was calculated by dividing the number of worms inside the circle by the total number of worms on the plate. Motor behavior assays were run with a total of at least 200 animals tested per compound concentration. The motor index score ranges from 0% (animals that exhibit the same motor defect as untreated CL2006 animals) to 100% (animals that exhibit motor behavior comparable to WT animals). All results included in the figures are calculated using the following formula:

$$Motor\ index(\%) = \frac{LD\ CL2006_{vehicle} - LD\ CL2006_{drug}}{LD\ CL2006_{vehicle} - LD\ WT_{vehicle}} x100$$

4.6.4. Chemotaxis assay

Nematodes were sampled after the treatments with memantine and **IIc** and washed with M9 buffer (3 g/L KH_2PO_4, 6 g/L Na_2HPO_4, 5 g/L NaCl, 1 mL/L 1 mM $MgSO_4$, 800 mL/L ddH_2O). In brief, the assay was performed in 100 mm NGM plates. 10 μL of odorant (0.025% benzaldehyde in 96% ethanol) was added to the "attractant" spot, and on the oppose side of the NGM, 10 μL of control odorant (96% ethanol) was added. Then, 70–80 worms were positioned in the center of the plate. Assay plates were incubated at 23 °C for 1 h and were scored according to the chemotaxis index (CI) as follows: CI = (number of worms at attractant-number of worms at control)/(number of worms at attractant spot + number of worms at control spot). Two trials were performed in triplicate. In each experiment, at least 250 worms from each group were analyzed.

4.6.5. 5XFAD mice

The 5XFAD strain is a well-established and suitable transgenic AD mouse model expressing five familial mutations of human AD. 5XFAD mice also exhibit early-onset cognitive impairment and Aβ pathology [88]. Six months old female Wild Type (WT) and 5XFAD mice (n = 43) were randomly divided into four groups: WT (n = 14), 5XFAD Control (Control) (n = 8), 5XFAD treated with memantine (Mem) (n = 11) and 5XFAD treated with **IIc** (**IIc**) (n = 10). Animals had free access to food and water under standard temperature conditions (22 ± 2 °C) and were maintained on 12 h: 12 h light-dark cycles (300 lux/0 lux). Water consumption was controlled each week; drug concentrations were adjusted accordingly to reach the appropriate dose for each cage. Memantine and **IIc** were dissolved in 1.8% 2-hydroxypropyl-β-cyclodextrin and administered at 5 mg/kg/day through drinking water for four weeks and up to euthanasia. Studies were approved by the Animal Experimentation Ethics Committee (CEEA) at the University of Barcelona. All efforts were made to reduce the number of animals used and their suffering.

4.6.6. Novel object recognition test (NORT)

NORT is a cognitive test used to assess short- and long-term recognition memories. The apparatus used consisted of a 90°, two-arm, 25-cm-long, 20-cm-high, and a 5-cm-wide black maze of

black polyvinyl chloride. The objects to be discriminated were made of plastic and chosen not to frighten mice and without any part likely to be bitten. The test was performed over 5 days. On the first three days, animals were individually habituated to the apparatus for 10 min each day. On the fourth day, the animals were individually exposed during 10 min to the apparatus and were allowed to freely explore the zone inside the apparatus (First trial/ Familiarization) where we had placed two identical novel objects (A + A′ or B + B′) at the end of each arm. After 10 min, the animals were removed and returned to their home cage, and 2 h later the retention trial (second trial) was performed. In this second trial, objects A′ and B′ were swapped (A + B′ or A'+B) and the mice were allowed to explore the maze for 10 min. Twenty-four hours after the first trial, animals were exposed again to the apparatus, and in this case, objects A′ and B′ were substituted by two new objects with different shapes and colours (A + C or B + C'), and animals were allowed to explore them for 10 min. The time exploring the novel object (TN) and the old object (TO) were measured and recorded using a camera. Exploration of an object was defined as pointing the nose towards the object at a distance ≤2 cm and/or touching it with the nose. Turning or sitting around the object was not considered exploration. To avoid object preference biases objects A and B were counterbalanced so that one-half of the animals in each experimental group were first exposed to object A and then to object B, whereas the other half first saw object B and then object A. Finally, to quantify cognitive performance, the Discrimination Index (DI) was calculated, which is defined as (TN-TO)/(TN + TO).

4.6.7. Brain tissue preparation

Mice groups were euthanized by cervical dislocation and brains were immediately removed from the skull. For molecular experiments, the hippocampus was isolated and frozen in powdered dry ice. Hippocampi were maintained at −80 °C for further use for protein extraction, RNA and DNA isolation. For thioflavin-S staining, mice were anesthetized (ketamine 100 mg/kg and xylazine 10 mg/kg, intraperitoneally) and then perfused with 4% paraformaldehyde (PFA) diluted in 0.1 M phosphate buffer solution intracardially. Brains were removed and postfixed in 4% PFA overnight at 4 °C. Afterwards, brains were changed to PFA +15% sucrose. Finally, the brains were frozen on powdered dry ice and stored at −80 °C until sectioning. Brain coronal sections of 30 μm were obtained (Leica Microsystems CM 3050S cryostat, Wetzlar, Germany) and kept in a cryoprotectant solution at −20 °C until use.

4.6.8. Protein level determination by Western Blotting

For Western Blotting (WB), aliquots of 15 μg of hippocampal protein extraction per sample were used. In brief, tissues were homogenized in lysis buffer containing phosphatase and protease inhibitors (Cocktail II, Sigma-Aldrich). Total protein levels were obtained, and protein concentration was determined by the Bradford method. Protein samples were separated by Sodium dodecyl sulphate-Polyacrylamide gel electrophoresis (SDS-PAGE) (8−20%) and transferred onto Polyvinylidene difluoride (PVDF) membranes (Millipore). Afterwards, membranes were blocked in 5% non-fat milk in Tris-buffered saline (TBS) solution containing 0.1% Tween 20 TBS (TBS-T) for 1 h at rt, followed by overnight incubation at a 4 °C with the primary antibodies listed in Table S4. Then, membranes were washed and incubated with secondary antibodies for 1 h at RT. Immunoreactive proteins were viewed with the chemiluminescence-based detection kit, following the manufacturer's protocol (ECL Kit, Millipore), and digital images were acquired using ChemiDoc XRS + System (BioRad). Semi-quantitative analyses were done using ImageLab software (BioRad), and results were expressed in Arbitrary Units (AU), considering control protein levels as 100%. Protein loading was routinely monitored by immunodetection of Glyceraldehyde-3-phosphate dehydrogenase (GAPDH).

4.6.9. Data Acquisition and statistical analysis

Data analysis was conducted using GraphPad Prism ver. 6 statistical software. Data are expressed as the mean ± standard error of the mean (SEM) of at least 3 samples per group. Statistical analysis was performed by way of two-tail Student's t-test or one-way analysis of variance (ANOVA) followed by Tukey post-hoc analysis. Statistical significance was defined as p-value < 0.05. Statistical outliers were determined with Grubbs' test and, when necessary, were removed from the analysis. The cognitive analysis was performed blindly: an experimenter unaware of the treatment groups performed the tests and recorded the number of animals. Another experimenter analyzed the videos and the behavioral scoring.

4.7. Cytotoxicity

The cytotoxicity of **IIc** was measured in Neuro2A cells. Cells were plated in 96-well plates at a density of 40.000 cells/well and grown under conventional conditions (0,2 mL per well in RPMI medium 10%FBS and supplemented with pyruvate and antibiotics). The day after, cells were exposed during 24 h to 1, 10 or 100 μM EV-19. Afterwards, cell viability was assessed using the MTT method. Briefly, 20 μL of a solution of 5 mg/ml of 3-(4,5-dimethyl-2-thiazolyl)-2,5-diphenyl-2*H*-tetrazolium bromide in PBS was added in each well and after 1 h in the cell incubator the supernatant was discarded and cells lysed with 200 μL DMSO. After shaking, absorbance was measured at 595 nm in a Biotek PowerWave HT plate reader. Assays were performed in triplicate and no difference was found between controls and drug-treated cells at any concentration.

Contributions

A.L.T. and J.C.-A. contributed equally. S.V. conceived the idea. A.L.T synthesized and chemically characterized the compounds. F.X.S. performed the intracellular calcium-based determination of the IC_{50}s in cells. A.L.T., M.B.P., D.S. and J.W.J. designed and carried out electrophysiological studies. D.S.P. and M.G.K designed and performed MD calculations. M.I.L., J.M.B. and B.P. carried out DMPK studies. J.C.-A., C.G.-F. and M.P. designed and carried out the *in vivo* experiments. A.L.T. wrote the first draft of the manuscript. A.L.T., D.S., M.B.P, J.W.J, D.S.P, M.G.K., J.C.-A, C.G.-F, M.P. and S.V. wrote the definitive manuscript with feedback from all the authors. All authors have given approval to the final version of the manuscript.

Declaration of competing interest

The authors declare that they have no known competing financial interests or personal relationships that could have appeared to influence the work reported in this paper.

Acknowledgements

This research was funded by the Spanish *Ministerio de Economía, Industria y Competitividad* (Grant SAF2017-82771-R to S.V. and PID2019-106285RB-I00 to M.P.), the María de Maeztu Unit of Excellence (Institute of Neurosciences, Universitat de Barcelona, MDM-2017-0729, to M.P. and D.S.), and 2017SGR106 (AGAUR, Catalonia to S.V. and M.P.), the Spanish *Ministerio de Ciencia e Innovación* (Grant PID2020-119932 GB-I00/AEI /10.13039/ 5011000011033 to D. S.), the European Regional Development Fund (ERDF), the *Xunta de Galicia* (ED431G 2019/02 and ED431C 2018/

21), and the United States National Institutes of Health (Grant R01AG065594to J.W.J., M.G.K., and S.V; Grant F31NS113477 to M.B.P). J.C.-A acknowledges the Spanish *Ministerio de Ciencia e Innovación* for a FPI fellowship (MDM-2017-0729-19-2). A.L.T. acknowledges a PhD fellowship (FPU grant) from the Spanish *Ministerio de Educación, Cultura y Deporte* and the Spanish Society of Medicinal Chemistry (SEQT) and Enantia S. L. for an "Award for Novel Researchers in the Discovery and Development of New Drugs". Computational work used the Extreme Science and Engineering Discovery Environment (XSEDE) Bridges 2 at Pittsburgh Supercomputing Center, allocation to M.G.K. TG-MCB180173, which is supported by the United States National Science Foundation grant number ACI-1548562.

Appendix A. Supplementary data

Supplementary data to this article can be found online at https://doi.org/10.1016/j.ejmech.2022.114354.

References

[1] M.W. Bondi, E.C. Edmonds, D.P. Salmon, Alzheimer's disease: past, present, and future, J. Int. Neuropsychol. Soc. 23 (2017) 818–831.
[2] Alzheimer's Disease International, Alzheimer's Disease International, London, 2019.
[3] GBD 2016 Dementia Collaborators, Global, regional, and national burden of Alzheimer's disease and other dementias, 1990-2016: a systematic analysis for the Global Burden of Disease Study 2016, Lancet Neurol. 18 (2019) 88–106.
[4] M. Vaz, S. Silvestre, Alzheimer's disease: recent treatment strategies, Eur. J. Pharmacol. 887 (2020), 173554.
[5] J. Sevigny, P. Chiao, T. Bussière, P.H. Weinreb, L. Williams, M. Maier, R. Dunstan, S. Salloway, T. Chen, Y. Ling, J. O'Gorman, F. Qian, M. Arastu, M. Li, S. Chollate, M.S. Brennan, O. Quintero-Monzon, R.H. Scannevin, H.M. Arnold, T. Engber, K. Rhodes, J. Ferrero, Y. Hang, A. Mikulskis, J. Grimm, C. Hock, R.M. Nitsch, A. Sandrock, The antibody aducanumab reduces Aβ plaques in Alzheimer's disease, Nature 537 (2016) 50–56.
[6] S. Jaffe, USA FDA defends approval of Alzheimer's disease drug, Lancet 398 (2021) 32.
[7] L.A. Hershey, R. Tarawneh, Clinical efficacy, drug safety and surrogate endpoints: has aducanumab met all of its expectations? Neurology 97 (2021) 517–518.
[8] S. Salloway, J. Cummings, Aducanumab, amyloid lowering, and slowing of Alzheimer disease, Neurology 97 (2021) 543–544.
[9] D.S. Knopman, J.S. Perlmutter, Prescribing aducanumab in the face of meager efficacy and real risks, Neurology 97 (2021) 545–547.
[10] G. Marucci, M. Buccioni, D.D. Ben, C. Lambertucci, R. Volpini, F. Amenta, Efficacy of acetylcholinesterase inhibitors in Alzheimer's disease, Neuropharmacology 190 (2021), 108352.
[11] J.M. López-Arrieta, L. Schneider, Metrifonate for Alzheimer's disease, Cochrane Database Syst. Rev. 2 (2006), CD003155.
[12] Klein.J. Phenserine, Expet Opin. Invest. Drugs 16 (2007) 1087–1097.
[13] O. Weinreb, T. Amit, O. Bar-Am, M.B. Youdim, A novel anti-Alzheimer's disease drug, ladostigil neuroprotective, multimodal brain-selective monoamine oxidase and cholinesterase inhibitor, Int. Rev. Neurobiol. 100 (2011) 191–215.
[14] M. Son, C. Park, S. Rampogu, A. Zeb, K.W. Lee, Discovery of novel ncetylcholinesterase inhibitors as potential candidates for the treatment of Alzheimer's Disease, Int. J. Mol. Sci. 20 (2019) 1000.
[15] M. Saxena, R. Dubey, Target enzyme in Alzheimer's disease: acetylcholinesterase inhibitors, Curr. Top. Med. Chem. 19 (2019) 264–275.
[16] M. Bortolami, D. Rocco, A. Messore, R. Di Santo, R. Costi, V.N. Madia, L. Scipione, F. Pandolfi, Acetylcholinesterase inhibitors for the treatment of Alzheimer's disease – a patent review (2016–present), Expert Opin. Ther. Pat. 31 (2021) 399–420.
[17] T. Kishi, S. Matsunaga, K. Oya, I. Nomura, T. Ikuta, N. Iwata, Memantine for Alzheimer's disease: an updated systematic review and meta-analysis, J. Alzheimers Dis. 60 (2017) 401–425.
[18] S. Matsunaga, T. Kishi, I. Nomura, K. Sakuma, M. Okuya, T. Ikuta, N. Iwata, The efficacy and safety of memantine for the treatment of Alzheimer's disease, Expet Opin. Drug Saf. 17 (2018) 1053–1061.
[19] C.G. Parsons, A. Stoffler, W. Danysz, Memantine: a NMDA receptor antagonist that improves memory by restoration of homeostasis in the glutamatergic system–too little activation is bad, too much is even worse, Neuropharmacology 53 (2007) 699–723.
[20] W. Danysz, C.G. Parsons, Alzheimer's disease, β-amyloid, glutamate, NMDA receptors and memantine—searching for the connections, Br. J. Pharmacol. 167 (2012) 324–352.
[21] P. Xia, H.-S.V. Chen, D. Zhang, S.A. Lipton, Memantine preferentially blocks extrasynaptic over synaptic NMDA receptor currents in hippocampal autapses, J. Neurosci. 30 (2010) 11246–11250.
[22] K.E. Gilling, C. Jatzke, M. Hechenberger, C.G. Parsons, Potency, voltage-dependency, agonist concentration-dependency, blocking kinetics and partial untrapping of the uncompetitive N-methyl-D-aspartate (NMDA) channel blocker memantine at human NMDA (GluN1/GluN2A) receptors, Neuropharmacology 56 (2009) 866–875.
[23] Rammes.G. Neramexane, A moderate-affinity NMDA receptor channel blocker: new prospects and indications, Expet Rev. Clin. Pharmacol. 2 (2009) 231–238.
[24] Y. Wang, J. Eu, M. Washburn, T. Gong, H.S.V. Chen, W.L. James, S.A. Lipton, J.S. Stamler, G.T. Went, S. Porter, The pharmacology of aminoadamantane nitrates, Curr. Alzheimer Res. 3 (2006) 201–204.
[25] Y. Wang, J. Eu, M. Washburn, T. Gong, H.S. Chen, W.L. James, S.A. Lipton, J.S. Stamler, G.T. Went, S. Porter, Memantine-sulfur containing antioxidant conjugates as potential prodrugs to improve the treatment of Alzheimer's disease, Eur. J. Pharmaceut. Sci. 49 (2013) 187–198.
[26] H. Takahashi, P. Xia, J. Cui, M. Talantova, K. Bodhinathan, W. Li, S. Saleem, E.A. Holland, G. Tong, J. Piña-Crespo, D. Zhang, N. Nakanishi, J.W. Larrick, S.R. McKercher, T. Nakamura, Y. Wang, S.A. Lipton, Pharmacologically targeted NMDA receptor antagonism by nitromemantine for cerebrovascular disease, Sci. Rep. 5 (2016) 14781.
[27] S.O. Bachurin, E.F. Shevtsova, G.F. Makhaeva, V.V. Grigoriev, N.P. Boltneva, N.V. Kovaleva, S.V. Lushchekina, P.N. Shevtsov, M.E. Neganova, O.M. Redkozubova, E.V. Bovina, A.V. Gabrelyan, V.P. Fisenko, V.B. Sokolov, A.Y. Aksinenko, V. Echeverria, G.E. Barreto, G. Aliev, Novel conjugates of aminoadamantanes with carbazole derivatives as potential multitarget agents for AD treatment, Sci. Rep. 30 (2017) 45627.
[28] R. Leiva, M.B. Phillips, A.L. Turcu, E. Gratacòs-Batlle, L. León-García, F.X. Sureda, D. Soto, J.W. Johnson, S. Vázquez, Pharmacological and electrophysiological characterization of novel NMDA receptor antagonists, ACS Chem. Neurosci. 9 (2018) 2722–2730.
[29] T. Kumamoto, M. Nakajima, R. Uga, N. Ihayazaka, H. Kashihara, K. Katakawa, T. Ishikawa, R. Saiki, K. Nishimura, K. Igarashi, Design, synthesis, and evaluation of polyamine-memantine hybrids as NMDA channel blockers, Bioorg. Med. Chem. 26 (2018) 603–608.
[30] S. Sestito, S. Daniele, D. Pietrobono, V. Citi, L. Bellusci, G. Chiellini, V. Calderone, C. Martini, S. Rapposelli, Memantine prodrug as a new agent for Alzheimer's disease, Sci. Rep. 9 (2019) 4612.
[31] L. Wu, X. Zhou, Y. Cao, S.H. Mak, L. Zha, N. Li, Z. Su, Y. Han, Y. Wang, M.P. Man Hoi, Y. Sun, G. Zhang, Z. Zhang, X. Yang, Therapeutic efficacy of novel memantine nitrate MN-08 in animal models of Alzheimer's disease, Aging Cell 20 (2021), e13371.
[32] S. Couly, M. Denus, M. Bouchet, G. Rubinstenn, T. Maurice, Anti-amnesic and neuroprotective effects of fluoroethylnormemantine in a pharmacological mouse model of Alzheimer's disease, Int. J. Neuropsychopharmacol. 24 (2021) 142–157.
[33] http://www.rest-therapeutics.com/ (accessed 2021-12-29).
[34] https://eumentistx.com/ (accessed 2021-12-29).
[35] G. Bernstein, K. Davis, C. Mills, L. Wang, M. McDonnell, J. Oldenhof, C. Inturrisi, P.L. Manfredi, O.V. Vitolo, Characterization of the safety and pharmacokinetic profile of d-methadone, a novel N-Methyl-D-Aspartate receptor antagonist in healthy, opioid-naive subjects: results of two phase 1 studies, J. Clin. Psychopharmacol. 39 (2019) 226–237.
[36] https://www.relmada.com/product-development (accessed 2021-12-29).
[37] D. Vandame, G. Desmadryl, J. Becerril Ortega, M. Teigell, N. Crouzin, A. Buisson, A. Privat, H. Hirbec, Comparison of the pharmacological properties of GK11 and MK801, two NMDA receptor antagonists: towards an explanation for the lack of intrinsic neurotoxicity of GK11, J. Neurochem. 103 (2007) 1682–1696.
[38] https://www.otonomy.com/pipeline/ (accessed 2021-08-26).
[39] https://www.nrxpharma.com/ (accessed 2021-08-26).
[40] R.S. Duman, G.K. Aghajanian, G. Sanacora, J.H. Krystal, Synaptic plasticity and depression: new insights from stress and rapid-acting antidepressants, Nat. Med. 22 (2016) 238–249.
[41] https://aurismedical.com/science/inner-ear-therapeutics (accessed 2021-08-27).
[42] M.D. Duque, P. Camps, E. Torres, E. Valverde, F.X. Sureda, M. López-Querol, A. Camins, S.R. Prathalingam, J.M. Kelly, S. Vázquez, New oxapolycyclic cage amines with NMDA receptor antagonist and trypanocidal activities, Bioorg. Med. Chem. 18 (2010) 46–57.
[43] T. Torres, M.D. Duque, M. López-Querol, M.C. Taylor, N. Naesens, C. Ma, L.H. Pinto, F.X. Sureda, J.M. Kelly, S. Vázquez, Synthesis of benzopolycyclic cage amines: NMDA receptor antagonist, trypanocidal and antiviral activities, Bioorg. Med. Chem. 20 (2012) 942–948.
[44] E. Valverde, F.X. Sureda, S. Vázquez, Novel benzopolycyclic amines with NMDA receptor antagonist activity, Bioorg. Med. Chem. 22 (2014) 2678–2683.
[45] R.D. Tung, Deuterium medicinal chemistry comes of age, Future Med. Chem. 8 (2016) 491–944.
[46] T. Pirali, M. Serafini, S. Cargnin, A.A. Genazzani, Applications of deuterium in medicinal chemistry, J. Med. Chem. 62 (2019) 5276–5297.
[47] J.F. Liu, S.L. Harbeson, C.L. Brummel, R. Tung, R. Silverman, D. Doller, A decade of deuteration in medicinal chemistry, Annu. Rep. Med. Chem. 50 (2017)

519–542.
[48] S. Cargnin, M. Serafini, T. Pirali, A primer of deuterium in drug design, Future Med. Chem. 11 (2019) 2039–2042.
[49] P. Camps, M.D. Duque, S. Vázquez, L. Naesens, E. De Clercq, F.X. Sureda, M. López-Querol, A. Camins, M. Pallàs, S.R. Prathalingam, J.M. Kelly, V. Romero, D. Ivorra, D. Cortés, Synthesis and pharmacological evaluation of several ring-contracted amantadine analogs, Bioorg. Med. Chem. 16 (2008) 9925–9936.
[50] R.A. Bishop, The intramolecular cyclization of unsaturated benzo derivatives of Bicyclo[3.3.2]decane, Aust. J. Chem. 36 (1983) 2465–2472.
[51] R. Bishop, G. Burgess, Ritter reactions. II. Reductive deamidation of N-bridgehead amides, Tetrahedron Lett. 28 (1987) 1585–1588.
[52] E. Sánchez-Larios, J.M. Holmes, C.L. Daschner, M. Gravel, NHC-Catalyzed spiro bis-indane formation via domino Stetter-Aldol-Michael and Stetter-Aldol-Aldol reactions, Org. Lett. 12 (2010) 5772–5775.
[53] C.J. Moody, G.J. Warrellow, Vinyl azides in heterocyclic synthesis. Part 10. Synthesis of the isoindolobenzazepine alkaloid lennoxamine, J. Chem. Soc. Perkin Trans. 1 (1990) 2929–2936.
[54] O. Farooq, Oxidation of aromatic 1,2-dimethanols by activated dimethyl sulfoxide. O, Synthesis 10 (1994) 1035–1036.
[55] J.J. Pappas, W.P. Keaveney, M. Berger, R.V. Rush, Directional effects of substituents in the ozonolysis of naphthalenes. Synthesis of o-phthalaldehydes, J. Org. Chem. 33 (1968) 787–792.
[56] A.K. Gupta, X. Fu, J.P. Snydert, J.M. Cook, General approach for the synthesis of polyquinenes via the Weiss reaction, Tetrahedron 47 (1991) 3665–3710.
[57] A.M. Canudas, D. Pubill, F.X. Sureda, E. Verdaguer, P. Camps, D. Muñoz-Torrero, A. Jiménez, A. Camins, M. Pallàs, Neuroprotective effects of (+/-)-huprine Y on in vitro and in vivo models of excitoxicity damage, Exp. Neurol. 180 (2003) 123–130.
[58] X. Song, M.O. Jensen, V. Jogini, R.A. Stein, C.-H. Lee, H.S. Mchaourab, D.E. Shaw, E. Gouaux, Mechanism of NMDA receptor channel block by MK-801 and memantine, Nature 556 (2018) 515–519.
[59] W. Limapichat, W.Y. Yu, E. Branigan, H.A. Lester, D.A. Dougherty, Key binding interactions for memantine in the NMDA receptor, ACS Chem. Neurosci. 4 (2013) 255–260.
[60] E. Gratacòs-Batlle, N. Yefimenko, H. Cascos-García, D. Soto, AMPAR interacting protein CPT1C enhances surface expression of GluA1-containing receptors, Front. Cell. Neurosci. 8 (2015) 469.
[61] I. Bresink, T.A. Benke, V.J. Collett, A.J. Seal, C.G. Parsons, J.M. Henley, G.L. Collingridge, Effects of memantine on recombinant rat NMDA receptors expressed in HEK 293 cells, Br. J. Pharmacol. 119 (1996) 195–204.
[62] C.G. Parsons, V.A. Panchenko, V.O. Pinchenko, A.Y. Tsyndrenko, O.A. Krishtal, Comparative patch-clamp studies with freshly dissociated rat hippocampal and striatal neurons on the NMDA receptor antagonistic effects of amantadine and memantine, Eur. J. Neurosci. 8 (1996) 446–454.
[63] T.A. Blanpied, F.A. Boeckman, E. Aizenman, J.W. Johnson, Trapping channel block of NMDA-activated responses by amantadine and memantine, J. Neurophysiol. 77 (1997) 309–323.
[64] T.A. Blanpied, R.J. Clarke, J.W. Johnson, Amantadine inhibits NMDA receptors by accelerating channel closure during channel block, J. Neurosci. 25 (2005) 3312–3322.
[65] C.G. Parsons, A. Stöffler, W. Danysz, Memantine: a NMDA receptor antagonist that improves memory by restoration of homeostasis in the glutamatergic system–too little activation is bad, too much is even worse, Neuropharmacology 53 (2007) 699–723.
[66] C.G. Parsons, K. Gilling, Memantine as an example of a fast, voltage-dependent, open channel N-methyl-D-aspartate receptor blocker, Methods Mol. Biol. 403 (2007) 15–36.
[67] S.E. Kotermanski, J.W. Johnson, Mg2+ imparts NMDA receptor subtype selectivity to the Alzheimer's drug memantine, J. Neurosci. 29 (2009) 2774–2779.
[68] H.J. Otton, A. Lawson McLean, M.A. Pannozzo, C.H. Davies, D.J. Wyllie, Quantification of the Mg2+-induced potency shift of amantadine and memantine voltage-dependent block in human recombinant GluN1/GluN2A NMDARs, Neuropharmacology 60 (2011) 388–396.
[69] M.L. Vallano, B. Lambolez, E. Audinat, J. Rossier, Neuronal activity differentially regulates NMDA receptor subunit expression in cerebellar granule cells, J. Neurosci. 16 (1996) 631–639.
[70] M. Llansola, A. Sánchez-Pérez, O. Cauli, V. Felipo, Modulation of NMDA receptors in the cerebellum. 1. Properties of the NMDA receptor that modulate its function, Cerebellum 4 (2005) 154–161.
[71] L. Cathala, C. Misra, S. Cull-Candy, Developmental profile of the changing properties of NMDA receptors at cerebellar mossy fiber-granule cell synapses, J. Neurosci. 20 (2000) 5899–5905.
[72] N. Burnashev, H. Monyer, P.H. Seeburg, B. Sakmann, Divalent ion permeability of AMPA receptor channels is dominated by the edited form of a single subunit, Neuron 8 (1992) 189–198.
[73] H. Mori, H. Masaki, T. Yamakura, M. Mishina, Identification by mutagenesis of a Mg(2+)-block site of the NMDA receptor channel, Nature 358 (1992) 673–675.
[74] K. Kashiwagi, T. Masuko, C.D. Nguyen, T. Kuno, I. Tanaka, K. Igarashi, K. Williams, Channel blockers acting at N-methyl-d-aspartate receptors: differential effects of mutations in the vestibule and ion channel pore, Mol. Pharmacol. 61 (2002) 533–545.
[75] H.S. Chen, S.A. Lipton, Pharmacological implications of two distinct mechanisms of interaction of memantine with N-methyl-D-aspartate-gated channels, J. Pharmacol. Exp. Therapeut. 314 (2005) 961–971.
[76] J.F. MacDonald, M.C. Bartlett, I. Mody, P. Pahapill, J.N. Reynolds, M.W. Salter, J.H. Schneiderman, P.S. Pennefather, Actions of ketamine, phencyclidine and MK-801 on NMDA receptor currents in cultured mouse hippocampal neurones, J. Physiol. 432 (1991) 483–508.
[77] M.V. Nikolaev, L.G. Magazanik, D.B. Tikhonov, Influence of external magnesium ions on the NMDA receptor channel block by different types of organic cations, Neuropharmacology 62 (2012) 2078–2085.
[78] N.G. Glasgow, M.R. Wilcox, J.W. Johnson, Effects of Mg2+ on recovery of NMDA receptors from inhibition by memantine and ketamine reveal properties of a second site, Neuropharmacology 137 (2018) 344–358.
[79] A.M. Woodhull, Ionic blockage of sodium channels in nerve, J. Gen. Physiol. 61 (1973) 687–708.
[80] C.G. Parsons, W. Danysz, G. Quack, Memantine is a clinically well tolerated N-methyl-D-aspartate (NMDA) receptor antagonist–a review of preclinical data, Neuropharmacology 38 (1999) 735–767.
[81] K.E. Gilling, C. Jatzke, M. Hechenberger, C.G. Parsons, Potency, voltage-dependency, agonist concentration-dependency, blocking kinetics and partial untrapping of the uncompetitive N-methyl-D-aspartate (NMDA) channel blocker memantine at human NMDA (GluN1/GluN2A) receptors, Neuropharmacology 56 (2009) 866–875.
[82] Oral Administration of IIc (5 Mg/kg) to Mice Led to its Fast Absorption from the Gastrointestinal Tract, Reaching a Maximum Plasma Concentration (C_{max}) of 1.12 ± 0.76 ᴍM after 45 Min. Interestingly, a Much Higher Concentration of UB-ALT-EV Was Found in Brain as Compared to Plasma, Indicating a Fast and Very High BBB Penetration. A C_{max} of 17.10 ± 6.06 μM was Determined in Brain Which Was Reached after about 1 H (T_{max} = 56 Min). Thus, the C_{max} in Brain Was 15-fold Higher than that in Plasma. A Brain/plasma Ratio of 32 Was Observed after 1 H at C_{max} (Brain). Companys-Alemany, J.; Turcu, A. L.; Schneider, M.; Müller, C. E.; Vázquez, S.; Griñán-Ferré, C.; Pallàs, M. NMDA Receptor Antagonists Reduce Amyloid-β Deposition by Modulating Calpain-1 Signaling and Autophagy, Rescuing Cognitive Impairment in 5XFAD Mice, Unpublished Results.
[83] W.A.M. de Almeida, J.P. de Andrade, D.S. Chacon, C.R. Lucas, E. Mariana, L. de Santis Ferreira, T. Guaratini, E.G. Barbosa, J.A. Zuanazzi, F. Hallwass, W. de Souza Borges, R. de Paula Oliveira, R.B. Giordani, Isoquinoline alkaloids reduce beta-amyloid peptide toxicity in *Caenorhabditis elegans*, Nat. Prod. Res. (2020) 1–5.
[84] T. Limana da Silveira, M. Lopes Machado, F. Bicca Obetine Baptista, D. Farina Gonçalves, D. Duarte Hartmann, L. Marafiga Cordeiro, A. Franzen da Silva, C. Lenz Dalla Corte, M. Aschner, F.A. Antunes Soares, *Caenorhabditis elegans* as a model for studies on quinolinic acid-induced NMDAR-dependent glutamatergic disorders, Brain Res. Bull. 175 (2021) 90–98.
[85] T. Kano, P.J. Brockie, T. Sassa, H. Fujimoto, Y. Kawahara, Y. Lino, J.E. Mellem, D.M. Madsen, R. Hosono, A.V. Maricq, Memory in *Caenorhabditis elegans* is mediated by NMDA-type ionotropic glutamate receptors, Curr. Biol. 18 (2008) 1010–1015.
[86] P.J. Brockie, A.V. Maricq, Ionotropic glutamate receptors in *Caenorhabditis elegans*, Neurosignals 12 (2003) 108–125.
[87] M.K. Back, S. Ruggieri, E. Jacobi, J. von Engelhardt, Amyloid beta-mediated changes in synaptic function and spine number of neocortical neurons depend on NMDA receptors, Int. J. Mol. Sci. 22 (2021) 6298.
[88] S.D. Girard, M. Jacquet, K. Baranger, M. Migliorati, G. Escoffier, A. Bernard, M. Khrestchatisky, F. Féron, S. Rivera, F.S. Roman, E. Marchetti, Onset of hippocampus-dependent memory impairments in 5XFAD transgenic mouse model of Alzheimer's disease, Hippocampus 24 (2014) 762–772.
[89] L. Devi, M. Ohno, Cognitive benefits of memantine in Alzheimer's 5XFAD model mice decline during advanced disease stages, Pharmacol. Biochem. Behav. 144 (2016) 60–66.
[90] M. Jürgenson, T. Zharkovskaja, A. Noortoots, M. Morozova, A. Beniashvili, M. Zapolski, A. Zharkovsky, Effects of the drug combination memantine and melatonin on impaired memory and brain neuronal deficits in an amyloid-predominant mouse model of Alzheimer's disease, J. Pharm. Pharmacol. 71 (2019) 1695–1705.
[91] X. Chen, J.W. Barclay, R.D. Burgoyne, A. Morgan, Using *C. elegans* to discover therapeutic compounds for ageing-associated neurodegenerative diseases, Chem. Cent. J. 9 (2015) 65.
[92] C. Griñán-Ferré, A. Bellver-Sanchis, M. Olivares-Martín, O. Bañuelos-Hortigüela, M. Pallàs, Synergistic neuroprotective effects of a natural product Mixture against AD hallmarks and cognitive decline in *Caenorhabditis elegans* and an SAMP8 mice model, Nutrients 13 (2021) 2411.
[93] A.L. Oblak, P.B. Lin, K.P. Kotredes, R.S. Pandey, D. Garceau, H.M. Williams, A. Uyar, R. O'Rourke, S. O'Rourke, C. Ingraham, D. Bednarczyk, M. Belanger, Z.A. Cope, G.J. Little, S.G. Williams, C. Ash, A. Bleckert, T. Ragan, B.A. Logsdon, L.M. Mangravite, S.J. Sukoff Rizzo, P.R. Territo, G.W. Carter, G.R. Howell, M. Sasner, B.T. Lamb, Comprehensive evaluation of the 5XFAD mouse model for preclinical testing applications: a MODEL-AD study, Front. Aging Neurosci. 13 (2021), 713726.
[94] G.E. Hardingham, H. Bading, Synaptic versus extrasynaptic NMDA receptor signaling: implications for neurodegenerative disorders, Nat. Rev. Neurosci. 11 (2010) 682–696.
[95] Y. Liu, T.P. Wong, M. Aarts, A. Rooyakkers, L. Liu, T.W. Lai, D.C. Wu, J. Lu, M. Tymianski, A.M. Craig, Y.T. Wang, NMDA receptor subunits have differential roles in mediating excitotoxic neuronal death both *in vitro* and *in vivo*,

J. Neurosci. 27 (2007) 2846–2857.
[96] D.T. Proctor, E.J. Coulson, P.R. Dodd, Post-synaptic scaffolding protein interactions with glutamate receptors in synaptic dysfunction and Alzheimer's disease, Prog Neurobiol 93 (2011) 509–521.
[97] Z. Liu, C. Lv, W. Zhao, Y. Song, D. Pei, T. Xu, NR2B-containing NMDA receptors expression and their relationship to apoptosis in hippocampus of Alzheimer's disease-like rats, Neurochem. Res. 37 (2012) 1420–1427.
[98] Y.-N. Wu, S.W. Johnson, Memantine selectively blocks extrasynaptic NMDA receptors in rat substantia nigra dopamine neurons, Brain Res. 1603 (2015) 1–7.
[99] R. Wang, P.H. Reddy, Role of glutamate and NMDA receptors in Alzheimer's Disease, J. Alz. Dis. 57 (2017) 1041–1048.
[100] F.J. Carvajal, R.G. Mira, M. Rovegno, A.N. Minniti, W. Cerpa, Age-related NMDA signaling alterations in SOD2 deficient mice, Biochim. Biophys. Acta (BBA) - Mol. Basis Dis. 1864 (2018) 2010–2020.
[101] R. Knox, C. Zhao, D. Miguel-Perez, S. Wang, J. Yuan, D. Ferriero, X. Jiang, Enhanced NMDA receptor tyrosine phosphorylation and increased brain injury following neonatal hypoxia-ischemia in mice with neuronal Fyn overexpression, Neurobiol. Dis. 51 (2013) 113–119.
[102] K. Prybylowski, K. Chang, N. Sans, L. Kan, S. Vicini, R.J. Wenthold, The synaptic localization of NR2B-containing NMDA receptors is controlled by interactions with PDZ proteins and AP-2, Neuron 47 (2005) 845–857.
[103] M. Xie, Y. Li, S.H. Wang, Q.T. Yu, X. Meng, X.M. Liao, The involvement of NR2B and tau protein in MG132-induced CREB dephosphorylation, J. Mol. Neurosci. 62 (2017) 154–162.
[104] M. Amidfar, J. de Oliveira, E. Kucharska, J. Budni, Y.-K. Kim, The role of CREB and BDNF in neurobiology and treatment of Alzheimer's disease, Life Sci. 257 (2020), 118020.
[105] S.L. Angulo, T. Henzi, S.A. Neymotin, M.D. Suarez, W.W. Lytton, B. Schwaller, H. Moreno, Amyloid pathology-produced unexpected modifications of calcium homeostasis in hippocampal subicular dendrites, Alzheimer's Dementia 16 (2020) 251–261.
[106] O. Trott, A.J. Olson, AutoDock Vina, Improving the speed and accuracy of docking with a new scoring function, efficient optimization and multithreading, J. Comput. Chem. 31 (2010) 455–461.
[107] S. Jo, T. Ki, V.G. Iyer, W. Im, CHARMM-GUI: a web-based graphical user interface for CHARMM, J. Comput. Chem. 29 (2008) 1859–1865.
[108] E.L. Wu, S. Jo, H. Rui, K.C. Song, E.M. Dávila-Contreras, Y. Qi, J. Lee, V. Monje-Galvan, R.M. Venable, J.B. Klauda, W. Im, CHARMM-GUI *Membrane Builder* toward realistic biological membrane simulations, J. Comput. Chem. 35 (2014) 1997–2004.
[109] D.A. Case, I.Y. Ben-Shalom, S.R. Brozell, D.S. Cerutti, T.E.I. Cheatham, V.W.D. Cruzeiro, T.A. Darden, R.E. Duke, D. Ghoreishi, M.K. Gilson, H. Gohlke, A.W. Goetz, D. Greene, R. Harris, N. Homeyer, S. Izadi, A. Kovalenko, T. Kurtzman, T.S. Lee, S. LeGrand, P. Li, C. Lin, J. Liu, T. Luchko, R. Luo, D.J. Mermelstein, K.M. Merz, Y. Miao, G. Monard, C. Nguyen, H. Nguyen, I. Omelyan, A. Onufriev, F. Pan, R. Qi, D.R. Roe, A. Roitberg, C. Sagui, S. Schott-Verdugo, J. Shen, C.L. Simmerling, J. Smith, R. Salomon-Ferrer, J. Swails, R.C. Walker, J. Wang, H. Wei, R.M. Wolf, X. Wu, L. Xiao, D.M. York, P.A. Kollman, AMBER 2018, University of California, San Francisco, 2018.
[110] J.A. Maier, C. Martinez, K. Kasavajhala, L. Wickstrim, K.E. Hauser, C. Simmerling, ff14SB: improving the accuracy of protein side chain and backbone parameters from ff99SB, J. Chem. Theor. Comput. 11 (2015) 3696–3713.
[111] C.J. Dickson, B.D. Madej, A.A. Skjevik, R.M. Betz, K. Teigen, I.R. Gould, R.C. Walker, Lipid14: the Amber lipid force field, J. Chem. Theor. Comput. 10 (2014) 865–879.
[112] J. Wang, R.M. Wolf, J.W. Caldwell, P.A. Kollman, D.A. Case, Development and testing of a general amber force field, J. Comput. Chem. 25 (2004) 1157–1174.
[113] J.-P. Ryckaert, G. Ciccotti, H.J.C. Berendsen, Numerical integration of the cartesian equations of motion of a system with constraints: molecular dynamics of *n*-alkanes, J. Comp. Phys. 23 (1977) 327–341.
[114] T. Darden, D. York, L. Pedersen, Particle mesh Ewald: an N-log(N) method for Ewald sums in large systems, J. Chem. Phys. 98 (1993) 10089–10092.
[115] W. Humphrey, A. Dalke, K. Schulten, VMD: visual molecular dynamics, J. Mol. Graph. 14 (1996) 33–38.
[116] D.R. Roe, T.E. Cheatham III., PTRAJ and CPPTRAJ: software for processing and analysis of molecular dynamics trajectory data, J. Chem. Theor. Comput. 9 (2013) 3084–3095.
[117] N.G. Glasgow, J.W. Johnson, Whole-cell patch-clamp analysis of recombinant NMDA receptor pharmacology using brief glutamate applications, Methods Mol. Biol. 1183 (2014) 23–41.
[118] F. Yi, S. Bhattacharya, C.M. Thompson, S.F. Traynelis, K.B. Hansen, Functional and pharmacological properties of triheteromeric GluN1/2B/2D NMDA receptors, J. Physiol. 597 (2019) 5495–5514.
[119] A.M. Woodhull, Ionic blockage of sodium channels in nerve, J. Gen. Physiol. 61 (1973) 687–708.
[120] S.M. Antonov, V.E. Gmiro, J.W. Johnson, Binding sites for permeant ions in the channel of NMDA receptors and their effects on channel block, Nat. Neurosci. 1 (1998) 451–461.
[121] L. Di, E.H. Kerns, K. Fan, O.J. McConnell, G.T. Carter, High throughput artificial membrane permeability assay for blood-brain barrier, Eur. J. Med. Chem. 38 (2003) 223–232.